NASA CONTRACTOR REPORT

NASA CR-605

EVALUATION OF A MINIATURIZED DOUBLE-FOCUSING MASS SPECTROMETER

by Wayne H. Brigden

Prepared by
SPACELABS, INC.
Van Nuys, Calif.
for Flight Research Center

NATIONAL AERONAUTICS AND SPACE ADMINISTRATION • WASHINGTON, D. C. • NOVEMBER 1966

EVALUATION OF A MINIATURIZED DOUBLE-FOCUSING MASS SPECTROMETER

By Wayne H. Brigden

Prepared under Contract No. NAS 4-791 by
SPACELABS, INC.
Van Nuys, Calif.

for Flight Research Center

NATIONAL AERONAUTICS AND SPACE ADMINISTRATION

For sale by the Clearinghouse for Federal Scientific and Technical Information
Springfield, Virginia 22151 – Price $3.25

PREFACE

Particular acknowledgment should be made to Mr. Raymond W. Snyder without whose help this report would have been impossible. Only people active in the field of mass spectrometry can fully appreciate the amount of toil required to collect the quantity of experimental data found in the following pages.

Wayne H. Brigden

TABLE OF CONTENTS

TABLE OF CONTENTS continued

TABLE OF ILLUSTRATIONS

TABLE OF ILLUSTRATIONS continued

TABLE OF ILLUSTRATIONS continued

TABLE OF ILLUSTRATIONS continued

TABLE OF TABLES

TABLE OF TABLES continued

TABLE OF TABLES continued

TABLE OF TABLES continued

EVALUATION OF A MINIATURIZED DOUBLE-FOCUSING MASS SPECTROMETER

1. INTRODUCTION

The general conclusion drawn from this report is that the magnetic double-focusing mass spectrometer shows considerable promise as a practical means of measuring gas concentrations in a flight environment. It should be pointed out that the magnetic double-focusing mass spectrometer has several inherent advantages over other means of gas concentration measurement either in the air or on the ground. These advantages are the capability of simultaneously monitoring several different gases, the capability of scanning for unknown gases as well as the ability to obtain accurate readings in a tenth of a second or less. While any one of these features is available in other types of instruments, the double-focusing mass spectrometer is unique in that all of these capabilities are included in one instrument. The mass spectrometer investigated in this report demonstrates the feasibility of designing such an instrument for a flight environment.

Cost, complexity and physical size have been the principal obstacles to the wide spread use of the mass spectrometer. This has been particularly true in considering the mass spectrometer for flight applications. The instrument studied in this report demonstrates that reasonable sized mass spectrometers--which work--can be built. Future developments in the field should overcome the limitations of cost and complexity and make the magnetic double-focusing mass spectrometer a useful and practical research tool.

2. SUMMARY OF EVALUATION RESULTS

2.1 Sensitivity

The basic sensitivity of the mass spectrometer in amps per torr of input pressure is not the same for the various collector buckets due to the different ballistic paths. Furthermore, since much higher partial pressures are anticipated for some gases than for others, the different collector buckets monitor different current ranges. For this reason, electrometers of three different sensitivities are used: 2×10^{11}, 5×10^{11} and 5×10^{12} ohms. For operational purposes, it is only necessary to establish an overall instrument sensitivity in volts per torr of input pressure for each output regardless of the electrometer sensitivities. Should it be desired to monitor mixtures with lower concentrations of Nitrogen, Oxygen and Carbon Dioxide, the overall sensitivity for these gases could be increased simply by plugging in more sensitive electrometers. For this reason, two sensitivity factors are given in Table I for each gas. The first sensitivity factor is measured using the standard electrometer sensitivity for exhaled gas analysis. The second sensitivity factor given is that obtainable by using the most sensitive electrometer.

The curves from which the sensitivity slopes were obtained are shown in Figures 1, 2 and 3. The bending of the curves near the origin is due to the flow characteristics of the capillary with low total input pressure. The total input pressure less the partial pressure of any particular gas generally leaves a remainder of 150 torr. The sensitivity curves are, therefore, not distorted near the origin in typical operation since the total input pressure is maintained above the critical 150 torr level. The sensitivity slope for each gas is determined from the pure gas curve by taking one slope point at the 150 torr level and the second slope point at a higher pressure level. Thus for any particular gas, the sensitivity can be represented by a straight line passing through the origin of an output voltage vs. pressure curve as long as the total sample pressure less the partial pressure of the gas of interest remains above 150 torr. Below this pressure, inaccuracies occur due to the flow characteristics of the capillary line.

It should be noted that the sensitivity figures quoted in Table I are determined with the instrument tuned for best resolution. By opening the collector slits and retuning the instrument for better sensitivity (with less resolution), it is estimated that the instrument sensitivity could be improved by a factor of five from the values quoted in Table I.

TABLE I

Mass Spectrometer Sensitivity Factors

Gas	Operating Sensitivity	Instrument Sensitivity With Most Sensitive Electrometer
N_2	7.67×10^{-3} volts/torr	192×10^{-3} volts/torr
O_2	6.88×10^{-3} volts/torr	172×10^{-3} volts/torr
CO_2	17.8×10^{-3} volts/torr	178×10^{-3} volts/torr

2.2 Minimum Detectable Level

The Minimum Detectable Level is defined for the purposes of this report: as the concentration in parts per million of an atmospheric sample which will cause an output voltage rise on the most sensitive electrometer equal to the peak-to-peak random noise voltage on the same electrometer. The peak-to-peak noise voltage on the 5×10^{12} ohm electrometer is 50 millivolts. Although all the 5×10^{12} electrometers do not have noise levels of this value, this is a conservative value for a properly tuned amplifier. Since the electrometer noise is essentially a constant, the Minimum Detectable Level depends almost entirely upon the sensitivity. For example, should the sensitivity double, the Minimum

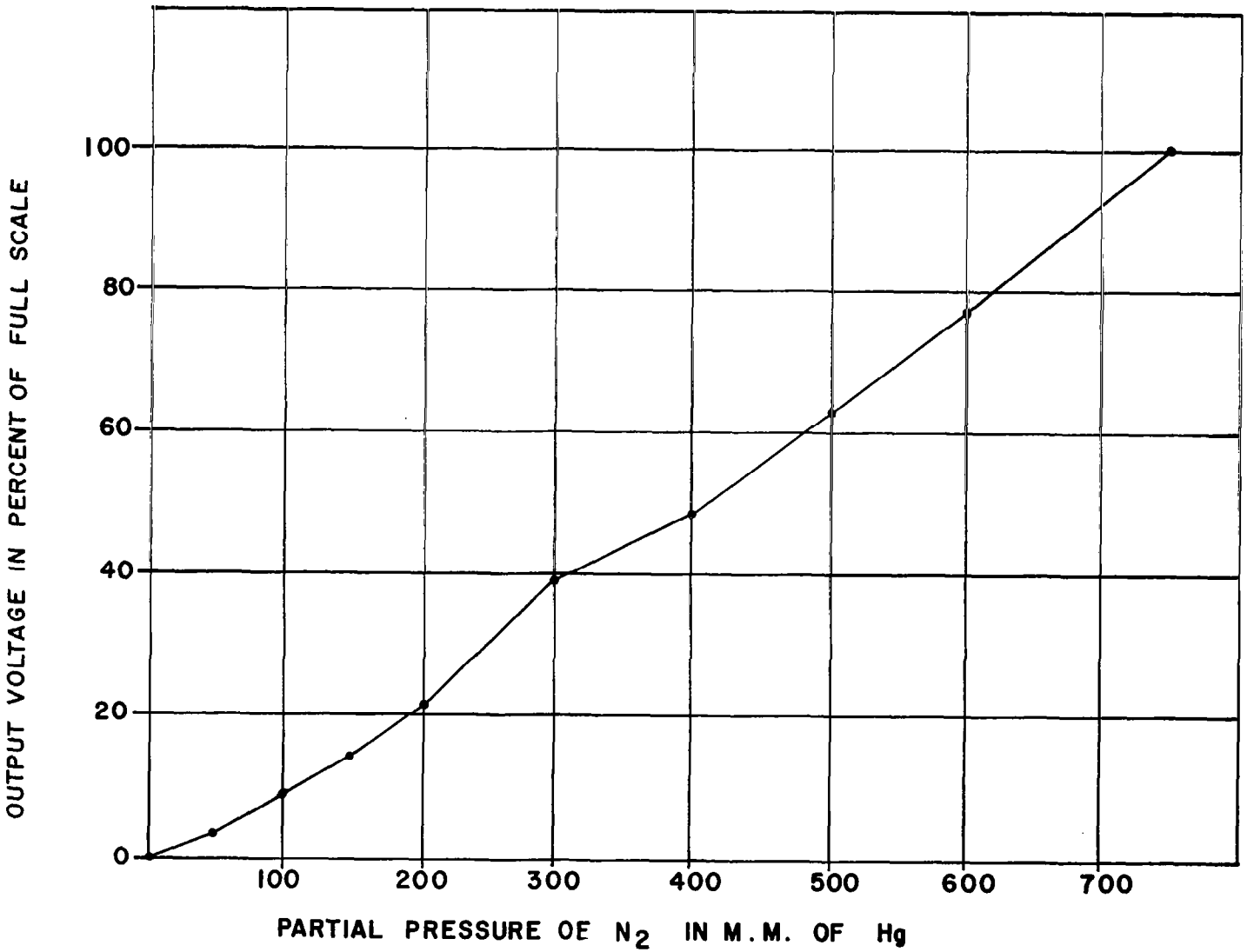

PURE GAS CALIBRATION OF NITROGEN

FIG. 1

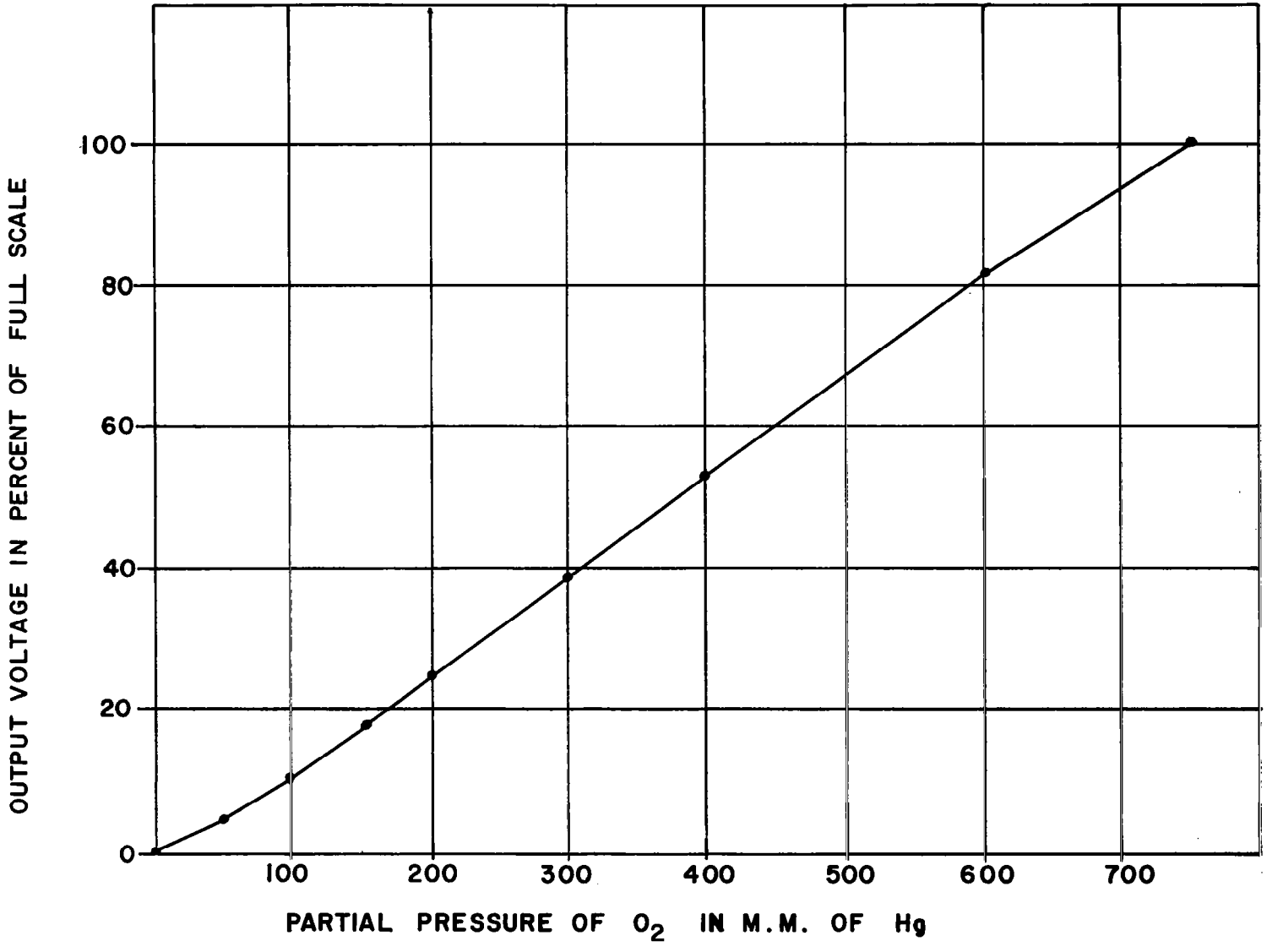

PURE GAS CALIBRATION OF OXYGEN

FIG. 2

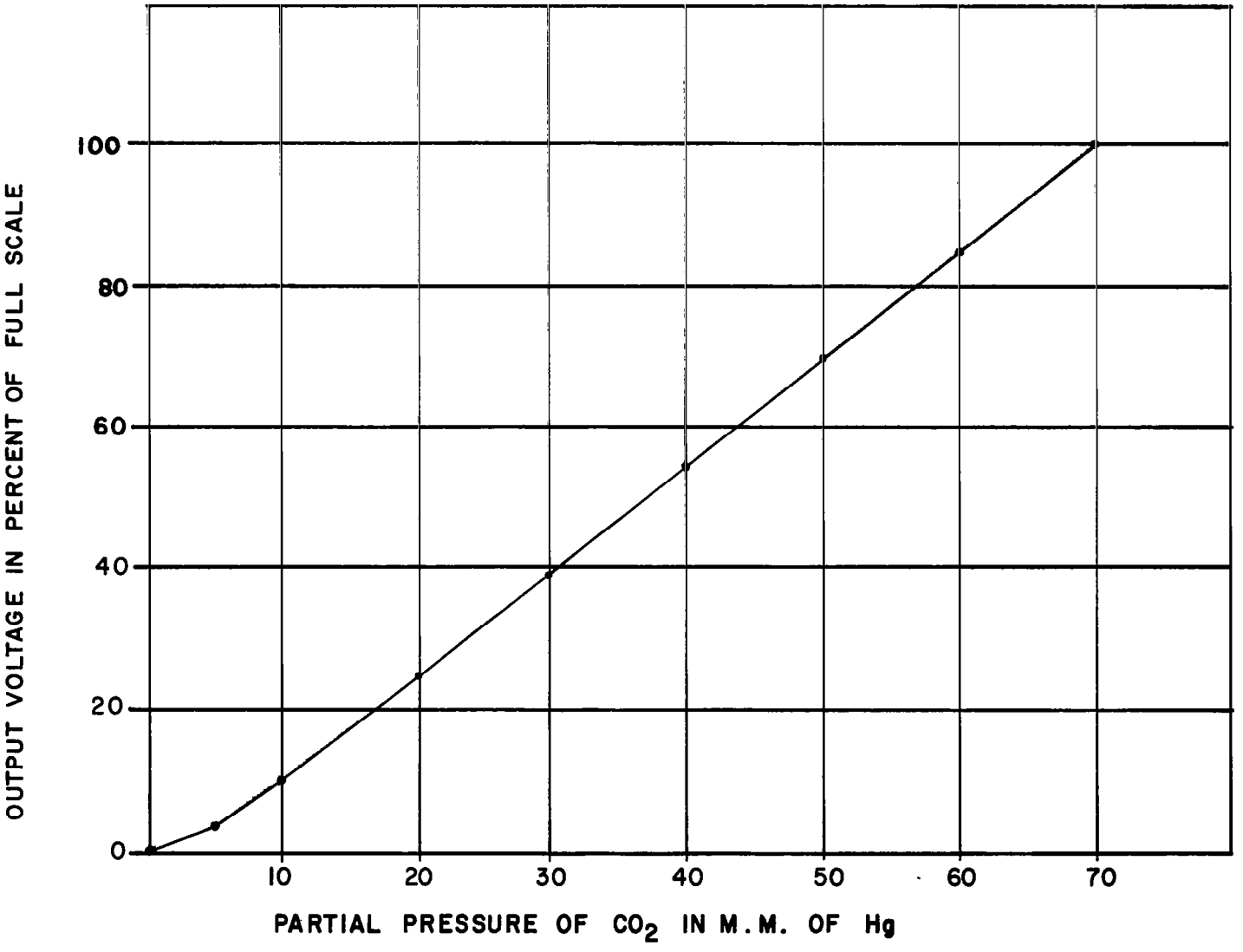

PURE GAS CALIBRATION OF CARBON DIOXIDE

FIG. 3

Detectable Level would be halved. With the mass spectrometer presently tuned for best resolution (poor sensitivity), the Minimum Detectable Level is 800 ppm. of an atmospheric sample. By changing the analyzer magnet, the Minimum Detectable Level could be reduced to 250 ppm without depreciation of the resolution. This has not been done since it involves an almost complete redesign of two circuit boards. As was mentioned in the section on sensitivity, it is estimated that the mass spectrometer sensitivity could be increased by a factor of five by tuning the instrument for less resolution and widening the collector slits. If such an improvement in sensitivity were achieved, the Minimum Detectable Level would be improved by a factor of five.

2.3 Accuracy

In normal operation, the mass spectrometer is calibrated once every two minutes by introducing a known gas mixture at fixed pressure from the Calibration Sample Bottle. Although regulated, the Calibration Sample Bottle output pressure is a function of time. Assuming the Calibration Sample Bottle is operated for two seconds every minute, the Sample Bottle is operated 8 minutes for each 4 hours of instrument operation. After 8 minutes of operation, the Calibration Sample Bottle output pressure increases .6% from its initial value. This is a predictable error which can be corrected if extreme accuracy is desired.

In operation, the output zero level is noted every two minutes with the sample off. Assuming a constant temperature and clean vacuum system, the zero level remains within .2 percent of full scale over this two minute period.

Knowing the variation in calibration pressure and zero stability, it is only necessary to know the sensitivity stability over a period of one minute, and the deviation of the pressure curve from the straight line sensitivity curve to be able to predict the accuracy of the measurement. Tests have shown that the sensitivity remains within .8 percent over a period of ten minutes and within 5.8 percent over a period of 3 hours. This data is shown in Table II.

TABLE II

Output vs. Time at Constant Input Pressure

Time in Minutes	Output in Percent of Initial Reading
0	100.0
10	100.3
20	100.8
30	100.0
40	100.3

TABLE II continued

Time in Minutes	Output in Percent of Initial Reading
50	100.3
60	100.0
80	98.5
105	96.7
135	95.8
155	95.8
180	95.0

From Figures 1 - 3 the maximum deviation from the straight line sensitivity curves is seen to be plus or minus 3.0 percent of full scale for N_2, plus or minus 2.0 percent for O_2 and plus or minus 3.0 percent for CO_2. The linearity figures are taken over the range from 150 to 750 mm of Hg. for O_2 and N_2. The 0 to 60 mm section of the curve was taken for CO_2 as this sample was part of a mixture. Here again, if extreme accuracy were desired, the error due to deviation from the sensitivity curve could be eliminated by a tedious mathematical procedure.

In considering measurement accuracy, it should be noted that a certain amount of ambiguity in reading the output results from the noise of the electrometers. In measuring small gas concentrations, where the most sensitive electrometers are used, this ambiguity can be as much as one percent of full scale.

2.4 Long Term Stability

The long term stability is limited by fluctuations in ionization current, decay of the magnet and the cleanliness of the vacuum system.

Over a period of several days the total emission current was noted to vary $\pm$ 1.25 percent. This figure discounts the 5 percent change which occurs immediately after turning the unit on. Assuming constant filament position and source voltages, the percentage change in total emission current should equal the percentage change in ionization current.

The rate of decay of the magnet is a function of the time elapsed since recharging being greatest immediately after recharging. Experiments indicate the rate of decay to be 2.2 percent per week immediately after recharging, but to be only .2 percent per week 3 months later. Since a change in magnetic field strength of .2 percent will cause the mass spectrometer to have short term instability, the High

Voltage supply should be adjusted regularly to compensate for this change in magnetic field. Good operating procedure would dictate a check of this adjustment before each flight.

Good operating procedure should maintain the cleanliness of the vacuum system for a period of several months. A dirty vacuum system can cause instability in two ways. When the electrodes in the ionization region become dirty, charged particles can collect in arbitrary numbers on these electrodes thus upsetting the established operating potentials. Instability is also caused by a dirty vacuum system outside of the ionization region. This phenomenon results when the outgassing from the vacuum system walls increases the throughput to the ion pump thus causing the pump pressure to increase. When this happens, the output becomes more susceptible to changes in pump speed.

2.5 Input Pressure

The mass spectrometer will operate over a pressure range of zero to atmospheric pressure; however, gross errors (such as 50 percent) would be experienced if caution were not taken to maintain the total sample pressure above some level. This is due to the flow characteristics of the capillary line. If the total sample pressure including the partial pressure of the gas of interest is maintained above 150 torr, errors due to changes in total pressure are limited to plus or minus 3 percent of full scale.

2.6 Mass Range

Ion beams with mass numbers ranging from 2 to 78 have been observed. There has been no particular emphasis in the testing program to monitor mass numbers outside of this range. If it were so desired, the mass range might possibly be extended by retuning the instrument.

2.7 Resolution

The resolution was found to be one part in forty-five using the criterion of one percent cross talk between adjacent peaks of equal height.

2.8 Output

The electrometers have a zero to minus five volts dc output. The electrometers are capable of driving a 10K ohm load and have a dynamic output impedance of less than one ohm.

2.9 Unattended Operating Time

The Unattended Operating Time is limited by the vacuum system and more partic-

ularly by the Sorption Pump. With the sorption pump Zeolite well pumped down, the instrument is capable of operating in a laboratory environment for a period of 9 hours from the time it is filled with liquid nitrogen. At the end of four and a half hours, .2 percent error will result from reduced sorption pumping, and at the end of 9 hours, two percent error will result from the reduced pumping. Operation beyond this time limit will result in gross errors. The Unattended Operating Time is decreased under vibration; however, the decrease in operating time due to vibration is not well documented. Two hour flights have been made without noticeable changes in performance.

2.10 Response Time

The zero to one hundred percent rise time is approximately .03 seconds for the higher concentration gases and .10 seconds for the gases of lower concentration. The response time is primarily limited by the characteristics of the capillary tube.

3. BASIC THEORY OF OPERATION

3.1 Explanation of Operation

A simple block diagram of the mass spectrometer is shown in Figure 4. The gas to be sampled is passed continuously through the capillary line and is pumped by the sorption pump. The capillary line is tapered in such a manner that the sample is being continuously expanded as it passes through the line. The inlet manifold pressure is approximately only one percent of the pressure being sampled. A small part of the capillary flow passes through the gold leak into the ion source. The gas which flows through the gold leak is further expanded by a factor of approximately 20,000. This sample gas in the ion source is being continually pumped by the 4 liter/sec ion pump.

The ion source contains an electron gun. This electron gun provides a narrow controlled beam of electrons which continually bombard the gas molecules passing through the source. The small number of molecules which are ionized by this process are acted upon by an electrical field in the ionization region which forces the ionized particles to pass out of the ion source through a narrow slit.

The beam of representative ions leaving the source is attracted to the analyzer section of the mass spectrometer. In this section, the single ion beam is focused and separated by electric and magnetic forces into a number (depending upon sample) of ion beams of unique mass over charge ratio. These individual beams pass through their respective collector slits each of which is unique to a given m/e ratio.

The ions of each beam are collected by the individual collector bucket, and the resulting current is measured by the respective electrometer. Since the various m/e ratios resulting from electron bombardment are known for each gas, it is possible to position the collector buckets in such a manner that each bucket will monitor an ion beam which is unique to any given gas.

3.2 Requirements for Stable Operation

The objective of this section is to categorically list the conditions necessary for stable operation. The advantages of such a list are twofold: first, it serves as a guide in outlining an evaluation program; second, it serves as a troubleshooting guide for unstable operation.

There are two fundamental requirements which must be met to achieve stable operation of the mass spectrometer described in this report. The first requirement is STABLE ION BEAM POSITION. In other words, for all conditions or combination of conditions such as input voltage, temperature and time, the ion beam position must be sufficiently stable to remain completely within the collector slit.

The second fundamental requirement of stable operation is STABLE ION BEAM

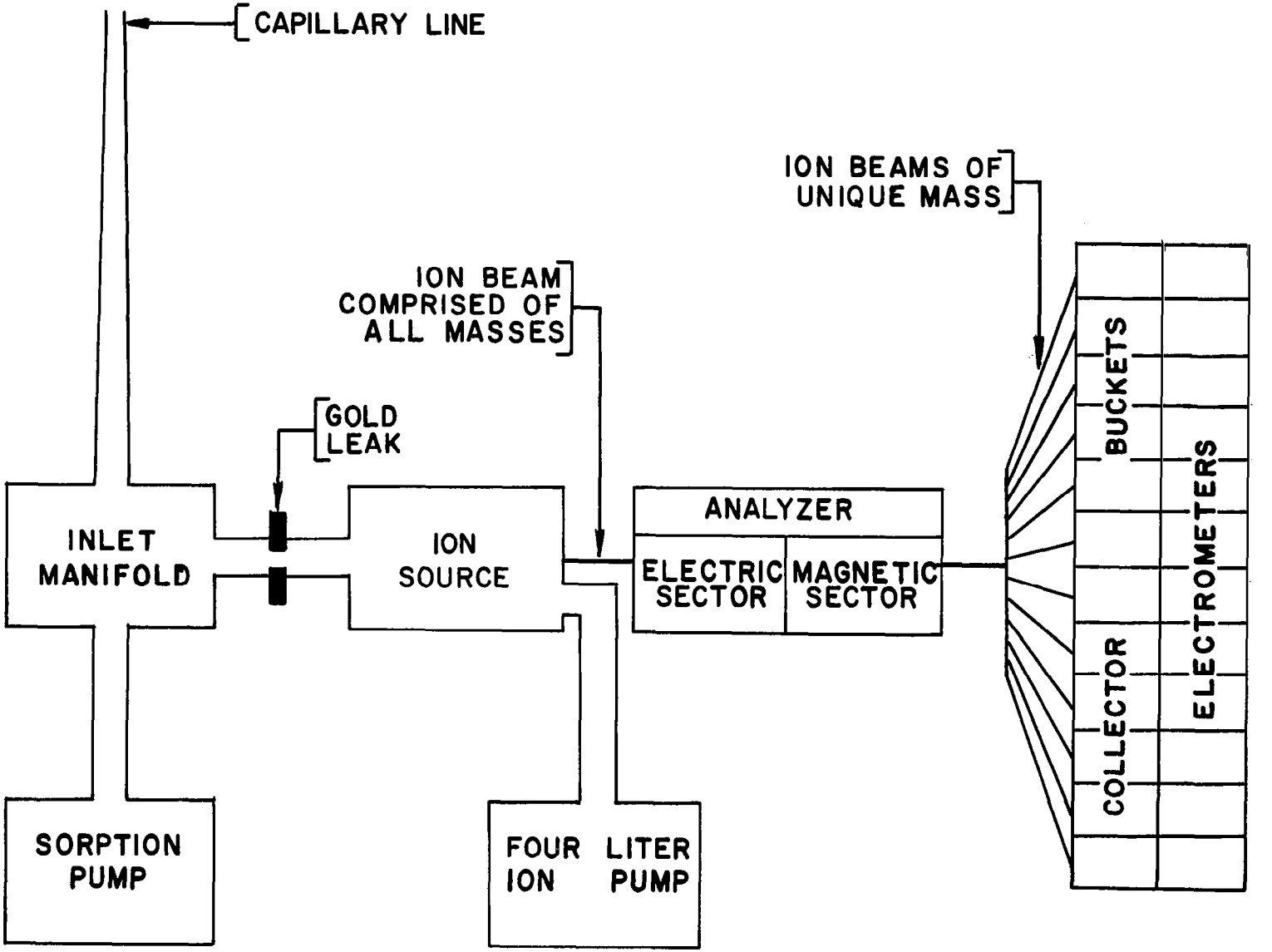

SIMPLE BLOCK DIAGRAM
FIG. FOUR

INTENSITY. That is, for a given capillary input pressure, the ion beam intensity (as measured at the collector bucket) must remain constant over all conditions of time, temperature, input voltage, etc. It is found that the two most fundamental requirements for stable operation can be achieved if the five conditions described below are met.

The first condition of mass spectrometer stability is an adequately large ratio of collector slit width to ion beam width as measured at the collector. The larger this ratio the wider can be the tolerances of the Fixed High Voltage Supply and Magnet. This is shown in Figure 5. If the ratio should drop to 1, any variation in the Fixed High Voltage or magnetic field will cause a decrease in ions entering the slit and thus decrease the output. The collector slit width determines the maximum resolution obtainable for a given beam width. The collector slit therefore has a practical upper limit. The beam width has a practical lower limit which is fixed by the required mass spectrometer sensitivity. Flat-topped peaks, observed when the mass spectrometer High Voltage Supply is scanned, indicate an adequate collector slit to beam width ratio. However, flat-topped peaks are <u>not</u> conclusive evidence of a ratio greater than 1. Flat-topped peaks can be observed with a collector slit to beam width ratio of less than 1 if a homogeneous beam is swept across the slit. Unstable operation will generally result when this ratio is less than 1.

The second condition of mass spectrometer stability is that the Ion Acceleration Voltage be sufficiently stable. The Ion Acceleration Voltage is defined as the voltage through which an ion is accelerated from the point of ionization to the point at which the ion enters the magnetic sector. This voltage is primarily determined by the Fixed High Voltage Supply; however, the Ion Acceleration Voltage is also partly determined by the Anode Supply. The allowable variation in this parameter is determined by the relative positioning of the collector slits of interest and the collector slit to beam width ratio. This is shown in Figure 6. In this example, should the beams move to the right, the middle beam will hit the side of the slit first. Should the beams move to the left, the right hand beam would hit the edge of the slit first. Thus the middle beam in the example would determine the one extreme of Ion Acceleration Voltage and the beam on the right would determine the other extreme. It should be mentioned that proximity to the slit edge does not solely determine which beam will first strike the edge since the change in beam position for a given change in Ion Acceleration Voltage is different for different mass beams. This must be taken into consideration when determining which beam will first strike the edge of its slit.

The third condition of mass spectrometer stability is a stable magnet. A change in Magnet strength will effect the beam positions as does a change in Ion Acceleration Voltage. For a given percentage change, the magnet's effect on beam position will be more pronounced than the effect of a change in Ion Acceleration Voltage. The same manner of determining the necessary stability is used for the Magnet as is used for the Ion Acceleration Voltage. It is assumed that the magnet strength will be some function of time and temperature.

The fourth condition of mass spectrometer stability is constant ionizing current. The ionizing current is that part of the total electron emission current which passes through the ionization region of the source. The ionization region is defined as that region of the Ion Source from which ions are selected and

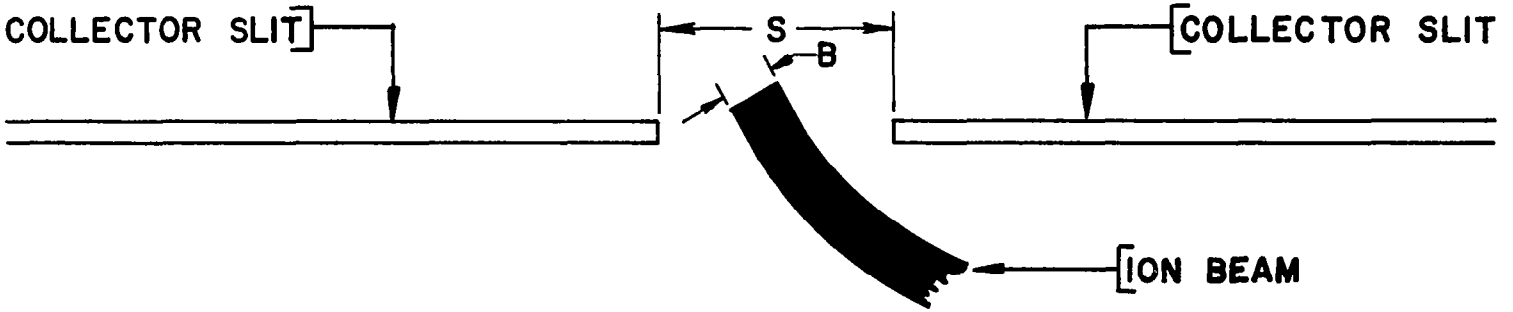

$$\frac{S}{B} = \frac{\text{COLLECTOR SLIT WIDTH}}{\text{ION BEAM WIDTH}}$$

FIG. FIVE

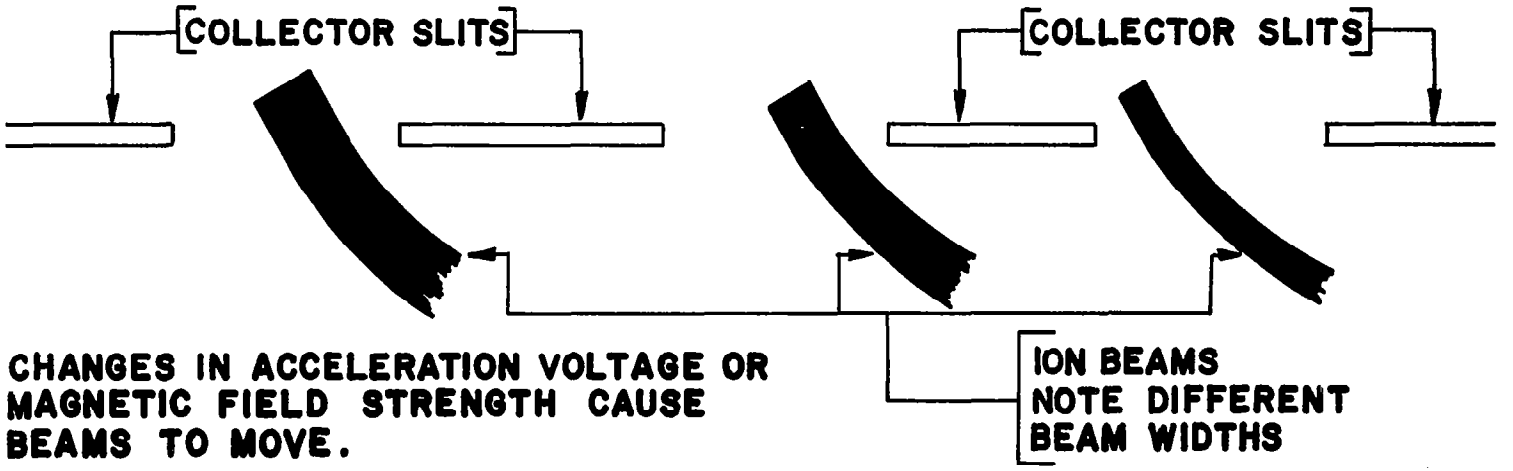

FIG. SIX

analyzed. The ionizing current, as defined, is thus varied by either a change in the number of electrons entering the source or a change in the distribution of those electrons which do enter. From this point of view, a change in magnetic configuration which changes the stray magnetic field in the source, for example, can be a cause of change in ionizing current because it changes the distribution of electrons within the source. Under proper operating conditions, the ion beam intensity is directly proportional to the ionizing current.

The fifth condition of mass spectrometer stability is that the source pressure remain constant for a given capillary input pressure. This condition is primarily determined by the operation of the capillary tube, gold leak and ion pump as well as the cleanliness of the vacuum system. Under proper operating conditions, the mass spectrometer output will be directly proportional to the source pressure.

4. DESCRIPTION OF LABORATORY LAYOUT AND EQUIPMENT

4.1 Trailer Layout and Outfitting

The testing of the mass spectrometer is conducted in a specially prepared trailer laboratory. The trailer is arranged so that about half its length is used for the laboratory per se and the other half for office space. Half of this office space is assigned to the mass spectrometry project. See Figure 7 and 8. A layout of the laboratory is shown in Figure 9.

Due to the dusty environment of the Mojave Desert, special consideration is given to maintaining a reasonably dust free work area. The doors and windows at the laboratory end of the trailer are made dust tight. One louver window was replaced with a single pane of glass. The outside door at the laboratory end of the trailer is not used, and the one outside door which is used has an electrostatic dust mat just inside it. Curtains were removed from the laboratory section to avoid the accumulation of dust. The floor of the trailer is cleaned and waxed regularly, and the dust mat is periodically changed. An Electronic Air Filter is installed in the laboratory section of the trailer.

Because of the several toxic and corrosive cleaning agents used, a necessary feature of the laboratory is a ventilated work area equipped with fan and non-corrodible work surface. See Figure 10.

As gas bottles are required in the laboratory both for samples and to pressurize the liquid nitrogen Dewar, bottle holders with chains and hooks were installed about the laboratory in convenient locations.

It is common for a number of different test instruments to be used simultaneously in testing. If the various test instruments and mass spectrometer were powered from a number of different power lines of arbitrary phase relation and ground reference, troublesome ground loops and ripple levels would undoubtedly occur. To avoid this problem, the laboratory was wired in such a manner that the mass spectrometer ground support power receptacle and all the power receptacles in the vicinity of the ground support system are connected to a single 100 amp. circuit. All benches in the laboratory are provided with AC receptacles spaced one foot apart.

4.2 Laboratory Vacuum and Pressure Equipment

In order to properly test and operate the mass spectrometer, a certain amount of vacuum and pressure equipment is required which is not found in the typical electronic laboratory. The largest single item in this group is a Leak Detector. The Leak Detector is not only used in leak checking the mass spectrometer itself but also the ground support equipment and component parts such as Capillary Lines and Inlet Valves. The Leak Detector proved invaluable in the fabrication of the Pure Gas Sample Inlet System and the Gold Leak Test System.

PHOTOGRAPH OF MASS SPECTROMETER LABORATORY

FIG. SEVEN

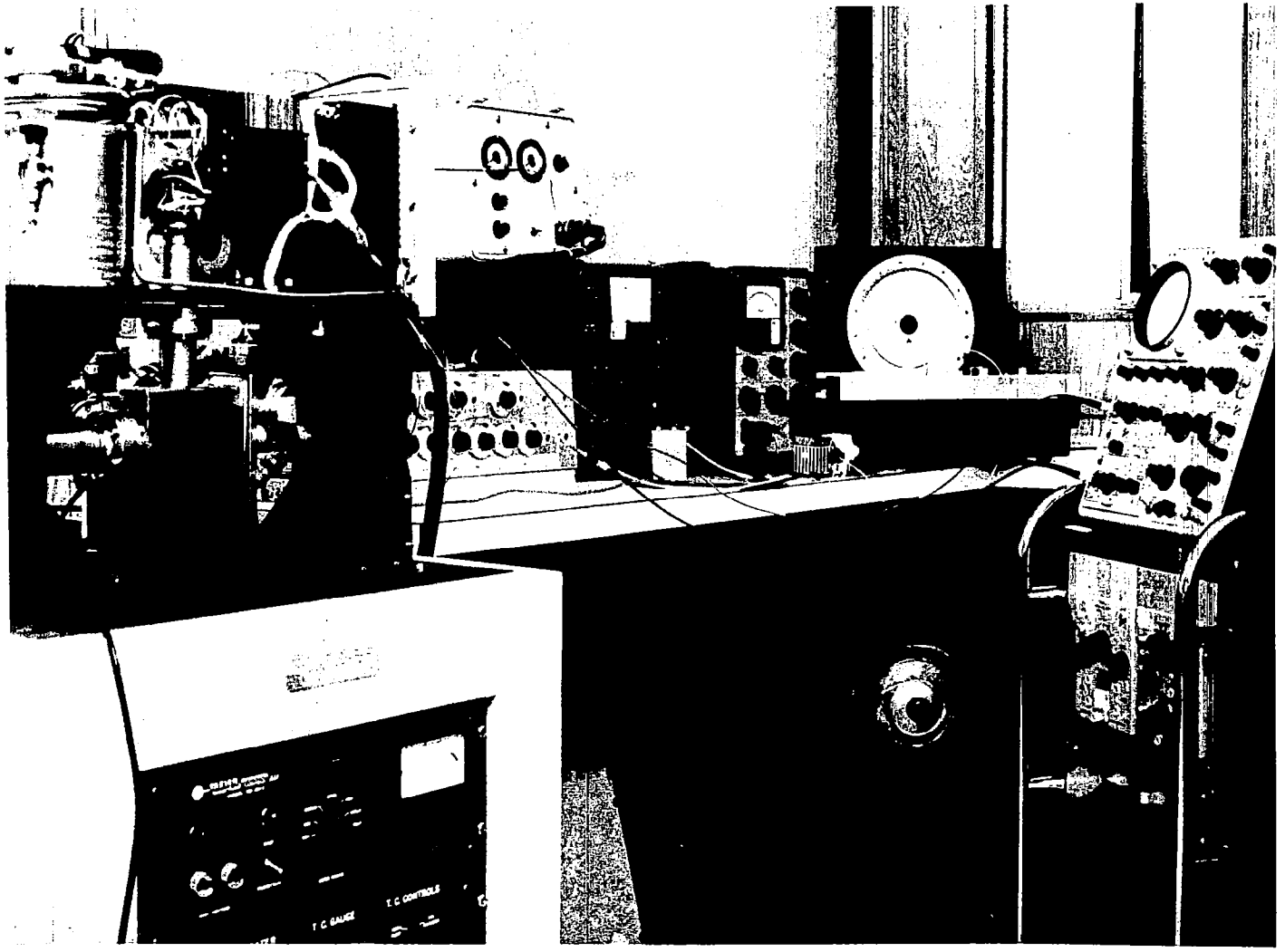

PHOTOGRAPH OF LABORATORY TESTING AREA

FIG. EIGHT

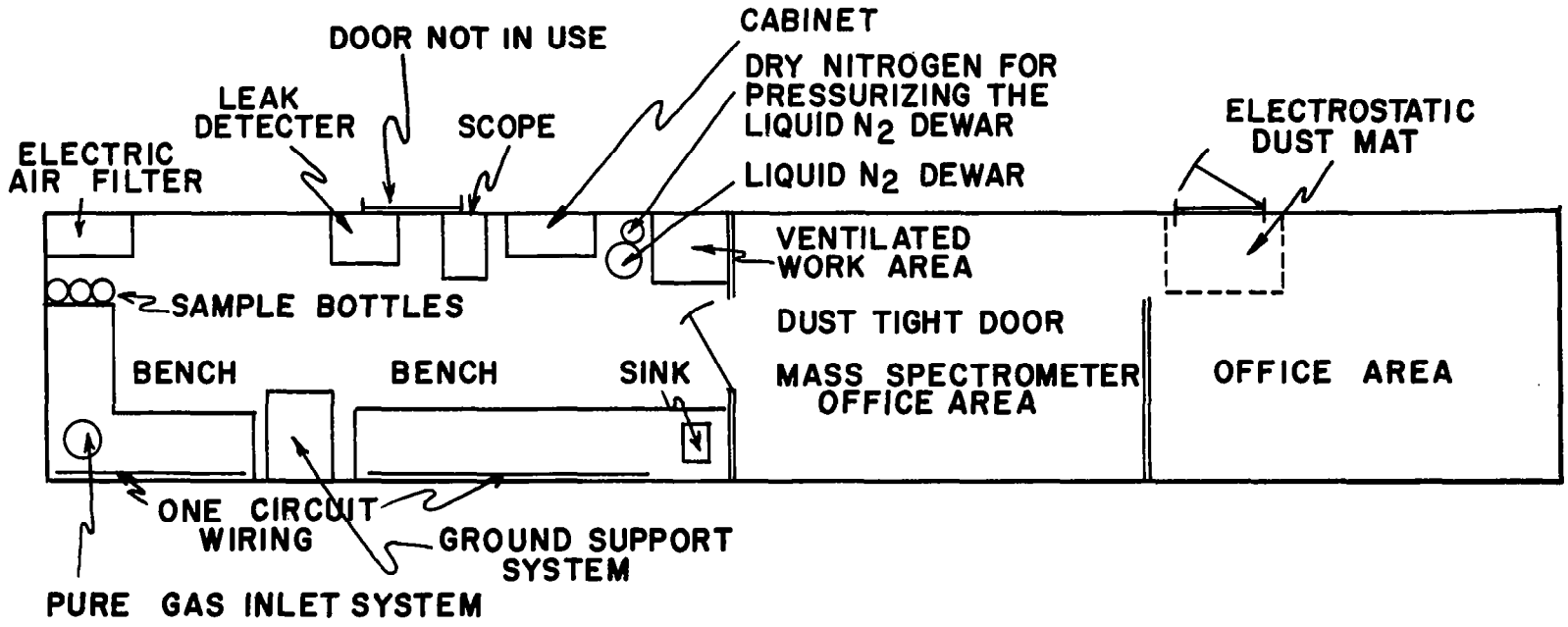

LABORATORY LAYOUT

FIG. NINE

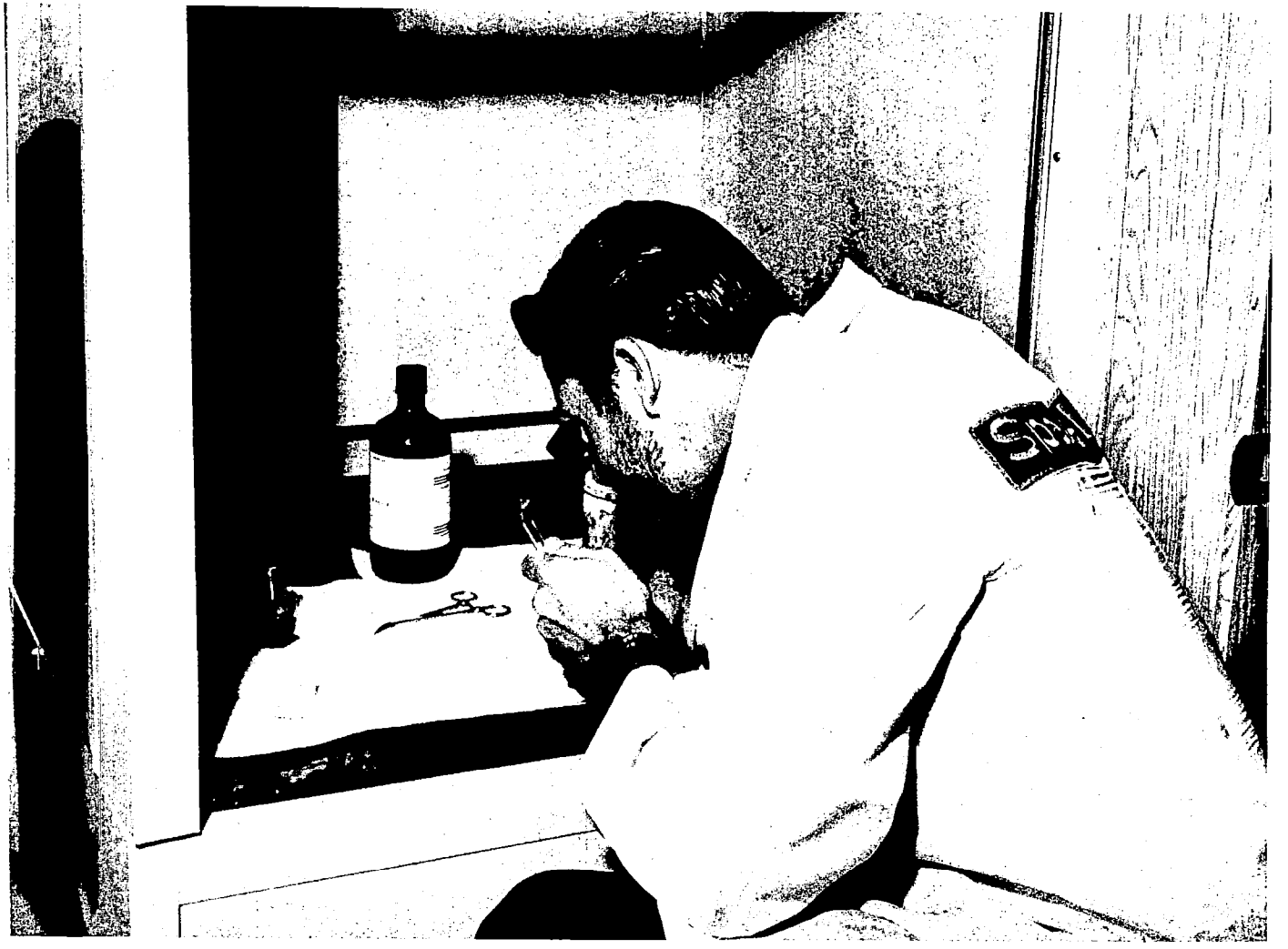

PHOTOGRAPH OF LABORATORY VENTED WORK AREA

FIG. TEN

Other pieces of lab equipment which fall in the above category are: an Ionization Gage (this is currently being used as an integral part of the Gold Leak Test System), an accurate 0 - 800 torr Absolute Pressure Gage to monitor the sample pressure, an accurate 0 - 20 torr Absolute Pressure Gage to monitor the Gold Leak input pressure on both the mass spectrometer and the Gold Leak Test System, appropriate Pressure Regulators for the sample gases used, the Sample Bottles themselves, a 50 liter Dewar for storage of liquid nitrogen, a large volume for introducing the sample at constant pressure and Forepumps for forepumping the inlet system and leak detector. In addition to the above are all the elbows, tees, flanges, tubing, fittings, etc. which are always required in working with vacuum systems.

In the first few months of work on the mass spectrometer, considerable difficulty was experienced with plugged or partially plugged Gold Leaks. Although a method was devised of checking the conductance of the leak in the mass spectrometer itself, half a day or more was required each time the Gold Leak was removed, cleaned and rechecked due to the time involved in venting and pumping down the mass spectrometer vacuum system. As the Gold Leaks often required several cleanings before they were unplugged, days were sometimes lost in obtaining a good Gold Leak. To solve this problem, the Gold Leak Test System was designed and fabricated. This system (which utilizes the vacuum pumps of the ground support equipment) provides a means of checking the conductance of a Gold Leak in less than an hour without venting the mass spectrometer vacuum system.

4.3 Laboratory Electronic Test Equipment

In addition to the more common types of electronic test equipment found in every electronic lab such as Multimeters, Oscilloscopes, Regulated Transistor Power Supplies, etc., there are a number of items of electronic test equipment which are particularly important in testing a mass spectrometer of this type. A list of such items which were used constantly during the testing is given: a Differential Voltmeter for measuring the high impedance electrode potentials to within an accuracy of .1 percent, a Pico-Amp Meter to measure the ion current into the electric sector, a Potentiometer Board to provide a means of changing the electrode potentials over wide voltage ranges during testing and experimentation, a Meter Panel to provide constant monitoring of various currents in the ion source, a 0 - 300 Volt Power Supply for ion beam energy measurements, an X-Y Recorder for observing the outputs as a function of the high voltage, a Gauss Meter for testing of the analyzer and ion pump magnets and a Standard Magnet for calibration of the gauss meter.

4.4 Other Equipment

In addition to the categories of equipment listed above, there is other equipment which was used and which was essential to the testing program. A small Spot Welder was used many times in changing filaments, moving collector slits and generally in working on the intricate mechanical parts of the mass spectrometer. A Water Welder was available for repairing the capillary lines. A Travelling Microscope was used several times in making small measurements. For example, the slit distances should be accurate in some cases to within .001 inch measured over a

distance of 3 inches. A small Temperature Chamber was borrowed on numerous occasions over the testing period. A larger chamber was required in temperature and altitude testing the overall instrument. A sonic cleaner was used on several occasions in cleaning small parts.

4.5 Special Supplies

Among other special items in the lab, good use was made of the following reference books: Experimental Nuclear Physics Vol. I, E. Segre; Mass Spectrometry, H. E. Duckworth; Mass Spectrometry, McDowell; High Vacuum Engineering, Alfred E. Barrington; Gas Data Book, Matheson Company; Catalog of Research Gases, Matheson Company. Due to the high degree of cleanliness required of the components located in the high vacuum sections of the instrument, several different cleaning agents were used. Distilled water, hand soap and Benzene and Ether of the purest grades were used frequently. Hydrofloric Acid and Baking Soda were used in cleaning the Gold Leaks. Operation and maintenance of the vacuum system as well as leak testing requires several special items such as low vapor pressure Duct Seal, Vacuum Grease, Spare Gaskets, Duo Seal Pump Oil for the forepumps, Zeolite for the sorption pumps, Molecular Sieve for the foreline trap and a Thermos bottle for filling the sorption pump with liquid nitrogen.

5. EVALUATION OF THE VACUUM SYSTEM

5.1 Function of the Vacuum System

The function of the mass spectrometer vacuum system is simply to provide an Ion Source pressure which is a representative sample of the gas to be analyzed. This Ion Source pressure must be: a) proportional to the input pressure, b) sufficiently high to provide adequate mass spectrometer sensitivity, c) sufficiently low to assure linear ionization of the sample, d) quickly responsive to changes in input pressure and e) unaffected by small changes in the pumping speed of either the Sorption Pump or Ion Pump.

5.2 Description of the Vacuum System

The Vacuum System is shown schematically in Figure 11. The gas to be monitored is selected from one of a possible four sources by opening the desired Inlet Valve. The sample gas selected flows down a capillary line to the Inlet Manifold. At this point, the pressure has been reduced by a factor of approximately one hundred from the inlet pressure. The main body of sample gas passes on through the Inlet Manifold, on through the orifice and is essentially consumed in the Sorption Pump by a combination of absorption and adsorption processes known known as sorption.[1]

A minute amount of the gas flowing through the capillary line is drawn into the Ion Source through a small hole (.3 mil dia.) in a gold foil. The assembly containing this gold foil is generally referred to as the Gold Leak. The amount of throughput (analogous to electrical current) flowing through the Gold Leak is proportional to the pressure difference across the leak and the conductance of the leak itself.[2] Since the pressure in the Inlet Manifold is several orders of magnitude larger than the pressure in the Ion Source, the throughput flowing through the Gold Leak is essentially proportional to the Inlet Manifold pressure and the conductance of the Gold Leak.

The Gold Leak throughput flows through the Ion Source, through the aperatures in the Source which comprise the source conductance, through the Analyzer to the Ion Pump. For a given throughput, the pump pressure is inversely proportional to the speed of the pump, or P_p equal Q/S where Q is the throughput in torr-liters per second, P_p is the pump pressure in torr and S is the speed of the pump in liters per second.[3] As the pressure drop in the analyzer section is negligible, the pressure drop across the source conductance is equal to the source pressure,

---

[1] Alfred E. Barrington, High Vacuum Engineering, (New Jersey: Prentice-Hall, Inc., 1963), p. 125

[2] ↑Ibid. p. 48

[3] ↑Ibid. p. 49

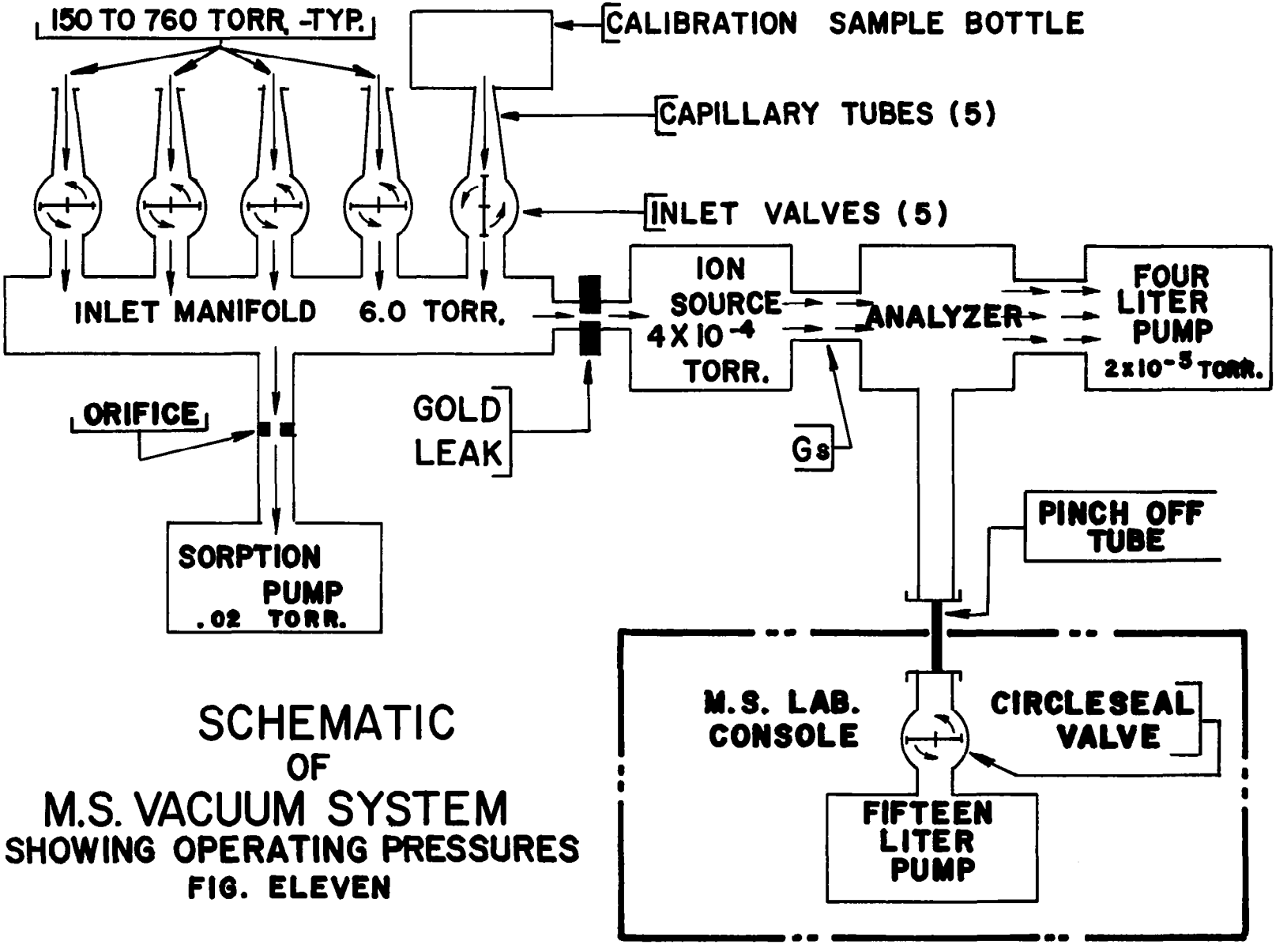

SCHEMATIC OF M.S. VACUUM SYSTEM SHOWING OPERATING PRESSURES

FIG. ELEVEN

P_s, minus the pump pressure, P_p. The equation $Q = (P_s - P_p)\ G_s$ can then be written. Substituting the expression Q/S for P_p and solving for P_s, the equation $P_s = Q(1/G_s + 1/S)$ is derived for the source pressure.

The equation derived in the preceeding paragraph is only valid in the case of the clean vacuum system. A more precise equation takes into account the outgassing from the walls of the vacuum system[4] and from the ion pump itself. To derive the more precise equation, the notation Q_s is used for the sample throughput flowing through the Gold Leak, and the notation Q_c is used for the contamination throughput which results from outgassing and small vacuum leaks. The more exact expression for pump pressure is then $P_p = Q_s/S + Q_c/S$. When this expression is substituted for P_p, the more precise equation, $P_s = Q_s\ (1/G_s + 1/S) + Q_c/S$, is derived.

In order to achieve good instrument stability, it is necessary that the source pressure remain constant with constant sample throughput. Since $1/G_s$ is determined by mechanical considerations such as aperature diameters etc., it is not difficult to maintain this quantity constant. The quantities $1/S$ and Q_c/S, however are a function of the condition of the ion pump, the cleanliness of the vacuum system, the sample throughput, the voltage on the ion pump and small vacuum leaks. For this reason, good mass spectrometer design dictates that the quantity $1/G_s$ be large compared to the quantity $1/S$ and the quantity Q_s/G_s be large with respect to the quantity Q_c/S. Under conditions of a clean vacuum system where Q_c is insignificant and the ion pump is operating at its rated speed of four liters per second, the quantity $1/G_s$ is 34 times as large as the quantity $1/S$ and the quantity Q_s/G_s meets the condition of being much larger than Q_c/S.

5.3 Four Liter Pump Evaluation

5.3.1 Objective

The objective of the following series of experiments was to evaluate the performance of the Four Liter Ion Pump.

5. 3. 2 Conclusions

It was concluded that the Four Liter Ion Pump does not perform to specifications. The pump speed under ideal conditions of voltage and pressure was found to vary between 1.9 liters/sec. and 3.0 liters/sec. Under the less ideal but more

[4] The outgassing from the walls of the ionization region itself is ignored in this analysis since the surface area of this region is small compared to the total surface area inside the vacuum system. An equation taking this throughput into consideration is only slightly more involved.

relevant conditions of lower voltage and pressure, the pump performance is even more inadequate. The combination of Ion Pump and Ion Pump Power Supply was found to be completely inoperable for throughputs of twice the design value. Throughputs of this value and greater are often experienced in operation due to outgassing and the use of oversized gold leaks. The disadvantage of these low pump speeds is cogently demonstrated in the section on Source Stability.

5.3.3 Equipment

Multimeter	Simpson Model 269
Front Panel Meter	Varian Console

5.3.4 Procedure

1. The Four Liter Ion Pump was reinstalled in the instrument after being reconditioned by the manufacturer.

2. Upon observing that the background pressure in the vacuum system was exceedingly high, the pump was heated at 470°C for several hours in the off condition. The fifteen liter ground support pump was pumping on the system at this time. The pump magnet had to be removed in this operation.

3. After cooling of the vacuum system, the Four Liter Pump Magnet was replaced, and the pump was activated using the flight Ion Pump Power Supply.

5. After the 15 liter and 4 liter pumps had both reached a stable pressure, the pump currents were measured and recorded. The purpose of these measurements was to establish typical background pressures.

5. The pumping speed of the 4 liter pump under the above conditions was noted by observing the change in the 15 liter pump current as the 4 liter pump was switched off.

6. In order to observe the performance of the pumps under operating conditions, a capillary tube was connected to the system and the appropriate inlet valve actuated. After one minute of operation with the valve open, the Gold Leak plugged. Several working days were required to correct this condition. This work is described in the section on Gold Leak cleaning procedures.

7. With the Gold Leak once again operating, the inlet valve was opened with only the 4 liter pump pumping on the system.

8. As the previous step indicated that the pumping speed of the 4 liter pump was inadequate, the pumping speed was checked under background conditions using the method outlined in the Results. This measurement was performed using the original flight pump supply.

9. Since all indications pointed to faulty ion pump operation, the four liter

pump was connected to the 15 liter pump power supply to assure sufficient pump voltage and power.

10. The pump speed was measured with the inlet valve open using the heavier supply. The method of measurement was again that method outlined in the Results.

11. The pump was baked while operating at a temperature of approximately 100°C in an attempt to improve the performance.

12. After an additional 72 hours of operation, the speed was again checked.

13. A measurement was made of the throughput through the Gold Leak. The method used is outlined in the Results.

14. As all tests indicated the 4 liter ion pump was not to specifications, a check was made on the field strength of the pump magnet.

5.3.5 Results

After the 4 Liter Ion Pump was baked out and the vacuum system had reached a stable condition, the background pressure at the 4 liter pump was 24 microamps or 8×10^{-7} torr. The pressure at the 15 liter pump at this time was 12.5 microamps or 4.5×10^{-8} torr.

When the 4 liter pump was turned off, the pressure measured at the 15 liter pump dropped from 12.5 to 7.5 microamps or 2×10^{-8} torr. This indicated that the 4 Liter Ion Pump was outgassing more than it was pumping at these pressures. In other words, the 4 Liter Pump effectively has a negative pumping speed at these pressures.

In Step #7 of the Procedure, an attempt was made to measure the speed of the 4 Liter Ion Pump under operational conditions. This was to be done by observing the rise in 4 liter pump pressure when the Inlet Valve was opened. The 15 liter pump was valved out of the system during this experiment. When the Inlet Valve was opened, the pressure rose quickly to approximately 700 microamps and then slowly continued to rise. As the pump current rose, the unregulated pump voltage dropped accordingly. Since ion pump speed is a function of pump voltage, particularly below about 4 kv, the pump speed decreased with pump voltage. Thus, a runaway, snowballing condition existed. The conclusion to be drawn was that the 4 Liter Ion Pump, the Gold Leak used, the Capillary Tube and Power Supply were an unworkable combination. As the runaway condition prevented measurement of the pumping speed with the inlet valve open, the valve was closed and the pressure allowed to drop back to 44 microamps or 1.3×10^{-6} torr. Both the 4 liter and the 15 liter pump were pumping on the vacuum system at this time. When the valve to the 15 liter pump was closed, the pressure at the 4 liter pump rose to 74 microamps or approximately 2.2×10^{-6} torr. The overall conductance of the 15 liter pump line is calculated below:

$$\frac{1}{G_{15}} = \frac{1}{G_A} + \frac{1}{G_P} + \frac{1}{G_V} + \frac{1}{S_{15}}$$

where G_{15} = overall conductance of line to 15 liter pump.

G_A = conductance of the aperature.

G_p = conductance of the pinch-off tube.

G_v = conductance of the valve.

S_{15} = speed of the 15 liter pump.

d = dia. of pinch-off tube = $\frac{7}{16}$" = .427" = 1.11 cm

$r = \frac{d}{2}$ = .555 cm

$A = \pi r^2 = \pi(.555)^2 = .97$ cm^2

l = length of pinch-off tube = 6" = 15.2 cm

$G_A = 3.62\ A\sqrt{\frac{T}{M}}$ L/sec. [5]

where A is the area in square centimeters

T is the temperature in degrees Kelvin

M is the average mass number

so $G_A = (3.62)\ (.97)\sqrt[6]{\frac{298}{29}} = 11.25$ L/sec. for air at room temperature

$G_p = (3.81)\ \frac{d^3}{l}\sqrt{\frac{T}{M}}$ L/sec.

where d is the diameter in centimeters
l is the length in centimeters

so $G_p = (3.81)\ \frac{1.11}{15.2}\sqrt[3]{\frac{298}{29}} = 1.09$ L/sec. for air at room temperature

G_v = 40 L/sec. as given by the manufacturer.

S_{15} = 15 L/sec. as given by the manufacturer.

$$\frac{1}{15} = \frac{1}{11.25} + \frac{1}{1.09} + \frac{1}{40} + \frac{1}{15}$$

[5] Alfred E. Barrington, High Vacuum Engineering, (New Jersey: Prentice-Hall, Inc., 1963) p. 53

[6] † Ibid. p. 55

$$\frac{1}{G_{15}} = .0889 + .918 + .025 + .0667 = 1.0985$$

$$G_{15} = \frac{1}{1.0985} = .910 \text{ L/sec.}$$

Now $Q = \Delta PG$

where Q is the throughput which is a constant in this experiment and comprised of outgassing from the chamber.

$G_1 = S_4 + G_{15}$ where G_1 is the total conductance with both the 4 liter pump and 15 liter pump pumping on the system.

$G_2 = S_4$ is the conductance with only the 4 liter pump operating.

P_1 and P_2 are measured at the 4 liter pump. Pump pressure is proportional to pump current.

$$\frac{Q}{G_2} = P_2 = KI_2$$

$$\frac{Q}{G_1} = P_1 = KI_1$$

Dividing one equation by the other, $\frac{G_1}{G_2} = \frac{I_2}{I_1} = \frac{74}{44} = 1.68$

$$G_1 = 1.68\ G_2 = 1.68\ \ S_4 = S_4 + G_{15}$$

$$.68\ \ S_4 = G_{15} = .910$$

$$S_4 = \frac{.910}{.68} = 1.34 \text{ L/sec.}$$

The 4 liter pump has a speed of 1.3 L/sec. with a pump voltage of 4,800 volts at a pressure of approximately 2×10^{-6} torr.

The general expression for the 4 liter pump speed which is derived in the manner shown above is $S_4 = \frac{G_{15}}{\left(\frac{I_2}{I_1}\right) - 1}$

Step #10 of the Procedure was taken to compare the pump speed with its specified value at a higher pressure and voltage, the most favorable conditions at which the speed could be checked. The measurement was repeated several times, and the results were consistently about a value of 2.3 L/sec. The equation developed on the previous pages was used in making the measurement.

---

[7] † Ibid. p. 48

In step #11 of the Procedure, the pump speed measurement was repeated after the pump had been baked. Immediately after cooling, the pump speed was measured and found to be lower than before baking. After several hours, the speed of the pump was again measured and found to be 2.3 L/sec.

With the speed of the pump accurately known from the above, the throughput of the Gold Leak is easily measured using the equation $Q = PS$. P is determined from the pump pressure vs. current curve. The throughput measured before the Inlet Valve is opened results from outgassing and small vacuum leaks. Since in this experiment only the Gold Leak throughput was of interest, the initial pump pressure due to outgassing was subtracted from the final pump pressure measured with the Inlet Valve open. The equation used to calculate the Gold Leak throughput is therefore:

$$Q_s = S(P_{p2} - P_{p1})$$

When the measurement was made in step #13 of the Procedure P_{p2} was 740 microamps or 2.3×10^{-5} torr. P_{p1} was 40 microamps or $.1 \times 10^{-5}$ torr. Therefore, $(P_{p2} - P_{p1})$ was equal to 2.2×10^{-5} torr, and Q_s was equal to 50×10^{-6} torr-liters/sec. This is roughly a factor of two higher than the design value.

In step #14 of the Procedure, the maximum field strength of the ion pump magnet was measured and found to be 1,200 gauss. This value is in the range to be expected.

5.3.6 Discussion

The series of experiments described above points out two variances from the design values: the pump speed is lower than specified and the throughput is higher than specified. The effects of these two discrepancies are examined below.

The effect of a slower pump speed is to raise the pump pressure. This in turn decreases the pressure ratio between the Ion Source and pump. The noticeable effect of this is an increased dependence of the mass spectrometer sensitivity upon pump speed. For example, with the design pump speed, a one hundred percent decrease in the speed of the pump would cause only a three percent increase in mass spectrometer output. However, with half the design speed, a one hundred percent decrease in pump speed would cause a five and a half percent increase in mass spectrometer output, and with one third the design pump speed, a one hundred percent decrease in pump speed would cause an eight percent increase in mass spectrometer output. Thus a lower initial pumping speed causes the mass spectrometer output to be more directly a function of ion pump speed.

The effect of having twice the throughput called for in the original design is to double the source pressure. This in turn will double the instrument sensitivity. If the source pressure was increased by much more than double the design value, non-linear operation would result. If no further increase takes place, the existing source pressure is tolerable.

5.3.7 Sequel

Following the writing of the above report, the pump speed was measured period-

ically over a period of four months. During this period the pump was operated with the ground support 15 liter pump power supply which maintained the pump voltage above 7 KV at all times. The pump speed was measured at the more optimum pressures. Under these ideal conditions, pump speeds as low as 1.9 liters/sec. and as high as 3.0 liters/sec. were measured.

5.4 EVALUATION OF GOLD LEAK CLEANING PROCEDURES

5.4.1 Objective

To report on the various techniques and procedures which have proven useful in cleaning a plugged Gold Leak.

5.4.2 Conclusion

Gold Leaks of the dimensions used on this mass spectrometer will become plugged from time to time. This phenomenon will occur most frequently after disassembly of the vacuum system. Past experience in clearing the leaks has indicated that success will be achieved only about fifty percent of the time and then only after several attempts.

5.4.3 Equipment

Dry Nitrogen Bottle with Regulator

Flexible Hose

Low Residue Ether

Small Beaker

Distilled Water

Liquid Hand Soap

Hydrofluoric Acid Solution

Baking Soda

Traveling Microscope

20 Power Eye Glass

5.4.4 Procedure

1. The plugged leak was cleaned by bubbling dry nitrogen through the leak in a beaker of ether.

2. An attempt was made to measure the diameter of the leak hole using a high power traveling microscope.

3. The hole was visually inspected with the aid of a bright light and 20 power eye glass.

4. The leak was installed and tested on the mass spectrometer.

5. The mass spectrometer was again vented, and the leak removed.

6. Hydrofluoric acid was applied to each side of the leak and allowed to stand for several minutes before being neutralized with baking soda and washed with distilled water.

7. After the acid treatment, the leak was again cleaned by bubbling dry nitrogen through the leak in a beaker of ether.

8. The leak was again visually inspected using the 20 power eye glass.

9. The Gold Leak was reinstalled on the mass spectrometer and tested under operating conditions.

10. The used ether was evaporated in a small pan using an air hose in order to test for residue.

11. Half a beaker of unused distilled water was evaporated in a small beaker using the hot plate to test for residue.

12. Dry nitrogen was bubbled into a beaker of unused distilled water, and the water was tested for residue.

13. Dry nitrogen was bubbled into a beaker of unused ether, and the ether was tested for residue.

14. The dry nitrogen hose was cleaned with liquid hand soap and distilled water.

15. Dry nitrogen was again bubbled into a beaker of unused distilled water, and the water was tested for residue.

16. The mass spectrometer was again vented and the leak removed.

17. Hydrofluoric acid was again applied to the Gold Leak. The leak was cleaned with baking soda and distilled water after the acid treatment.

18. The leak was then cleaned with hand soap and distilled water. The leak was rinsed thoroughly with distilled water after this operation.

19. The leak was placed in a beaker of clean ether and sonically vibrated at different frequencies.

20. Dry nitrogen was again bubbled through the leak in a beaker of clean ether.

21. The Gold Leak was reinstalled in the mass spectrometer and tested.

5.4.5 Results

In step #2 of the Procedure, the attempt to measure the diameter of the hole was disappointing. A value of .4 mills was finally reached after some difficulty. The microscope used did not have facilities for lighting beneath the object. It is felt that this would have been of help. The main objection to the microscope was the absence of underneath lighting as the travel resolution was more than satisfactory for the dimensions being measured. It was concluded that microscope observation is an inefficient and unreliable method of determining the condition of the Gold Leak.

In step #3 of the Procedure, the hole was visually inspected with the 20 power eye glass, the bright light behind the hole could be readily seen shining through the leak. The leak appeared completely unblocked and round in shape. When the leak was reinstalled in the mass spectrometer, it was found to behave as it had before. The leak would open when several hundred millimeters of pressure were placed across it. When the pressure was reduced to an operating level, the leak would again plug.

In steps 6, 7 and 8 of the Procedure, the leak was cleaned with Hydrofluoric acid and ether and then inspected with the 20 power eye glass. When the leak was reinstalled in the mass spectrometer and tested, the results were the same as before. At this point, it was concluded that the leak was being plugged by a clear oily or lacquer type substance.

In step #10 of the Procedure, the used ether was evaporated in a small pan to check for residue. An oily residue was observed.

When the unused distilled water was evaporated in step #11 of the Procedure, it was found to leave no residue. However, after the dry nitrogen was bubbled into a beaker of distilled water, the distilled water did leave an oily residue upon evaporation.

After cleaning the dry nitrogen hose, bubbling dry nitrogen through a beaker of distilled water did not contaminate the water.

Upon completing the cleaning procedure outlined in steps 20 through 21, the Gold Leak operated properly at a leak of twice the original calibrated value.

5.4.6 Discussion

This report gives the history of a successful attempt at unplugging a Gold Leak. As mentioned in the Conclusion, success in unplugging a leak is achieved only fifty percent of the time.

The manufacturer suggested that a small deflector (which has been fabricated and which is in our possession) be added to the Gold Leak assembly. Should another leak plug up while the instrument is in the operational mode, this will be done. Recently, plugging of the Gold Leak has only occurred upon disassembly.

5.4.7 Sequel

Since the writing of the above report, another Gold Leak cleaning method has been tried and proven partially successful. Success in clearing a Gold Leak has been achieved in two out of three attempts simply by using the abrasive action of rotating a soft pencil eraser in the foil cup of the leak while applying a light pressure. The success in one instance was somewhat debatable as the conductance of the leak increased by a factor of three in the process. This method definitely calls for a properly shaped pencil and a steady hand.

5.5 THEORY AND OPERATION OF THE GOLD LEAK TEST SYSTEM

5.5.1 Objectives

The objectives of this section are to describe the theory and the operation of the Gold Leak Test System and to measure the conductances of three spare Gold Leak assemblies.

5.5.2 Conclusion

It was concluded that none of the three Gold Leaks tested were plugged and that the conductances of the three leaks ranged from 4.5×10^{-6} to 8.4×10^{-6} liters per second.

5.5.3 Theory

The gold leak throughput $Q = (P_1 - P_2)\ G_{GL}$. (See Figure 12). P_2 is insignificant compared to P_1 so $Q \simeq P_1\ G_{GL}$.

Q also = $(P_2 - P_3)\ G_1$ where G_1 is a known conductance.

Therefore $Q = P_1\ G_{GL} = (P_2 - P_3)\ G_1$ or $G_{GL} = \dfrac{(P_2 - P_3)\ G_1}{P_1}$

P_1 is adjusted to 5 mm as read on the 20 mm gage

P_2 is read from the ion gage

P_3 is read from the 15 liter pump current.

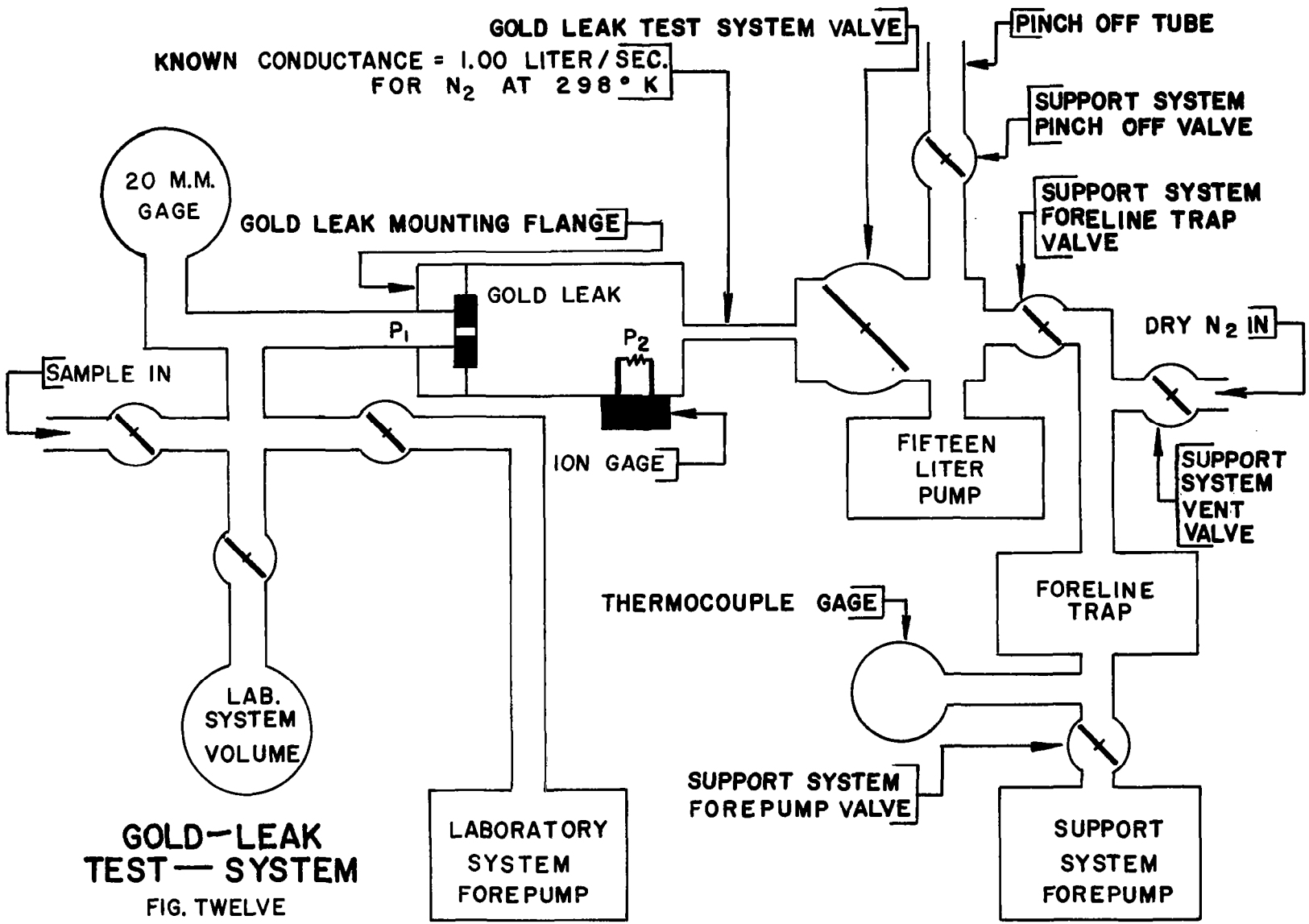

GOLD-LEAK TEST — SYSTEM

FIG. TWELVE

G_1 is calculated from the physical dimensions.

G_{GL} can therefore by calculated.

5.5.4 Equipment

Gold Leak Test System	-----	-----
Ion Gage Control Unit	Varian 971-0003	1009
Ion Gage	Varian UHV-24	-----

5.5.5 Procedure

1. A Roman numeral was engraved on each of the Gold Leaks.

2. The support system pinch-off valve was closed.

3. The support system forepump valve was closed.

4. The 15 liter pump was turned off and allowed to cool. The 4 liter pump in the mass spectrometer vacuum system remained in operation.

5. The support system foreline trap valve was opened.

6. The Gold Leak Test System valve was opened.

7. The line to the dry nitrogen bottle was purged and connected to the support system vent valve.

8. The vent valve was opened, and the 15 liter pump and Gold Leak Test System were pressurized to two p. s. i. with dry nitrogen.

9. The vent valve was closed.

10. The blank flange was removed, and the special Gold Leak mounting flange installed with the Gold Leak to be tested. At this time, the special flange was connected to the 20 mm gage and laboratory inlet system.

11. The support system forepump valve was opened, and the 15 liter pump and Gold Leak Test System were roughed down.

12. When the forepump pressure was down to 100 microns, the 20 mm gage and high side of the Gold Leak were roughed down using the laboratory inlet system forepump.

13. When the support system forepump pressure dropped to 10 microns, the 15 liter pump was turned on.

14. The ground support system foreline trap valve was closed.

15. When the 15 liter pump pressure dropped to approximately 3×10^{-7} torr, a pressure of 5 torr was applied to the high side of the Gold Leak through the laboratory inlet system volume. Dry nitrogen was used.

16. After adjusting the ion gage zero and emission current, the gage reading was recorded along with the 15 liter pump current.

17. The conductance of the Gold Leak was calculated using the known conductance of the Test System, the known input pressure of 5 mm, the ion gage pressure and the 15 liter pump pressure.

18. Steps 1 through 16 were repeated for three Gold Leaks.

5.5.6 Results

The results are given in Table III.

TABLE III

Results of Gold Leak Testing

Gold Leak No.	15 liter Pump Current	P_3 in torr	P_2 in torr	$P_2 - P_1$ in torr	Q in torr liter/sec.	G_{GL} in liters/sec.
II	800 microamps	2.5×10^{-6}	36.2×10^{-6}	33.6×10^{-6}	33.6×10^{-6}	6.74×10^{-6}
III	750 microamps	2.3×10^{-6}	44.0×10^{-6}	41.7×10^{-6}	41.7×10^{-6}	8.38×10^{-6}
IV	600 microamps	2.0×10^{-6}	29.0×10^{-6}	27.0×10^{-6}	27.0×10^{-6}	5.40×10^{-6}

5.5.7 Discussion

The Gold Leak Test System reduced the Gold Leak evaluation time to less than one hour. More than four hours were required to test a Gold Leak on the mass spectrometer. The Gold Leak Test System also eliminated the need for venting the mass spectrometer vacuum system in order to test a Gold Leak.

5.6 CAPILLARY LINE EVALUATION

5.6.1 Objective

The objectives of the following series of experiments are to determine if the six capillary lines are vacuum tight, to repair any that are not, to measure the various input pressures experienced with the different capillary lines, to determine if the operation of the capillary lines is a function of temperature and to record the input - output pressure characteristic of a typical capillary.

5.6.2 Conclusion

It was concluded that each of the six capillary lines had at least one vacuum leak. It was determined that one of the six lines was beyond repair. The remaining five lines were repaired by a water welding process. It was concluded that one of the five leak tight lines was partially obstructed. The four unobstructed lines have a Gold Leak input pressure between 6.11 and 6.41 torr. It was noted that the Gold Leak input pressure is a function of capillary temperature. The input - output pressure characteristic of the capillary lines was found to be non-linear at the lower pressures.

5.6.3 Equipment

Helium Leak Detector	CEC Model 24-120B	8034
20 mm pressure gage	Wallace & Tiernan FA 160	KK04-225
800 mm pressure gage	Wallace & Tiernan FA 129	JJ15468

5.6.4 Procedure

1. The end of each capillary was sealed with masking tape and duct seal. The capillary line was then pumped down and leak checked on the CEC leak detector.

2. The leaks detected in Step #1 of the Procedure were repaired by silver soldering with a water welder.

3. The capillary lines were again checked on the leak detector.

4. Those lines which still leaked were again soldered. It was necessary to repeat this process several times before five of the six lines were leak tight. The sixth line was considered irreparable.

5. A number was engraved on each line.

6. The 20 mm pressure gage was connected to a capillary input valve and pumped down using the laboratory inlet system forepump. See Figure 13.

7. The valve between the 20 mm gage line and the inlet system forepump was closed. It was noted that the 20 mm gage pressure did not rise upon closing the valve thus assuring a leak tight system.

8. The capillary line under test was connected to a second input valve.

9. Normal flow was established in the capillary line by opening the inlet valve. The mass spectrometer sorption pump was in operation at this time.

10. The inlet valve connected to the 20 mm gage line was opened.

11. After several minutes an equilibrium pressure was reached and the gage reading was recorded.

12. The capillary inlet valve was closed and the line removed.

13. Steps 8 through 12 were repeated for the remaining capillaries.

14. After obtaining a reading on the last capillary, the line was warmed with a heat gun while the gage pressure was observed.

15. The inlet end of the capillary was connected to the laboratory inlet system and pumped down.

16. The inlet pressure was increased in increments of 20 torr from 0 to 200 torr and in increments of 50 torr from 200 to 700 torr. CO_2 was used. The inlet manifold pressure was measured and recorded at each input pressure.

5.6.5 Results

1. In steps #1 through #4 of the Procedure, leaks in five of the six capillaries were repaired.

2. The results of Procedure steps #8 through #13 are given in Table IV. One capillary line was noted to be partially obstructed.

3. The result of heating the capillary in step #14 of the Procedure was to drop the manifold input pressure from 6.41 to 6.10 torr. The pressure returned to its original value as the line cooled.

4. The results of steps 15 and 16 of the Procedure are given in Table V and Figure 14.

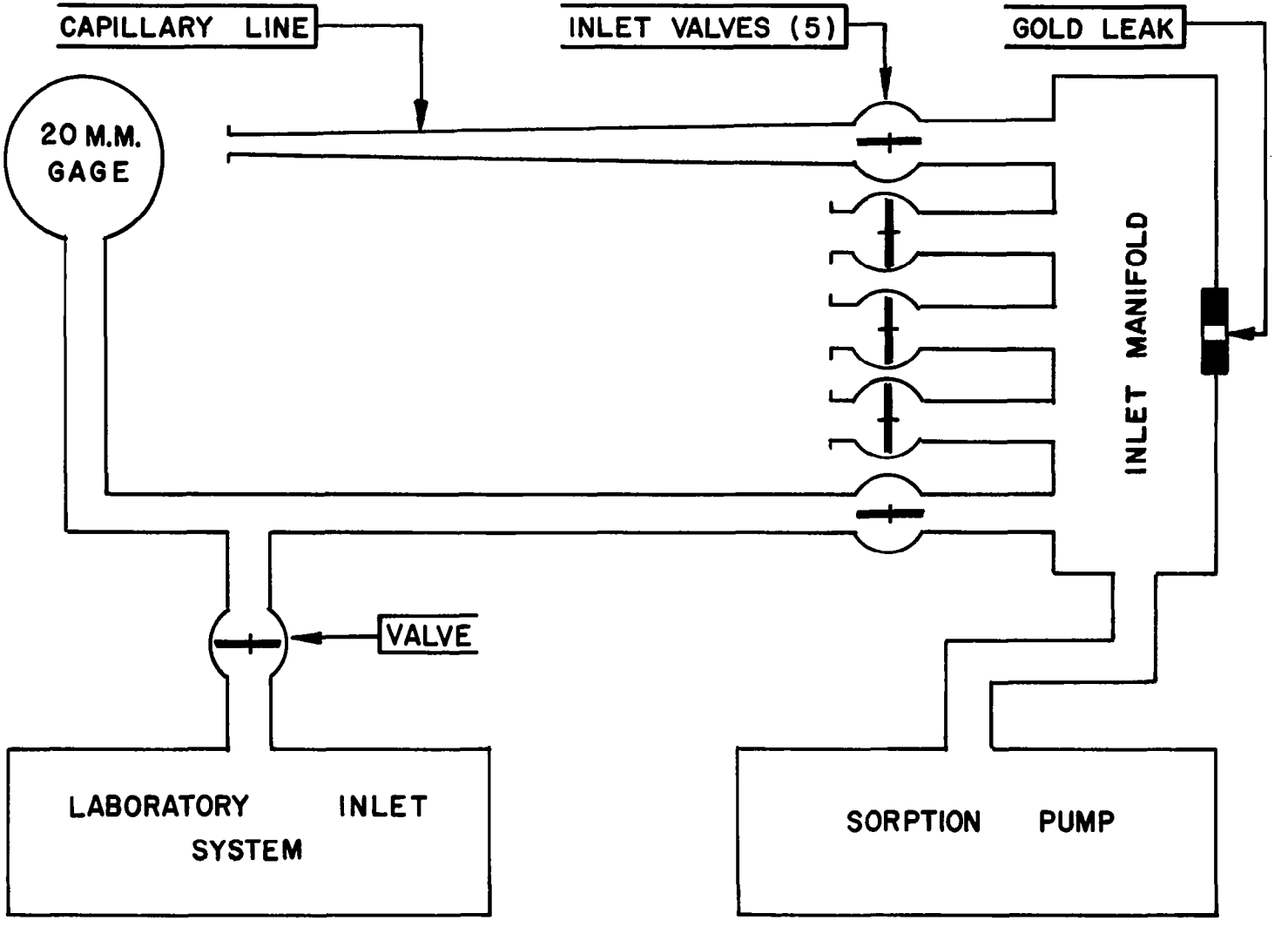

GOLD LEAK INPUT PRESSURE MEASUREMENT

FIG. THIRTEEN

TABLE IV

Gold Leak Input Pressure with Different Capillaries

Capillary No.	Inlet Manifold Pressure In Torr	Correction Factor
1 (Sample bottle line)	6.41	----
2	6.31	1.015
3	3.15	2.035
4	6.11	1.048
5	6.12	1.046

TABLE V

Capillary Line Pressure Characteristics

P_{in} in Torr	Inlet Manifold Pressure in Torr
0	0.00
20	0.00
40	0.00
60	0.30
80	0.50
100	0.65
120	0.82
140	1.0
160	1.20
180	1.4
200	1.62

TABLE V continued

P_{in} in Torr	Inlet Manifold Pressure In Torr
250	2.00
300	2.60
350	3.12
400	3.68
500	4.65
600	5.72
700	6.75

5.7 SORPTION PUMP EVALUATION

5.7.1 Objective

The objective of this section is to determine the unattended operating time of the Sorption pump.

5.7.2 Conclusion

Under laboratory conditions, the Sorption pump is capable of maintaining the inlet manifold pressure within plus or minus one percent for a period of nine hours.

5.7.3 Equipment

20 mm pressure gage	Wallace & Tiernan	FA160	KK04225

5.7.4 Procedure

1. The 20 mm gage was connected to one of the inlet valves and to the blending system forepump. See Figure 15.

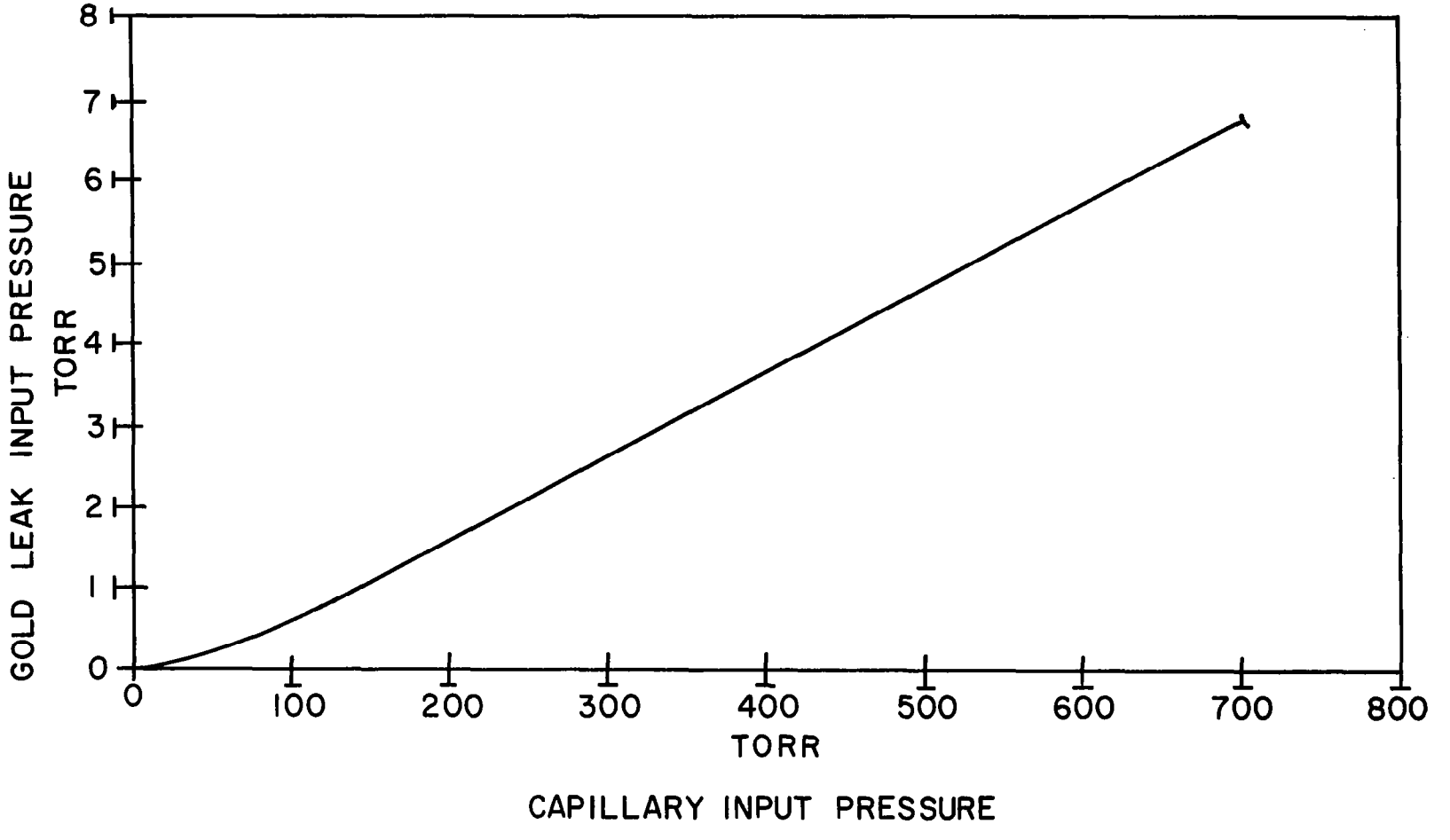

CAPILLARY LINE PRESSURE CHARACTERISTICS

FIG. FOURTEEN

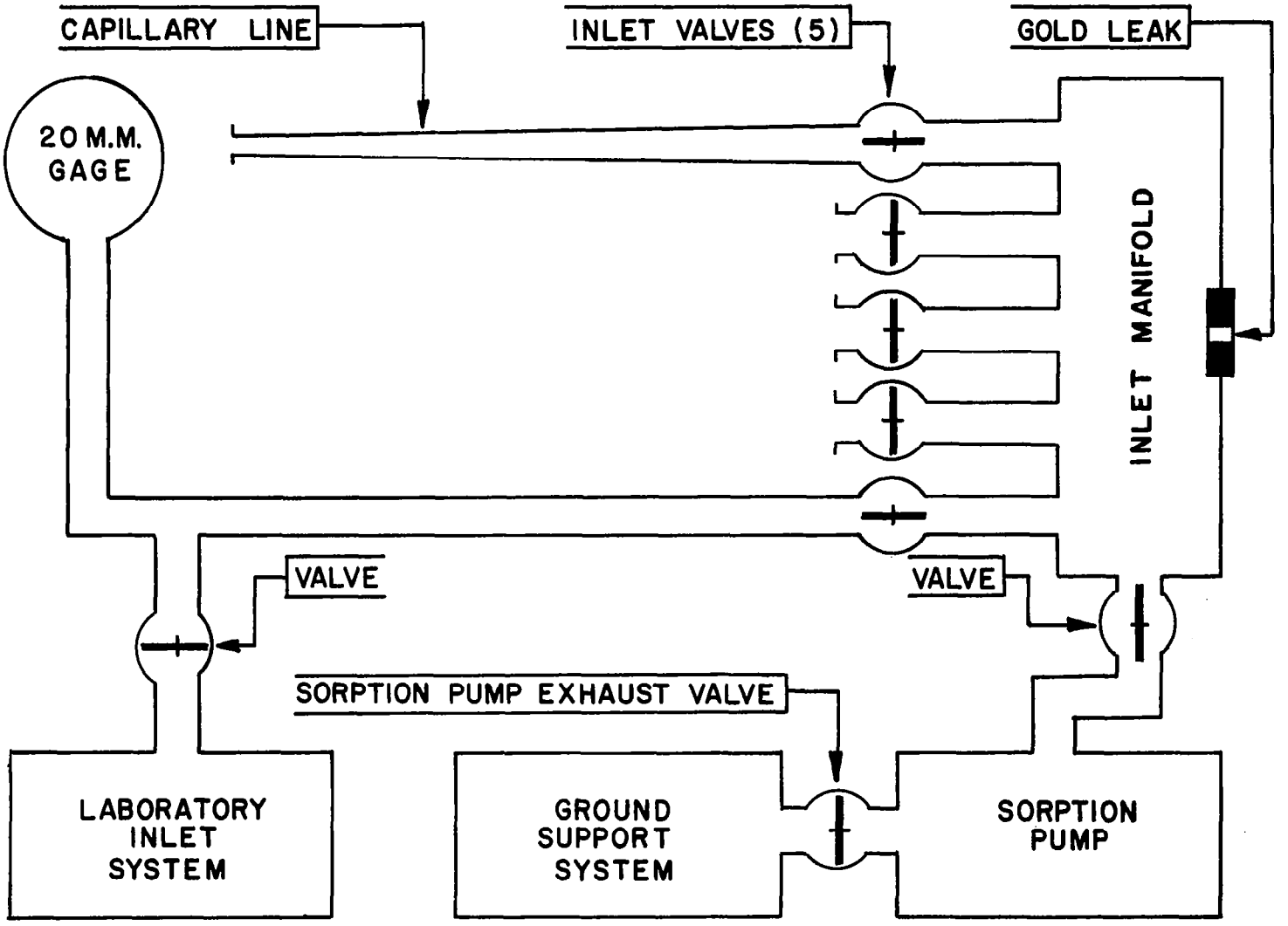

SORPTION PUMP TEST SETUP

FIG. FIFTEEN

2. A capillary line was connected to a second inlet valve.

3. The Sorption pump exhaust valve on the ground support system was closed. This isolated the Sorption pump from the ground support system. At the time that this valve was closed, the ground support system forepump had been pumping on the Sorption pump for a period of 15 hours. The inlet manifold to Sorption pump isolation valve was open during this period and remained open during the remainder of the experiment.

4. The Sorption pump was filled with liquid nitrogen.

5. The 20 mm pressure gage was pumped down with the laboratory inlet system. The valve to the inlet system was then closed.

6. Thirty minutes after the pump was filled with liquid nitrogen, the inlet valve to the 20 mm gage and the inlet valve to the capillary line was opened.

7. The pressure observed on the 20 mm gage was read and recorded. The time was noted beside the reading.

8. Manifold pressure readings were recorded every half hour until the pressure had risen to ten percent above its initial valve.

5.7.5 Results

The results of the experiment are given in Table VI.

TABLE VI

Manifold Inlet Pressure vs. Operating Time of Sorption Pump

Time in Operation in Hours	Inlet Manifold Pressure in Torr	Pressure Change in Torr	Pressure Change in Percent
0.0	6.40	.00	0.00
0.5	6.40	.00	0.00
1.0	6.40	.00	0.00
1.5	6.40	.00	0.00
2.0	6.40	.00	0.00
2.5	6.40	.00	0.00
3.0	6.40	.00	0.00

TABLE VI continued

Time in Operation in Hours	Inlet Manifold Pressure in Torr	Pressure Change in Torr	Pressure Change in Percent
3.5	6.40	.00	0.00
4.0	6.40	.00	0.00
4.5	6.41	+.01	+0.16
5.0	6.40	.00	0.00
5.5	6.40	.00	0.00
6.0	6.42	+.02	+0.31
6.5	6.46	+.06	+0.94
7.0	6.42	+.02	+0.31
7.5	6.46	+.06	+0.94
8.0	6.42	+.02	+0.31
8.5	6.50	+.10	+1.56
9.0	6.53	+.13	+2.04
9.5	7.30	+.90	+14.08

5.8 CALIBRATION SAMPLE BOTTLE EVALUATION

5.8.1 Objective

The objective of this section is to determine the variation in output pressure of the Calibration Sample Bottle as a function of time for different output pressure settings and different charging pressures.

5.8.2 Conclusion

It was concluded that the Calibration Sample Bottle exhibited better output pressure regulation with a charging pressure of 40 p. s. i. than with the recommended 50 p. s. i. The output pressure was found to have better regulation when adjusted to 250 torr than when adjusted to 500 torr. With a charging pressure of 40 p. s. i. and an output pressure of 270 torr, pressure variations remain within plus or minus half of one percent for a period of 30 minutes.

5.8.3 Equipment

Capillary Tube	-----	-----
Nitrogen Regulator and gage	Matheson Co.	_____
0 - 800 mm gage	Wallace & Tiernan FA129	JJ15468

5.8.4 Procedure

1. A capillary tube and the 0 - 800 mm gage were connected to the output port of the Calibration Sample Bottle.

2. With the high side of the bottle connected to the nitrogen regulator and the regulator adjusted to 50 p. s. i., the output pressure of the bottle as read on the 0 - 800 mm gage was adjusted to approximately 5 p. s. i.

3. The high side of the bottle was isolated from the nitrogen regulator by closing a valve and thus trapping a pressure of 50 p. s. i. on the high side of the bottle.

4. Data was taken to plot the output pressure as a function of time from the closing of the isolation valve.

5. Steps 2, 3 and 4 were repeated for an output pressure of approximately 10 p. s. i. and a charging pressure of 50 p. s. i.

6. Steps 2, 3 and 4 were repeated for an output pressure of approximately 10 p. s. i. and a charging pressure of 40 p. s. i.

7. Steps 2, 3 and 4 were repeated for an output pressure of approximately 5 p. s. i. and a charging pressure of 40 p. s. i.

5.8.5 Results

The results are given in Tables VII through X and in Figure 16.

TABLE VII

Calibration Sample Bottle Output Pressure
vs. Operating Time (50 p. s. i. input, 5 p. s. i. output)

Output Pressure in Torr	Percent of Initial Pressure	Elapsed Time in Min.
269.0	100.0	0
268.5	99.9	5

TABLE VII continued

Output Pressure in Torr	Percent of Initial Pressure	Elapsed Time in Min.
266.5	99.2	10
265.1	98.5	15
264.0	98.2	20
264.4	98.4	25
263.9	98.1	30
264.5	98.4	35
262.4	97.6	40

TABLE VIII

Calibration Sample Bottle Output Pressure
vs. Operating Time (50 p. s. i. input, 10 p. s. i. output)

Output Pressure in Torr	Percent of Initial Pressure	Elapsed Time in Min.
501.2	100.0	0
505.9	100.9	5
508.1	101.1	10
510.2	101.5	15
511.4	102.0	20
499.8	99.6	25
490.0	97.6	30
477.0	95.1	35

TABLE IX

Calibration Sample Bottle Output Pressure
vs. Operating Time (40 p. s. i. input, 5 p. s. i. output)

Output Pressure in Torr	Percent of Initial Pressure	Elapsed Time in Min.
271.0	100.0	0
272.0	100.4	2
272.2	100.4	4
272.2	100.4	6
272.1	100.4	8
271.9	100.3	10
271.0	100.3	12
271.9	100.3	14
272.0	100.4	16
272.2	100.4	18
272.5	100.6	20
272.7	100.6	22
273.0	100.8	24
273.3	100.9	26
273.4	100.9	28
273.3	100.9	30

TABLE X

Calibration Sample Bottle Output Pressure
vs. Operating Time (40 p. s. i. input, 5 p. s. i. output)

Output Pressure in Torr	Percent of Initial Pressure	Elapsed Time in Min.
502.5	100.0	0
503.0	100.1	2
504.0	100.3	4
505.3	100.6	6
505.7	100.6	8
506.8	100.9	10
507.5	101.0	12
508.7	101.2	14
509.5	101.4	16
510.1	101.5	18
510.6	101.6	20
508.4	101.2	22
503.4	100.2	24
498.3	99.2	26
493.5	98.2	28
488.6	97.2	30

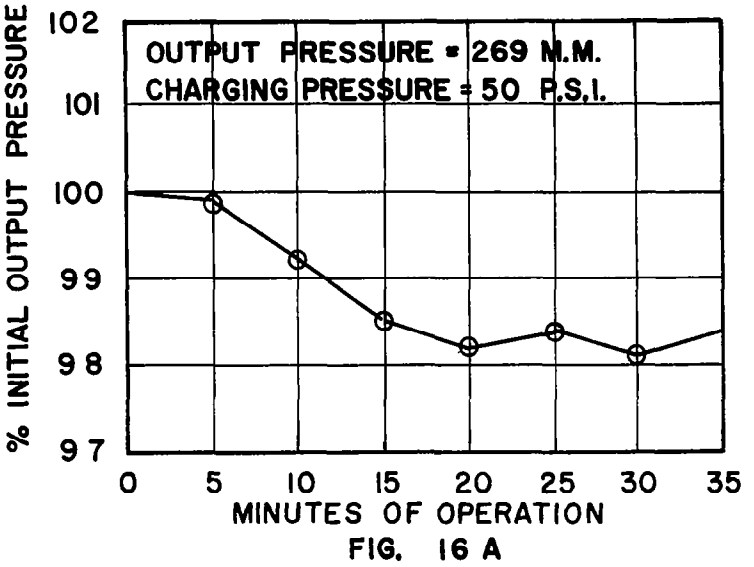

FIG. 16 A

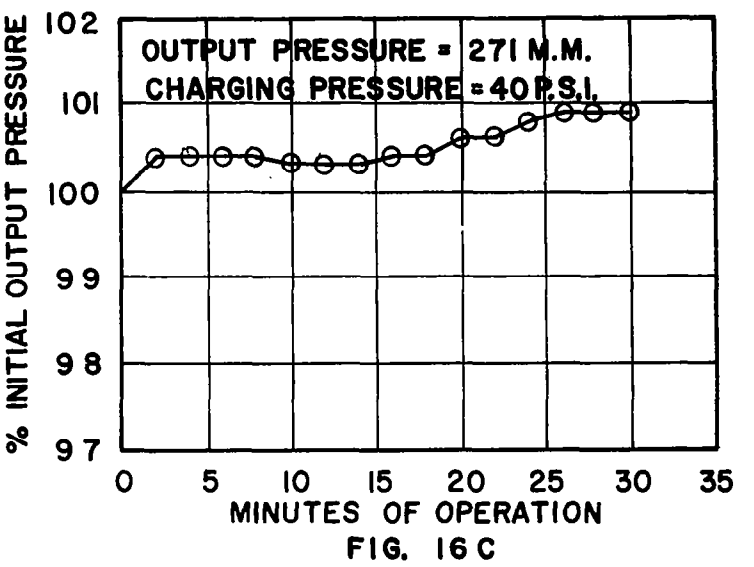

FIG. 16 C

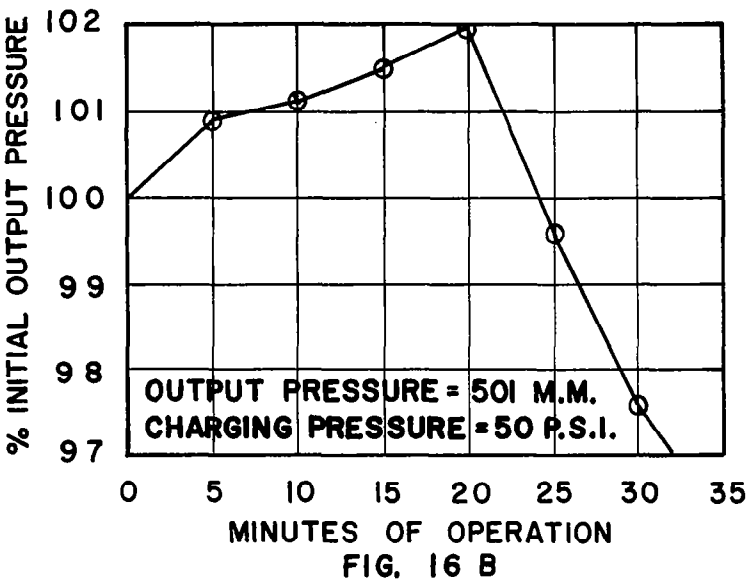

FIG. 16 B

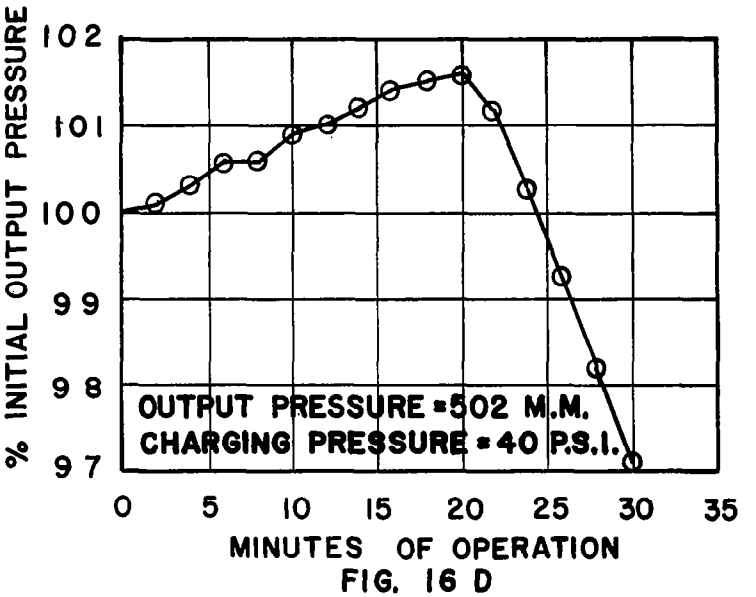

FIG. 16 D

CALIBRATION SAMPLE BOTTLE OUTPUT PRESSURE VERSUS TIME

5.9 INLET VALVE EVALUATION

Upon delivery of the mass spectrometer, it was apparent that the Inlet Valves were unsatisfactory. Due to inadequate spring tension, the valves would often remain open after removal of the actuating voltage. Even when closing was achieved, leaks would frequently reappear when the sample pressure was reduced.

After discussion with the valve manufacturer (Valcour Engineering Corp.), a new set of inlet valves with stiffer springs were ordered. Upon delivery each of the new valves was leak checked. The leak rates of the closed valves ranged from 2×10^{-7} to 1.1×10^{-4} atm-cc/sec. Each valve was operated a number of times before the reading was taken. All the valves were within or near the manufacturers specifications.

The manifold input pressure was monitored upon installation of the valve with the highest leak rate. The unused inlet valves were fitted with plugs to assure that they were leak tight. The inlet manifold pressure rise due to the valve leak was undetectable on the 0 - 20 mm gage, and thus it was concluded that an inlet valve leak rate of 1.1×10^{-4} atm-cc/sec. was tolerable.

Although the performance of the new valves has been significantly better than the original valves, an occasional malfunction still occurs.

6. EVALUATION OF THE ION SOURCE

6.1 Function of the Ion Source

The function of the Ion Source is to ionize a small part of the unknown input gas and to form these ionized particles into an ion beam of narrow energy spread. The ion beam thus formed is focused into the analyzer section of the mass spectrometer where it is separated into ion beams of different m/e ratios.

6.2 Description of Operation

As described in the section on the vacuum system, the ion source pressure is reduced from the input pressure by a factor of approximately two million. With an atmospheric sample, the source pressure is typically in the region of 4×10^{-4} torr; although this pressure is a function of the Gold Leak and Capillary used.

Ionization is accomplished by passing a narrow electron beam through the ionization region of the source. This electron beam has an energy of 70 to 80 electron-volts and an intensity which is normally adjusted to 40 microamps. The more narrow the electron beam, the smaller the energy spread of the ion beam will be. For this reason, it is important that the electron beam be of narrow physical dimensions in the ionization region.

Upon ionization, the ionized particles are forced by an electric field toward the Source Exit Slit. Some of the ions pass through the slit and thus form a ribbon-like beam. The larger part of the ionized particles will strike the metal about the slit and therefore be lost. The ions which do pass through the slit, and therefore comprise the ion beam, are accelerated toward the Entrance Slit in the electric sector of the analyzer due to the electric field existing in the region between the two slits. In passing between the slits, the ion beam comes under the influence of a focusing electrode known as Lens II. The function and operation of Lens II is described in the section on the Analyzer.

The performance of the Ion Source with respect to absolute energy spread[8] and ion beam intensity at the exit slit is almost independent of the Lens II potential and other electrode potentials. These two parameters are primarily a function of the Source Pressure, Emission Current and the Source Electrode Potentials with respect to each other. The percentage of ions leaving the exit slit which will also pass through the entrance slit is a function of the Lens II potential and the Exit Slit to Entrance Slit Potential (Ion Accelerator Voltage). The only provision for total ion beam measurement is in the electric sector. Therefore, when studying the source by monitoring the ion beam intensity, it is necessary to maintain a constant

[8] The term Absolute Energy Spread is differentiated from the terms Absolute Energy Distribution and Percentage Energy Distribution both of which would involve the exit to entrance slit voltage.

Ion Accelerator Potential and to operate the Lens II potential under constant conditions. This second condition is met in the following experiments by peaking the ion current with the Lens II potential before each current reading.

The Ion Source consists of the following nine electrodes:

Filament
Filament Shield
Electron Focus Slit
Electron Accelerator Slit
Ion Accelerator (of which the exit slit is an integral part)
Ion Repeller
Electron Rail I
Electron Rail II
Anode

A schematic type diagram of the physical relationships of the various electrodes is shown in Figure 17. The description and function of each electrode is given below.

Filament: The filament is a 5 mil. Rhenium wire bent into a semi-circular shape and mounted upon two relatively sturdy filament posts. A current of approximately two amperes is passed through the filament raising the temperature of its center to the point at which thermionic emission occurs. The total emission current is regulated at an adjusted level by controlling current through the filament. The total emission current can be adjusted to regulate from zero to over 100 microamps. As the filament is the starting point of the ionizing electron, it is used as the voltage reference in the Ion Source.

Filament Shield: The filament shield is mounted directly behind the filament. The shape of the shield is shown in Figure 18. The potential of the filament shield is negative with respect to the filament. The shape and potential of the shield in conjunction with the electron focus slit and to some degree the electron accelerator slit create an electric field about the filament which tends to focus the emitted electrons and accelerate them toward the electron focus and electron accelerator slits. This is shown in Figure 19.

Electron Focus Slit: The ~~electron focus slit~~, as stated above, operates in conjunction with the adjacent electrodes to focus the emitted electron into a ribbon-like beam which is accelerated toward the electron accelerator slit. The potential of the Electron focus slit is positive with respect to the filament.

Electron Accelerator: The electron accelerator further accelerates the electrons. It is more positive ~~than the~~ the electron focus. The physical dimensions of the Electron Accelerator also determines the source to pump pressure ratio.

Ion Repeller: The ion repeller in conjunction with the ion accelerator form a circular (in one plane) field which performs two functions: one, it causes a centripetal force, $F = eE = mv^2/R$, to act upon the electrons thus causing them to follow a circular path, and second, the repeller-accelerator field causes a centrifugal force to act upon the positive ionized particles forcing some of them through the exit slit.

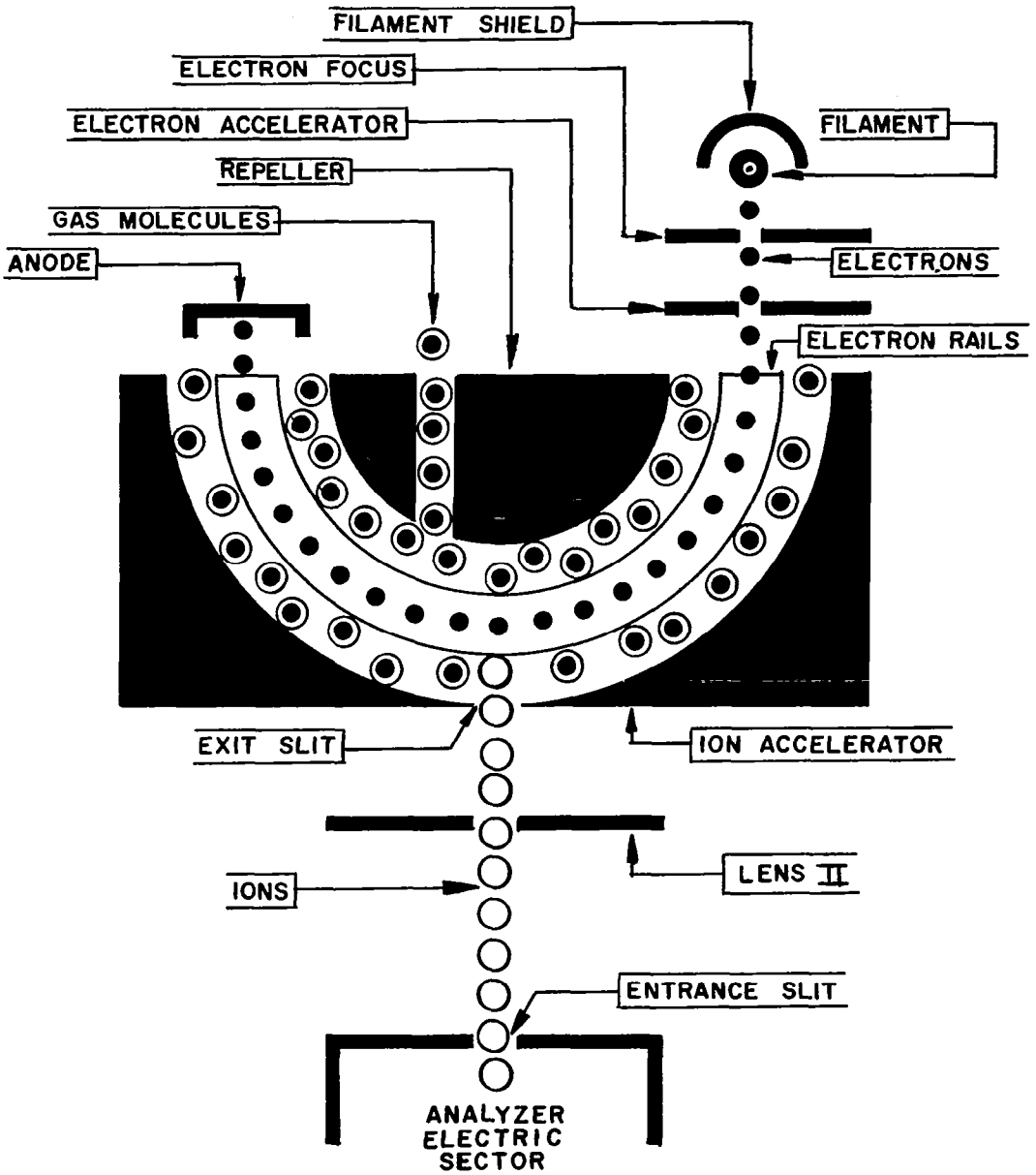

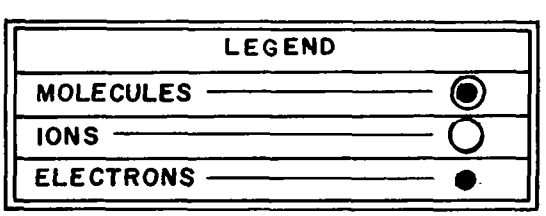

ION SOURCE SCHEMATIC

FIG. SEVENTEEN

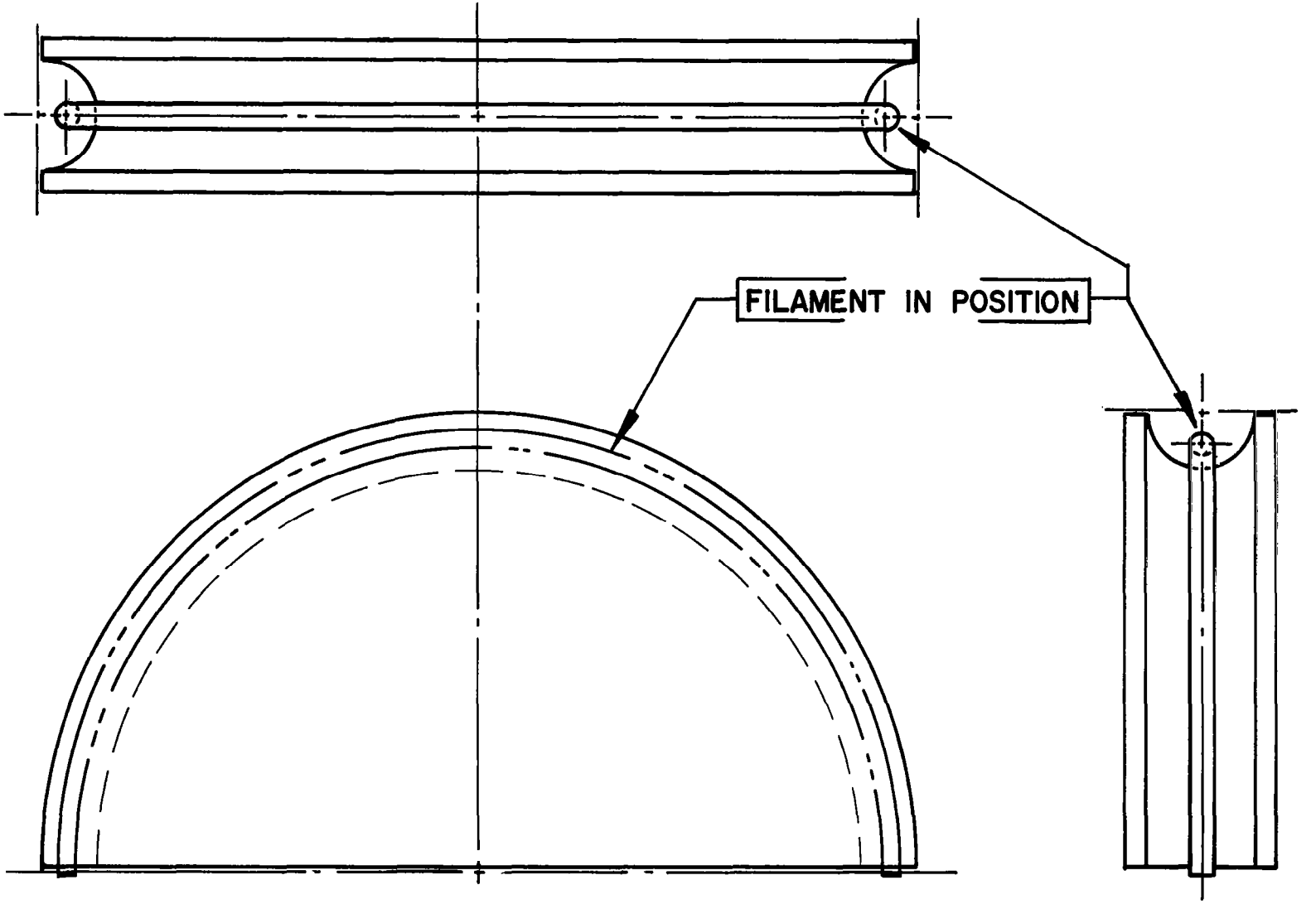

FILAMENT SHIELD

FIG. EIGHTEEN

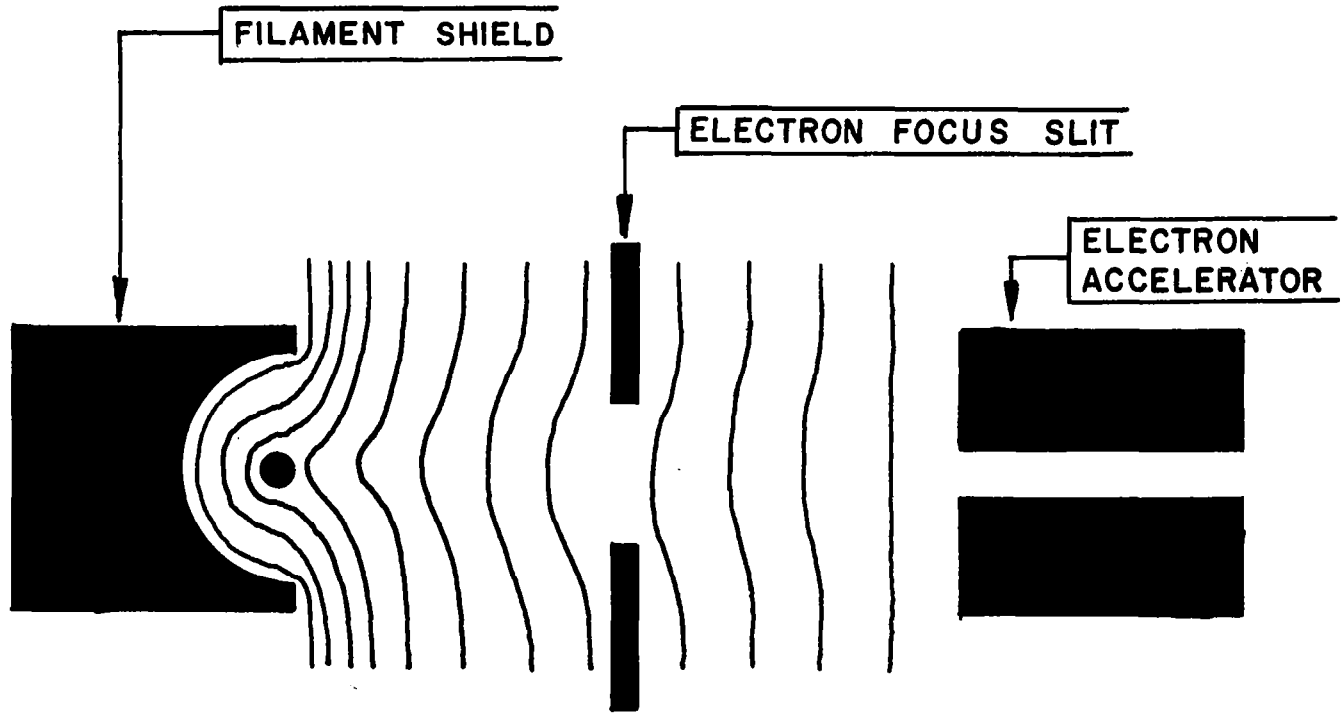

ELECTRIC FIELD IN FILAMENT REGION

FIG. NINETEEN

Ion Accelerator: As discussed above, the ion accelerator in conjunction with the ion repeller forms the repeller-accelerator field.

Anode: The function of the anode is to collect the electrons which pass through the ionization region. At one time, the current to the anode was considered the ionization current and was regulated rather than total emission current.

Electron Rails: The electron rails terminate the top and bottom of the repeller-accelerator field region. By placing a difference potential between Rail I and Rail II, the electron beam can be raised and lowered. This feature of the rails is not presently used, and the two rails are operated at a common potential. If the common rail potential were the repeller-accelerator center voltage, the repeller-accelerator field would be cylindrical. By operating the rails at a potential between the center voltage and accelerator voltage, the repeller-accelerator field approaches a spherical configuration. This is shown in Figure 20.

6.3 Selection of Source Variables

6.3.1 Objectives

The objectives of this section are: to determine the electron current distribution of the electron beam in the Ion Source, to measure the number and energy distribution of the ions generated by the Ion Source, to determine satisfactory operating potentials of the source electrodes, and to determine the proper operating ranges of the input pressure and emission current.

6.3.2 Conclusion

It was concluded that the energy spread of the ion beam generated by the Ion Source is relatively small. It was determined that the energy spread could be minimized by operating the source at a high electron accelerator voltage, a low emission current, a high ionization voltage and with an electron rail potential which lies between the rep. - acc. center voltage and the voltage of the ion accelerator. It was concluded that the electrode potentials tabulated in Table XXII of this report would provide satisfactory operation of the Ion Source. It was noted that the anode current (and thus probably the ionizing current) is a critical function of the repeller to ion accelerator potential. It was concluded that the mass spectrometer is operating in a linear region of the emission current vs. ion output curve. It was determined that the operation of the mass spectrometer is linear with input pressure from 150 to 700 mm of Hg. It was concluded that the ion beam generated by the Ion Source is not stable over time at constant input pressure and ambient temperature. The last conclusion implies that a study of Ion Source pressure stability and electron distribution stability are required.[9]

[9] The causes of Ion Source instability were later studied. The results of this study are given in the section on source stability and sensitivity.

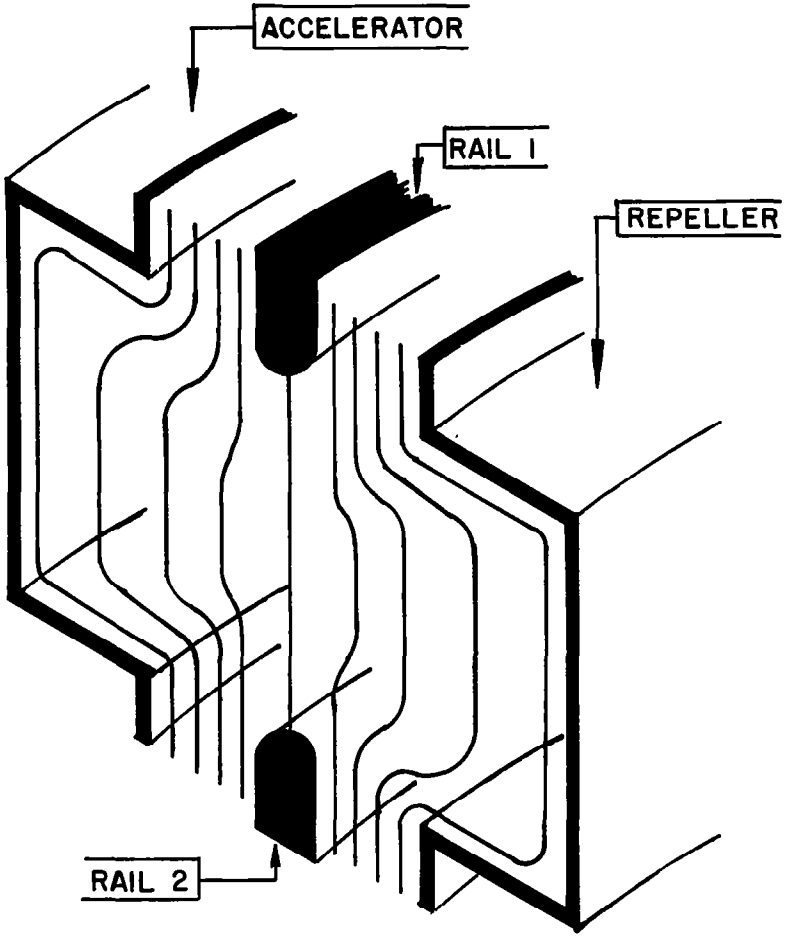

CROSS SECTION OF REPELLER-ACCELERATOR REGION SHOWING CYLINDRICAL FIELD WITH RAILS AT CENTER VOLTAGE.

FIG. TWENTY-A

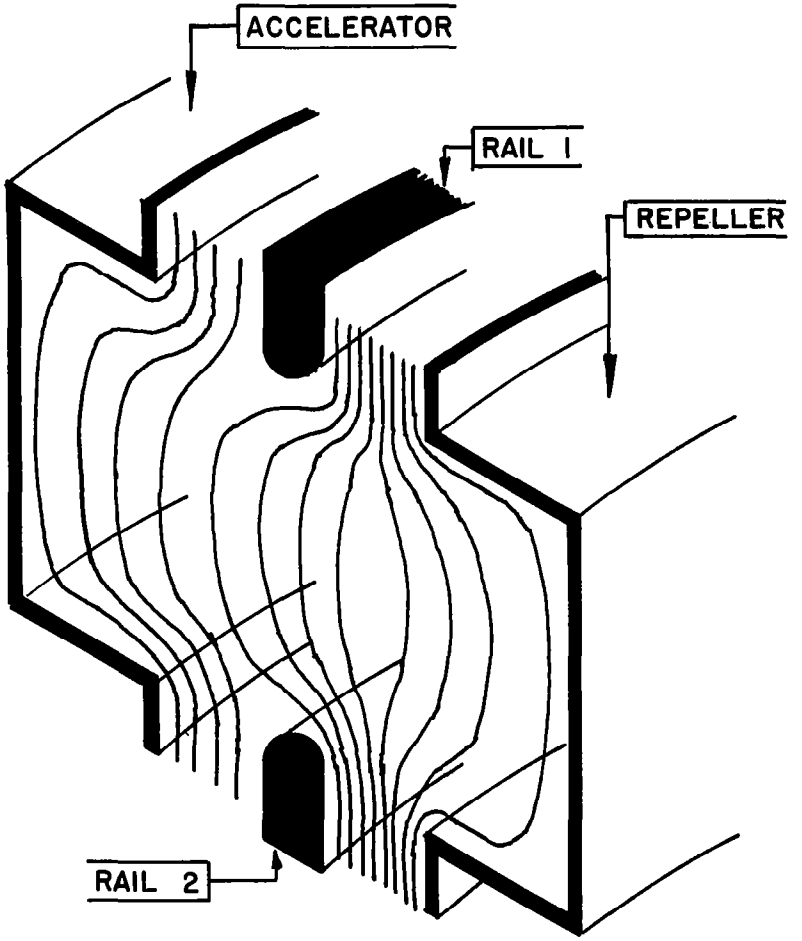

CROSS SECTION OF REPELLER-ACCELERATOR REGION SHOWING SPHERICAL FIELD WITH RAILS CLOSER TO ACCELERATOR POTENTIAL THAN REPELLER POTENTIAL.

FIG. TWENTY-B

ELECTRIC FIELD IN REPELLER - ION ACCELERATOR REGION

6.3.3 Equipment

Type of Instrument	Make & Model No.	Serial Number
(1) Differential Volt Meter	John Fluke 803B	3439
(1) Power Supply	John Fluke 407	1161
(1) Power Supply	Hewlett-Packard 721A	304-15768
(1) DC Micro Volt-Ammeter	Hewlett-Packard 425A	142-05861
(1) Pot Board	CSC	
(3) 0 - 50 microamp. meters	Triplet	
(2) 0 - 100 microamp. meters	Triplet	

6.3.4 Procedure

1. The circuit for energy spread measurements (shown in Figure 21) was connected.

2. With the mass spectrometer operating, the anode current was peaked with the repeller voltage, and the ion current was peaked with Lens II. Three plots of ion current vs. electrometer repelling voltage were made at different electron rail settings: (a) rails at the repeller-accelerator center voltage, (b) rails near the accelerator voltage and (c) rails at an intermediate potential.

3. Bar graphs were plotted of the percentage of ions rejected by a one volt increase in electrometer repelling voltage at different energy levels.

4. Using the method outlined above, energy spread measurements were made at different emission currents. This was done with the electron rails at the potential selected in Step 3. Curves were drawn for 20, 40 and 60 microamps.

5. An energy spread measurement was made with the electron accelerator voltage lowered to 61 volts from an initial value of 210.4 volts above the filament.

6. Maintaining the voltage relationship between them, the ion accelerator, ion repeller and electron rails were raised in potential with respect to the filament. This raised the ionization voltage[10] from 55 to 74.6 volts. Raising the ionization voltage decreases the transit time of the electrons and thus lessens the effects of space charge dispersion. Upon doing this, the anode current re-peaked

[10] The ionization voltage is primarily the voltage difference between the filament and the potential of the ionization region (injection voltage).

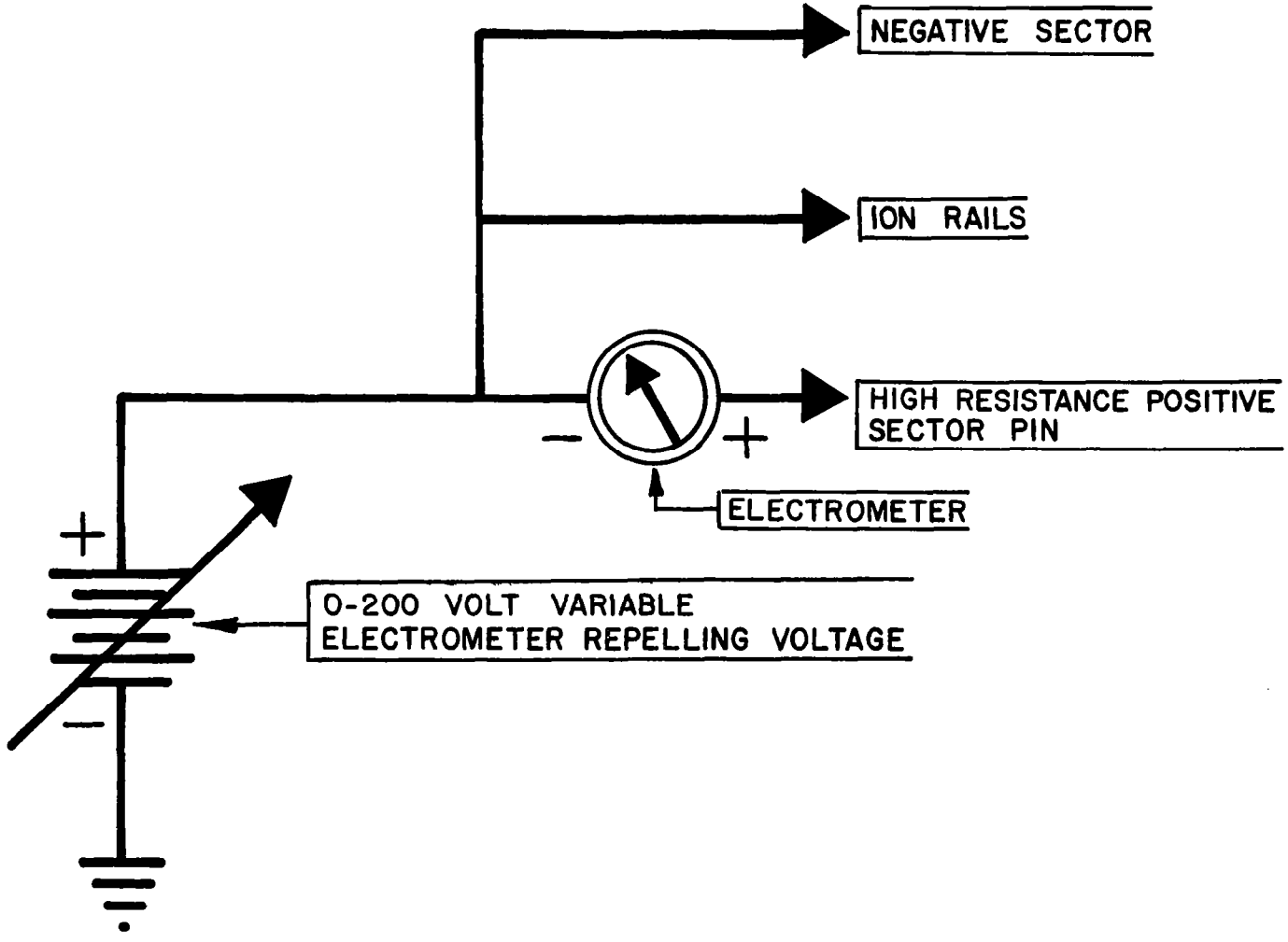

ENERGY SPREAD MEASUREMENT CIRCUIT CONNECTION

FIG. TWENTY-ONE

with the repeller. An energy spread measurement was then taken.

7. Data was taken and plotted of I_{anode}, $I_{rep.}$ and $I_{ion\ acc.}$ vs. the repeller to accelerator voltage.

8. Data was taken and a graph drawn of ion current vs. electron emission.

9. Data was taken and a graph drawn of ion current vs. input pressure.

10. Data was taken and a graph drawn of ion current over a period of six hours, with constant input pressure.

6.3.5 Results

1. The results obtained in Steps 2 and 3 of the Procedure are given in Tables XI, XII and XIII and in Figures 22, 23 and 24. It can be seen from the figures that the minimum energy spread occurs when the electron rails are at a potential which lies between the repeller-accelerator center voltage and the voltage of the ion accelerator.

2. The results obtained in Step 4 of the Procedure are given in Tables XIV and XV and Figures 25 and 26. These results should be compared to Table XII and Figure 23 for the 20 microamp. operation at the same rail voltage. Space charge dispersion of the electron beam due to high beam intensity appears to be negligible. It is interesting to note that the percentage of ions formed within a 4 volt potential is less for the 40 microamp. condition than for the 60 microamp. condition. This may be due to experimental error. It should be noted that the data was taken on different days and that there is less ion current for the 60 microamp condition than for the 40 microamp condition. This indicates there had been a change in source pressure.

3. When the electron accelerator to filament voltage was lowered from 210.4 volts to 61 volts (a voltage near the center of the repeller-accelerator field) the anode current dropped from 85 percent of the total emission current to 20 percent while the electron accelerator current rose from essentially zero to 55 percent of the total emission. The decrease in ionizing current caused a factor of 20 drop in the ion current. The decrease in electron accelerator voltage also had a deleterious effect upon the energy spread of the ion beam. This is shown by the data recorded in Table XVI and plotted in Figure 27. It should be noted that this change did not alter the ionization voltage ($V_{inj} - V_{fil}$) which is determined by the limits of the repeller and ion accelerator voltages. The change in source operating condition with electron accelerator voltage is due to the dispersion of the electron beam in the long, narrow electron accelerator slit. The dimensions of the slit have been selected for a given molecular flow conductance. These dimensions result in less than optimum electron ballistic characteristics.

4. In Step #6 of the Procedure, the ionization voltage was raised. As this raises the velocity of the electron particles, the repeller-accelerator voltage must be raised to maintain the $eE = mv^2/r$ relationship. The results of the energy spread measurement are tabulated in Table XVII and plotted in Figure 28. Figure 28 should be compared to Figure 23 to gage the improvement in energy spread. A voltage of 68.9 volts was subtracted from the electrometer voltage reading to make

TABLE XI

Ion Energy Spread Data

(Electron Rails at Rep.-Acc. Center Potential)

$V_{rep.}$ = 128.3, $V_{ion\ acc.}$ = 103.5, $V_{elec.\ rails}$ = 116. All voltages with respect to ground. Lens II adjusted for maximum ion current. Emission = 20 microamps.

Electrometer Repelling Voltage in Volts	Ion Current in Amps
100.0	$43. \times 10^{-12}$
110.5	$38. \times 10^{-12}$
111.4	$31. \times 10^{-12}$
111.8	$27. \times 10^{-12}$
112.1	$24. \times 10^{-12}$
112.4	$20. \times 10^{-12}$
112.8	$16. \times 10^{-12}$
113.3	11.5×10^{-12}
114.1	6.0×10^{-12}
114.7	3.5×10^{-12}
115.4	2.0×10^{-12}
116.0	1.0×10^{-12}
118.3	$.5 \times 10^{-12}$

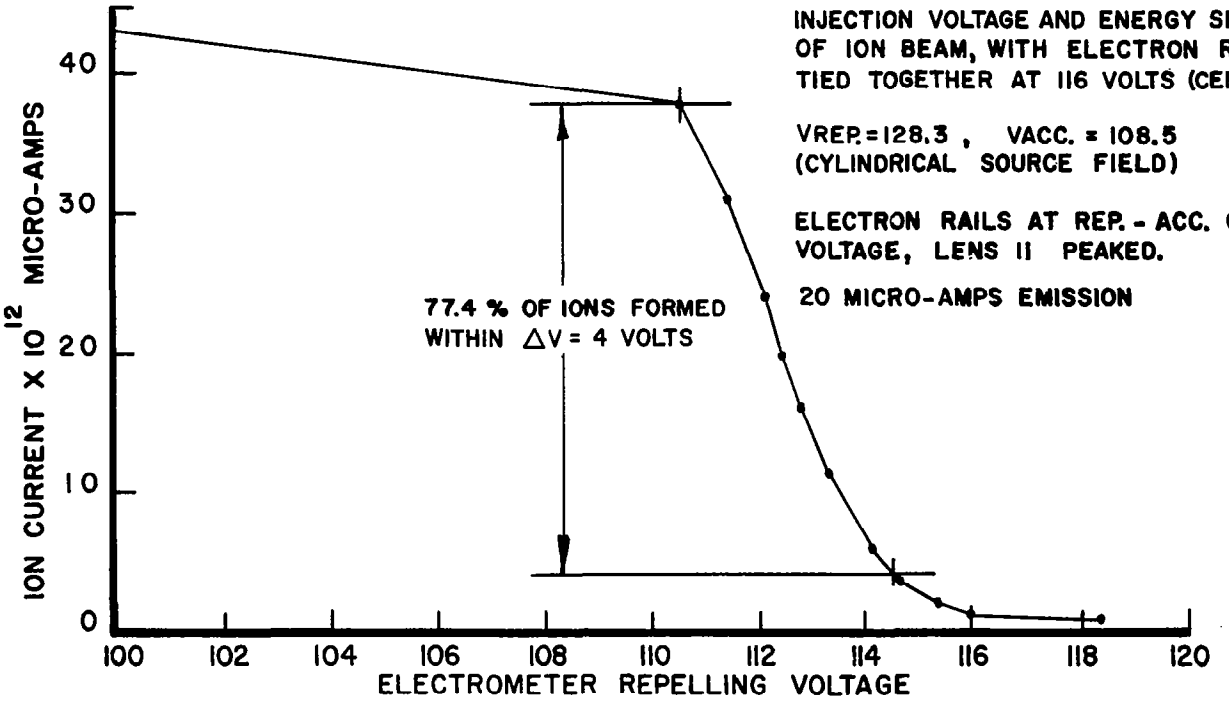

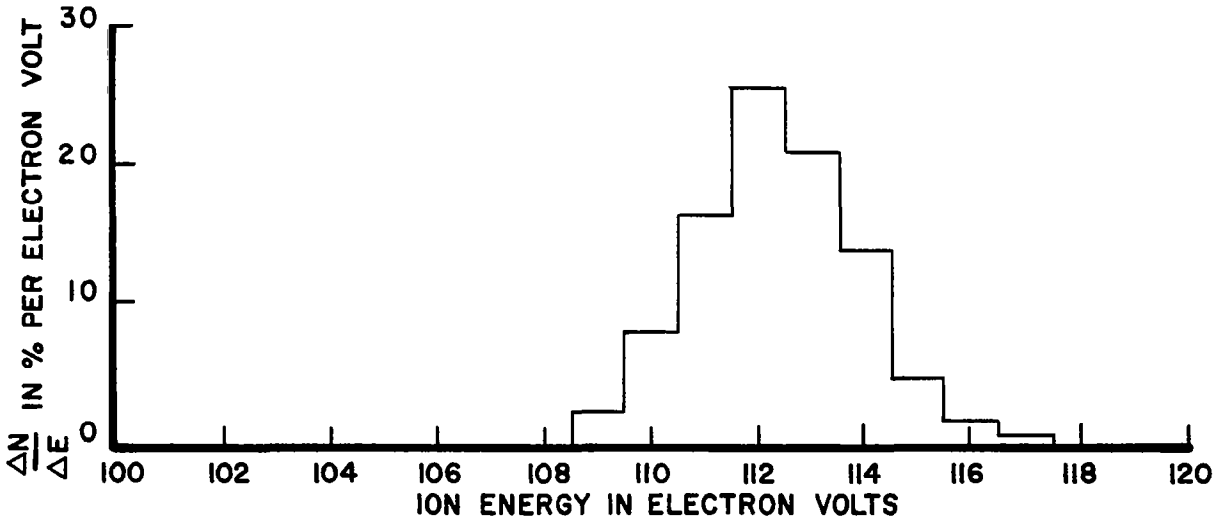

THESE TWO GRAPHS COMPRISE FIG. TWENTY-TWO

TABLE XII

Ion Energy Spread Data

(Electron Rails Between Rep.-Acc. Center Potential and Accelerator Potential)

$V_{rep.}$ = 128.3, $V_{ion\ acc.}$ = 103.5, $V_{elec.\ rails}$ = 116. All voltages with respect to ground. Lens II adjusted for maximum ion current. Emission = 20 microamps.

Electrometer Repelling Voltage in Volts	Ion Current in Amps
100	$16. \times 10^{-11}$
105	$16. \times 10^{-11}$
107.7	$15. \times 10^{-11}$
108.2	13.6×10^{-11}
108.7	12.0×10^{-11}
109.2	10.2×10^{-11}
109.5	9.0×10^{-11}
109.9	7.1×10^{-11}
110.3	5.4×10^{-11}
110.7	2.8×10^{-11}
111.2	2.3×10^{-11}
111.7	1.4×10^{-11}
112.4	$.8 \times 10^{-11}$
113.0	$.4 \times 10^{-11}$

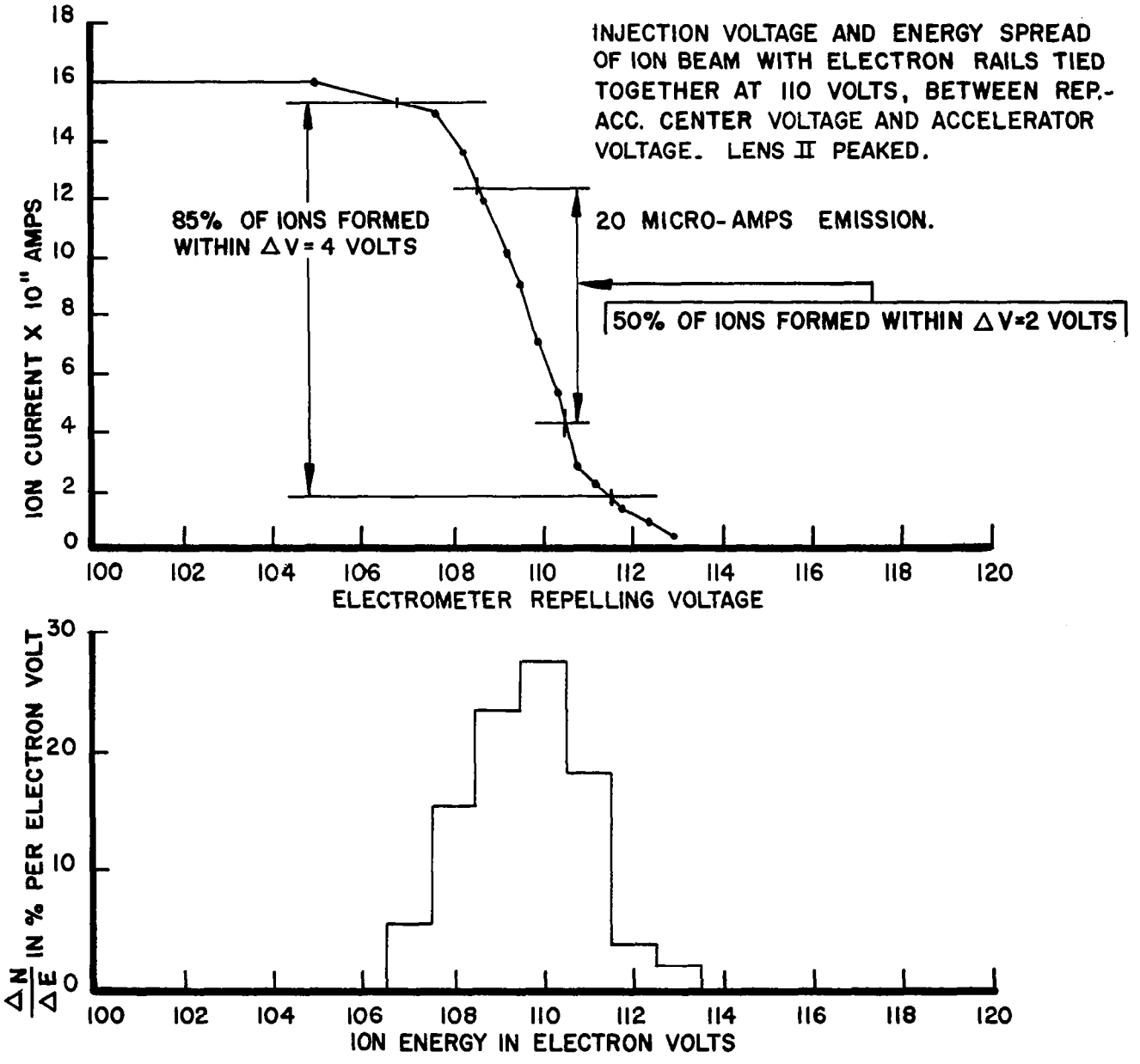

THESE TWO GRAPHS COMPRISE FIG. TWENTY-THREE.

TABLE XIII

Ion Energy Spread Data

(Electron Rails at Accelerator Potential)

$V_{rep.}$ = 128.3, $V_{ion\ acc.}$ = 103.5, $V_{elec.\ rails}$ = 103.8. All voltages with respect to ground. Lens II adjusted for maximum ion current. Emission = 20 microamps.

Electrometer Repelling Voltage in Volts	Ion Current in Amps
100.0	32.5×10^{-11}
102.9	32.5×10^{-11}
104.0	32.5×10^{-11}
105.2	32.5×10^{-11}
106.5	32.5×10^{-11}
107.3	32.0×10^{-11}
108.2	30.5×10^{-11}
109.0	28.5×10^{-11}
110.0	23.0×10^{-11}
110.6	17.5×10^{-11}
111.2	12.8×10^{-11}
111.7	9.6×10^{-11}
112.1	6.7×10^{-11}
112.6	4.6×10^{-11}
113.1	3.4×10^{-11}
113.6	2.4×10^{-11}
114.3	1.5×10^{-11}
115.0	$.9 \times 10^{-11}$
115.9	$.5 \times 10^{-11}$

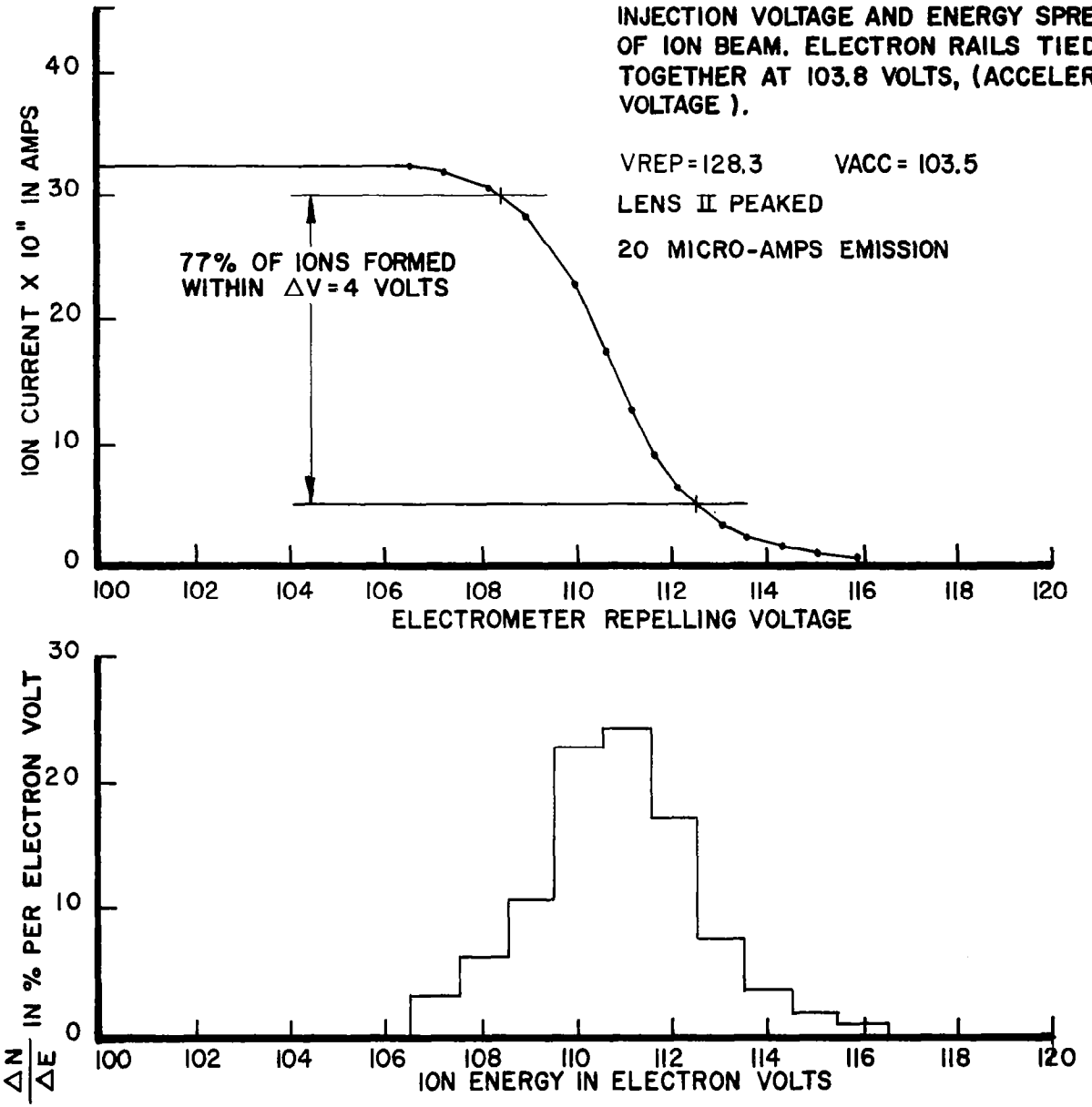

THESE TWO GRAPHS COMPRISE FIG. TWENTY - FOUR

TABLE XIV

Ion Energy Spread Data

(Emission Current at 40 microamps)

$V_{rep.} = 128.3$, $V_{ion\ acc.} = 103.5$, $V_{elec.\ rails} = 110.2$. All voltages with respect to ground. Lens II adjusted for maximum ion current.

Electrometer Repelling Voltage in Volts	Ion Current in Amps
100.0	27.2×10^{-11}
104.2	27.1×10^{-11}
105.0	27.0×10^{-11}
106.9	27.0×10^{-11}
107.8	26.9×10^{-11}
108.4	26.8×10^{-11}
109.4	26.0×10^{-11}
110.2	24.2×10^{-11}
111.0	21.2×10^{-11}
111.8	16.7×10^{-11}
112.6	10.4×10^{-11}
113.0	8.2×10^{-11}
113.3	5.8×10^{-11}
113.6	4.2×10^{-11}
113.9	3.0×10^{-11}
114.8	1.1×10^{-11}
115.5	$.6 \times 10^{-11}$

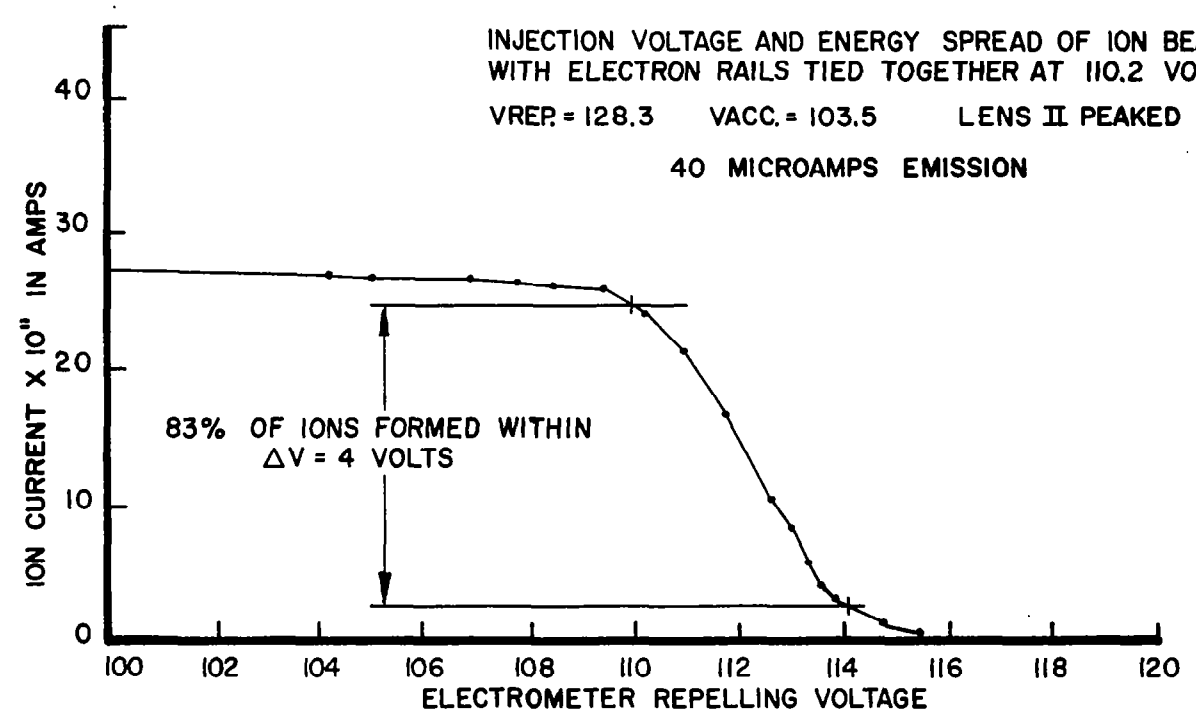

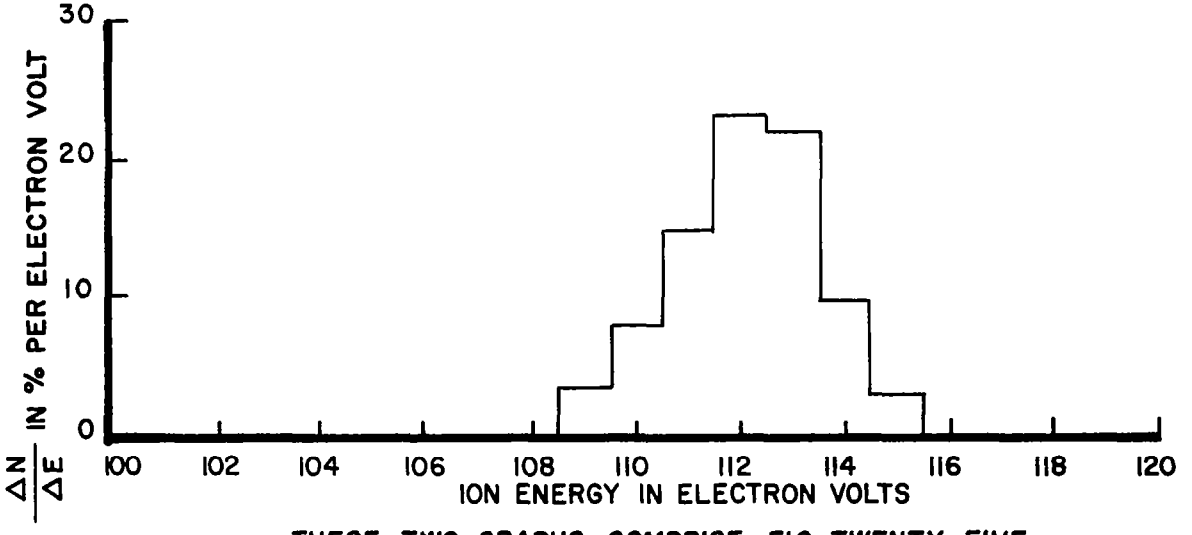

THESE TWO GRAPHS COMPRISE FIG. TWENTY-FIVE

TABLE XV

Ion Energy Spread Data

(Emission Current at 60 microamps)

$V_{rep.}$ = 128.3, $V_{ion\ acc.}$ = 103.5, $V_{elec.\ rails}$ = 110.2. All voltages with respect to ground. Lens II adjusted for maximum ion current.

Electrometer Repelling Voltage in Volts	Ion Current in Amps
100.1	21.5×10^{-11}
106.1	21.5×10^{-11}
107.1	20.3×10^{-11}
107.7	19.5×10^{-11}
108.2	18.1×10^{-11}
108.7	16.2×10^{-11}
109.2	14.2×10^{-11}
109.7	11.8×10^{-11}
110.3	8.1×10^{-11}
110.9	4.8×10^{-11}
111.5	2.3×10^{-11}
112.0	1.5×10^{-11}
112.5	$.95 \times 10^{-11}$
113.5	$.50 \times 10^{-11}$

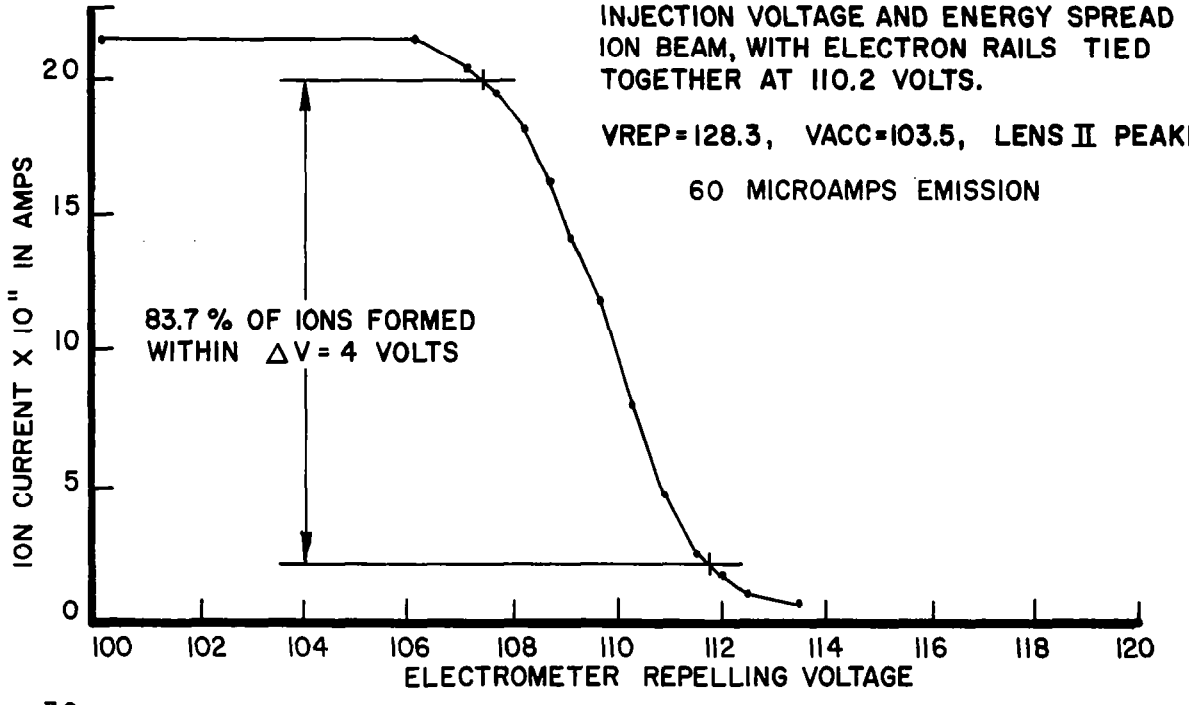

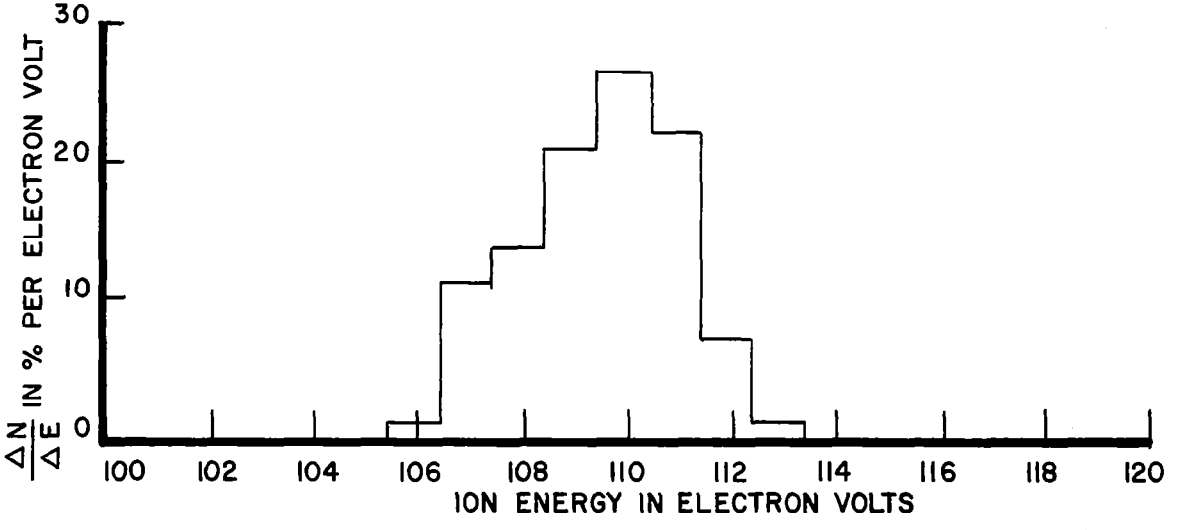

THESE TWO GRAPHS COMPRISE FIG. TWENTY - SIX

TABLE XVI

Ion Energy Spread Data

(Lowered Electron Accelerator Voltage)

$V_{rep.}$ = 128.3, $V_{ion\ acc.}$ = 103.5, $V_{elec.\ rails}$ = 110.2, $V_{fil.}$ = 55.0, $V_{elec.\ acc.}$ = 116.0. All voltages with respect to ground. Lens II adjusted for maximum ion current. Emission = 20 microamps. Electron accelerator potential lowered from 210 to 61 volts above the filament.

Electrometer Repelling Voltage in Volts	Ion Current in Amps
100.0	6.6×10^{-12}
104.2	6.6×10^{-12}
106.0	6.5×10^{-12}
106.5	6.4×10^{-12}
107.0	6.0×10^{-12}
107.5	5.8×10^{-12}
108.0	5.2×10^{-12}
108.5	4.8×10^{-12}
109.0	4.2×10^{-12}
109.5	3.4×10^{-12}
110.0	2.8×10^{-12}
110.5	2.4×10^{-12}
110.0	1.8×10^{-12}
111.5	1.3×10^{-12}
112.0	1.0×10^{-12}
112.5	$.6 \times 10^{-12}$
113.0	$.3 \times 10^{-12}$
114.0	$.0 \times 10^{-12}$

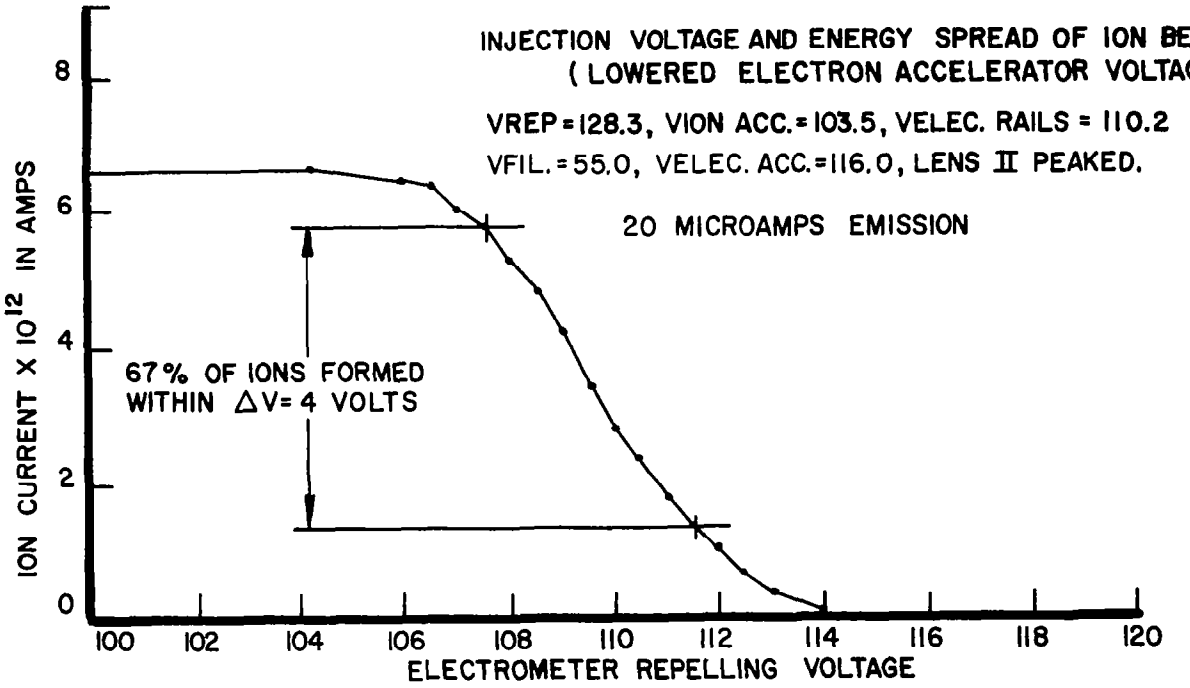

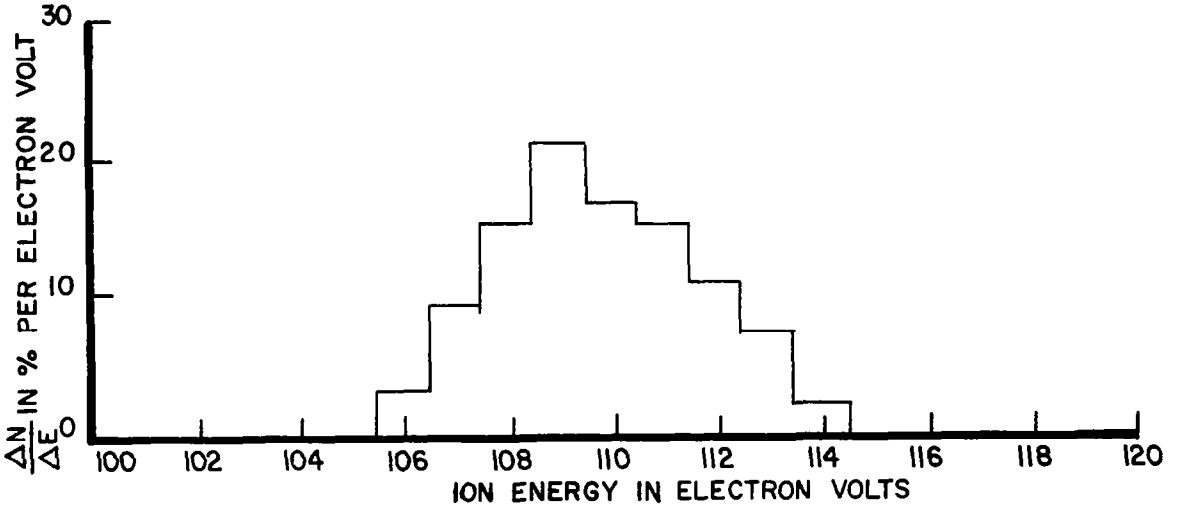

THESE TWO GRAPHS COMPRISE FIG. TWENTY-SEVEN

TABLE XVII

Ion Energy Spread Data

(Increased Ionization Voltage)

$V_{rep.}$ = 204.9, $V_{ion\ acc.}$ = 172.4, $V_{elec.\ rails}$ = 180.1, $V_{fil.}$ = 105.4, $V_{elec.\ acc.}$ = 315.4. All voltages with respect to ground. Lens II adjusted for maximum ion current. Emission = 20 microamps. V_{ion} raised from 61.0 to 74.6 volts. V_{ion} = ($V_{inj.}$ - $V_{fil.}$).

Electrometer Repelling Voltage in volts	Electrometer Repelling Voltage Minus 68.9	Ion Current in Amps
175.4	106.5	10.8×10^{-11}
177.7	108.8	10.2×10^{-11}
178.3	109.4	9.8×10^{-11}
178.8	109.9	8.6×10^{-11}
179.3	110.4	7.1×10^{-11}
179.8	110.9	5.3×10^{-11}
180.3	111.4	3.2×10^{-11}
180.8	111.9	2.0×10^{-11}
181.3	112.4	1.0×10^{-11}
181.8	112.9	$.7 \times 10^{-11}$
182.3	113.4	$.4 \times 10^{-11}$
182.7	113.8	$.3 \times 10^{-11}$

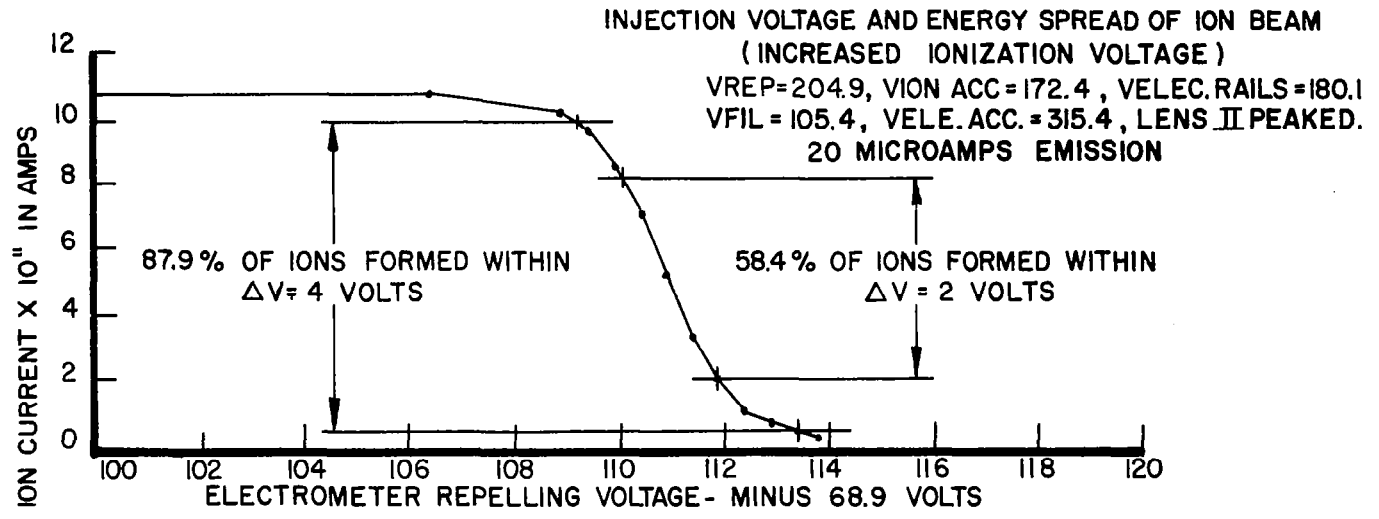

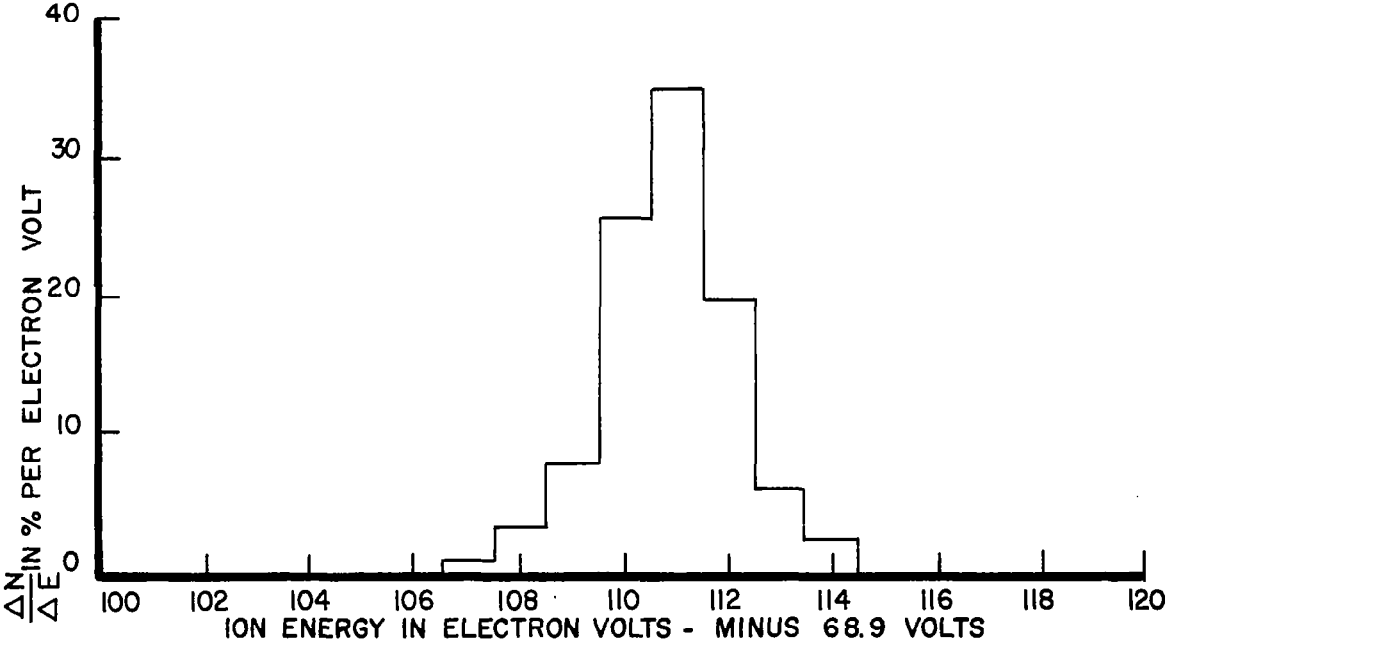

THESE TWO GRAPHS COMPRISE FIG. TWENTY-EIGHT

the ion accelerator voltage appear unchanged from the previous figures and thus make the figures more comparable.

5. In Step 7 of the Procedure, data was taken to plot the repeller, ion accelerator and anode currents vs. the repeller to accelerator voltage. In this experiment, it would be expected that the electron beam would strike the ion accelerator almost entirely at low rep.-acc. voltage. As the voltage is increased, it would be expected that the beam would move away from the accelerator and the anode current would increase. Further increases in repeller-accelerator voltage should cause the beam to strike the repeller almost exclusively. In other words, what would be expected is an ion accelerator curve sloping to the right, a repeller current curve sloping to the left and an anode current curve peaking in the center. The actual data taken is given in Table XVIII and plotted in Figure 29. The phenomenon described above is observed from a repeller-accelerator voltage of 30 volts and higher. The high repeller current at low repeller-accelerator voltage is presently unexplained.

6. In Step 8 of the Procedure, data was taken and a graph drawn of ion current vs. total emission current. The results are given in Table XIX, Figure 30. It is noted that non-linearity occurs at a current of approximately 60 to 70 microamps. The mass spectrometer would normally be operated below these currents.

7. In Step 9 of the Procedure, data was taken and a graph drawn of input pressure vs. ion current. The results are shown in Table XX and Figure 31. This curve indicates that the operation of the mass spectrometer will be linear over an input pressure range of 150 to 700 mm of Hg. At 150 mm and below, the flow characteristics of the capillary line cause a non-linear relationship between the input pressure and source pressure.

8. With the electrode voltages operated from well regulated supplies and the ambient temperature restricted to a small range, the ion current was monitored over a period of six hours. The result is given in Table XXI and Figure 32. The graph shows that a 25 percent change in ion current was observed over this period.[11]

9. Table XXII lists the source electrode potentials which were selected as providing satisfactory operation. These potentials are measured with respect to the filament. It should be mentioned that the potentials (particularly filament shield and electron focus potentials) required for proper operation are a function of the filament position. The potentials listed in Table XXII were somewhat modified when the filament was replaced. The values given, however, do provide a rough guide and were used during the analyzer evaluation.

[11] See section on Ion Source Stability.

TABLE XVIII

Source Electrode Currents vs. Rep.-Acc. Voltage

Total Emission = 20 microamps, $V_{ion\ acc,}$ = 172.9. All readings in microamps.

V_{rep}	$V_{rep.} - V_{ion\ acc.}$	$I_{rep.}$	$I_{acc.}$	I_{anode}
184.0	11.1	12.9	2.0	0.0
186.0	13.1	13.8	1.9	0.0
188.0	15.1	14.5	1.5	0.0
190.0	17.1	15.1	1.0	0.0
192.0	19.1	15.9	.9	0.0
194.0	21.1	16.3	.6	0.0
196.0	23.1	16.5	.8	0.0
198.0	25.1	16.5	1.0	0.0
200.0	27.1	15.9	1.8	0.0
202.0	29.1	15.0	2.7	0.0
204.0	31.1	14.5	3.2	0.0
206.0	33.1	14.0	1.5	2.0
207.0	34.1	1.0	.4	16.8
208.0	35.1	1.1	.5	16.6
209.0	36.1	3.7	.5	14.0
210.0	37.1	7.3	.5	10.3
211.0	38.1	10.4	.6	7.3
212.0	39.1	13.0	.6	4.8
213.0	40.1	14.8	.6	3.0
214.0	41.1	15.8	.6	2.0
215.0	42.1	16.0	.6	1.6
217.0	44.1	17.3	.6	.4

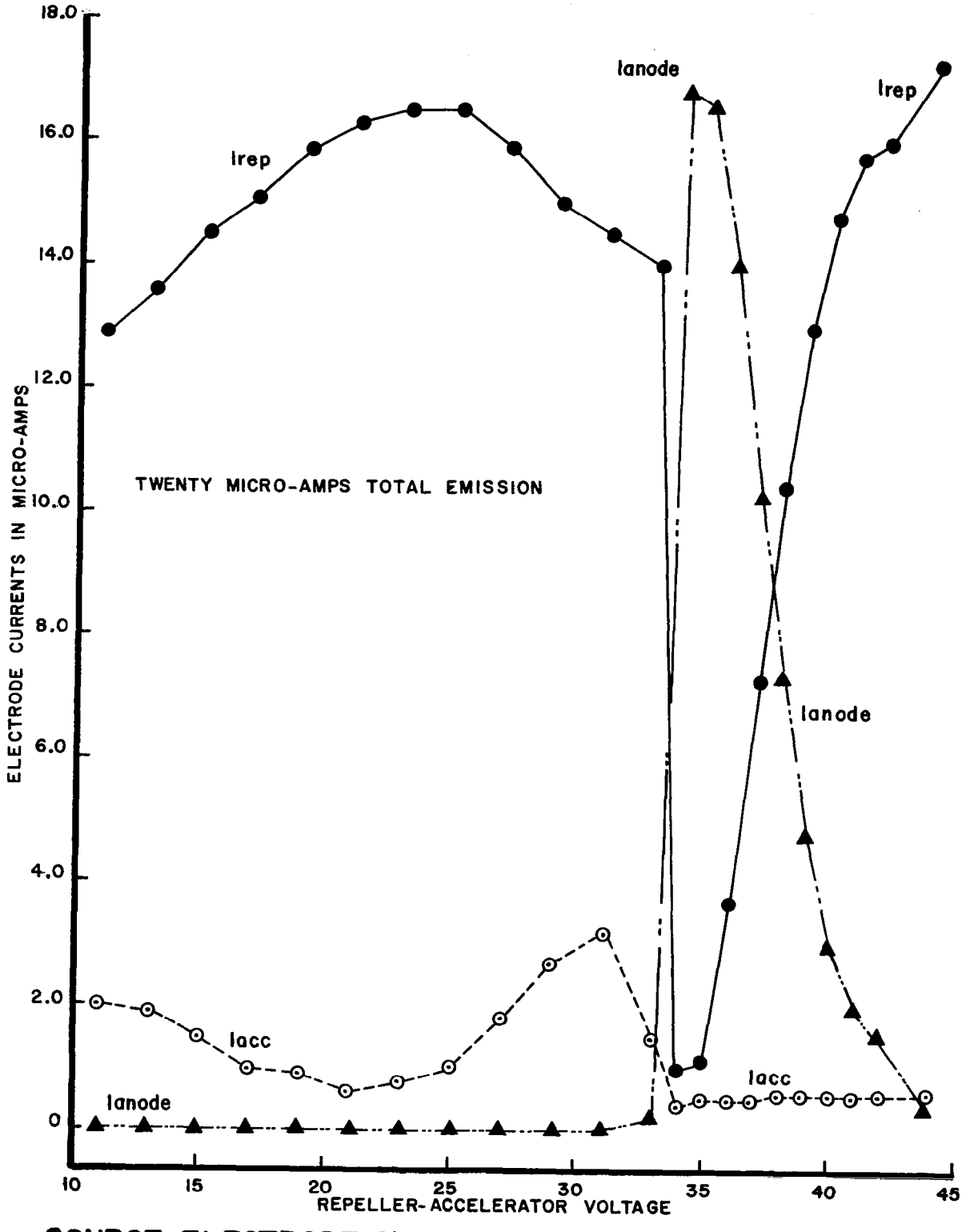

SOURCE ELECTRODE CURRENTS VS. REP.-ACC. VOLTAGE

FIG. TWENTY-NINE

TABLE XIX

Ion Current vs. Emission Current

Emission Current in Microamps	Ion Current in Amps
10	5.7×10^{-11}
20	10.9×10^{-11}
30	15.9×10^{-11}
40	23.2×10^{-11}
50	28.5×10^{-11}
60	33.5×10^{-11}
70	37.5×10^{-11}
80	40.0×10^{-11}
90	41.5×10^{-11}
100	43.0×10^{-11}

TABLE XX

Ion Current vs. Input Pressure

Input Pressure in Torr	Ion Current in Amps
698	10.5×10^{-11}
650	9.7×10^{-11}
600	8.95×10^{-11}
550	8.20×10^{-11}
500	7.40×10^{-11}
450	6.60×10^{-11}
400	5.85×10^{-11}
350	5.05×10^{-11}

TABLE XX continued

Input Pressure in Torr	Ion Current in Amps
300	4.35×10^{-11}
250	3.60×10^{-11}
200	2.95×10^{-11}
150	2.35×10^{-11}
100	1.75×10^{-11}
50	1.35×10^{-11}
2	1.20×10^{-11}

TABLE XXI

Ion Current vs. Operating Time

Time in Hours	Ion Current in Amps
0	23×10^{-11}
1	22.1×10^{-11}
2	20.6×10^{-11}
3	19.9×10^{-11}
4	19.3×10^{-11}
5	17.1×10^{-11}
6	17.1×10^{-11}

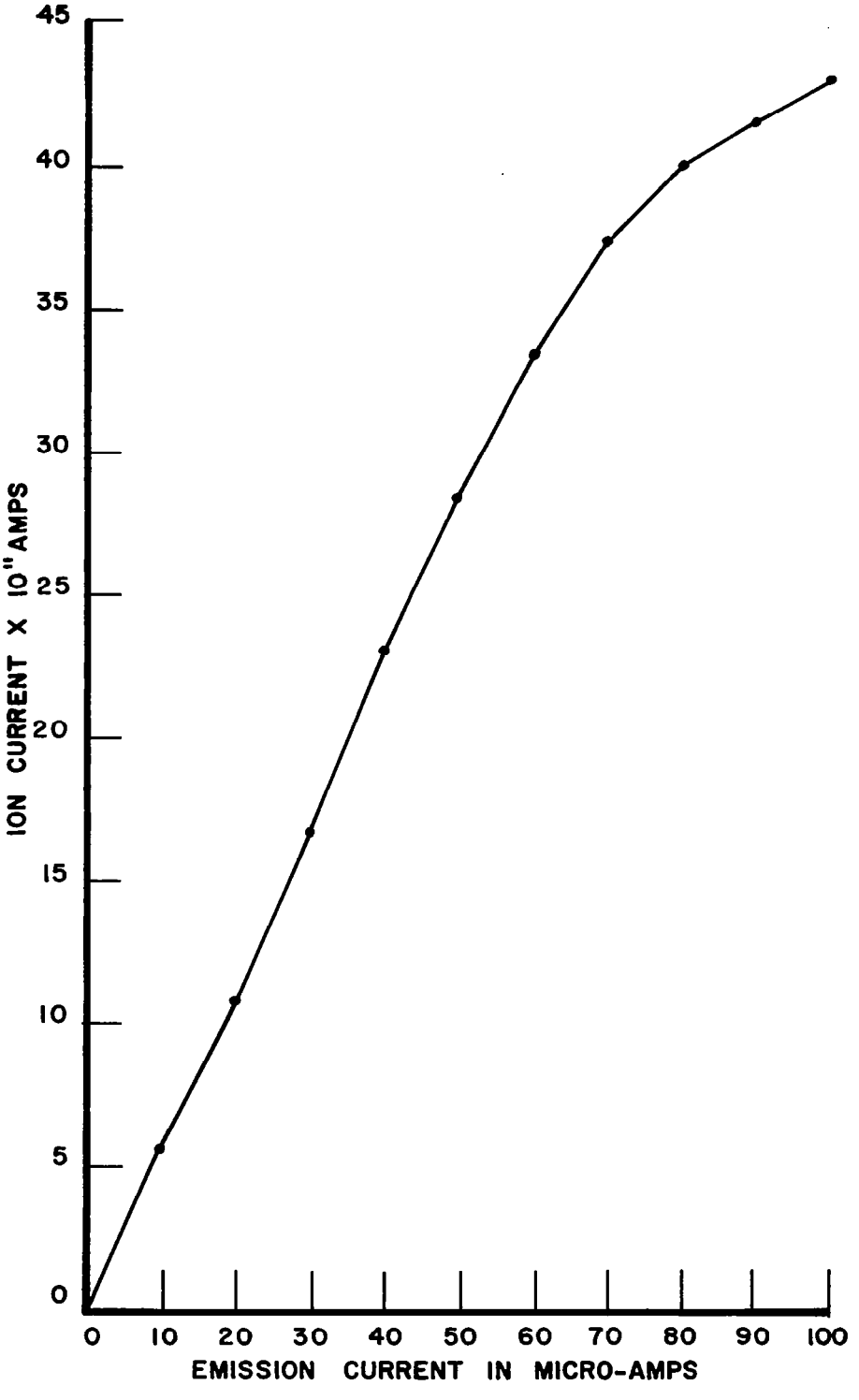

ION CURRENT VS. EMISSION CURRENT

FIG. THIRTY

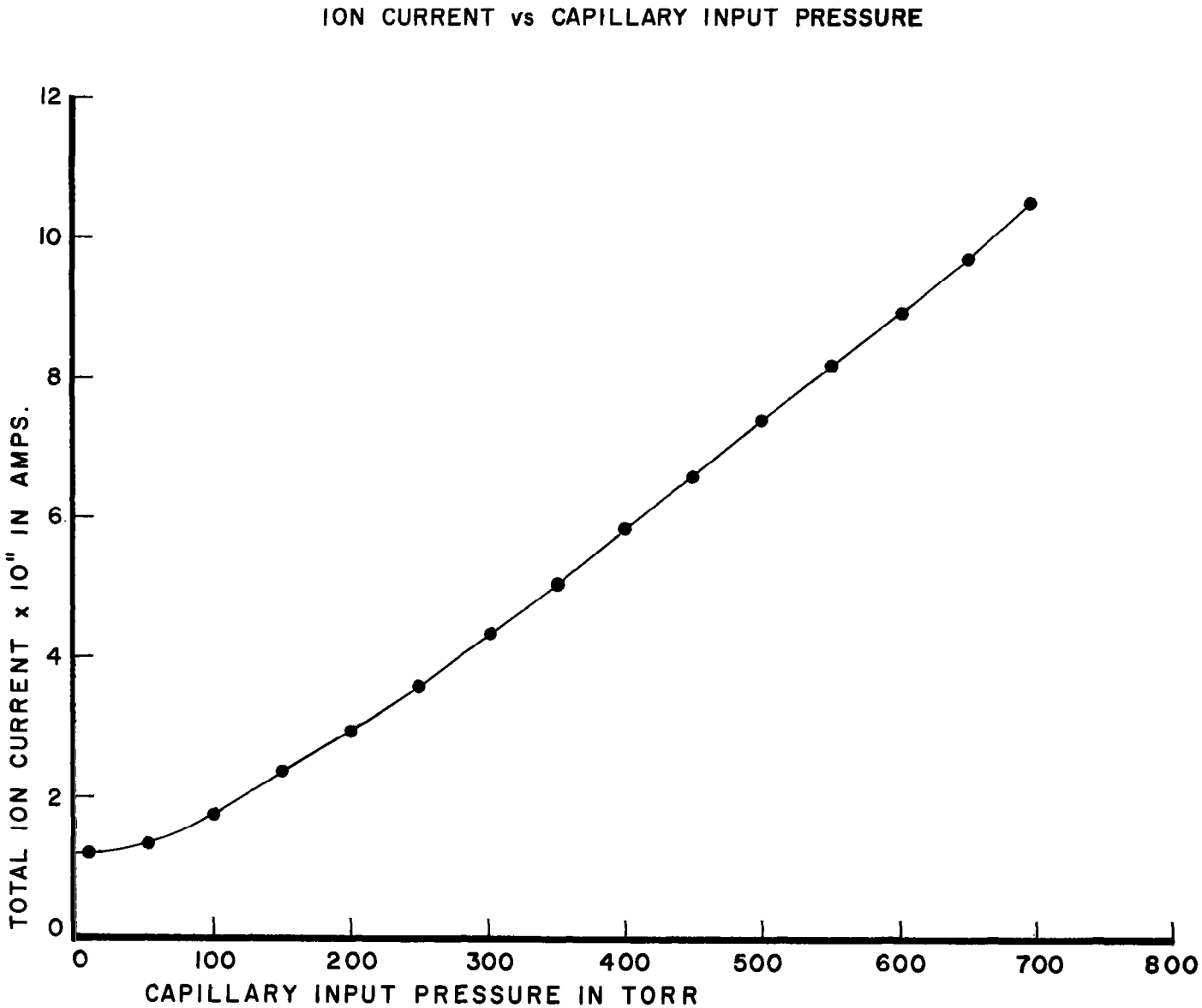

FIG. THIRTY-ONE

ION CURRENT vs OPERATING TIME

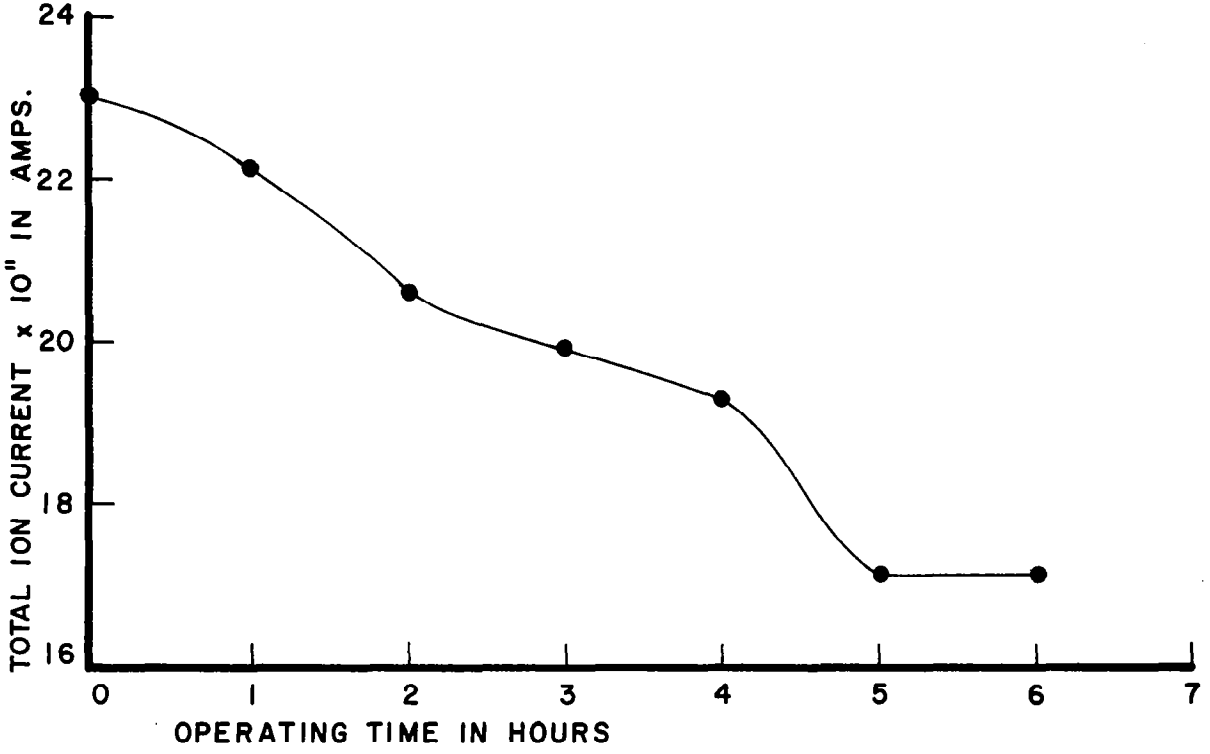

FIG. THIRTY - TWO

TABLE XXII

Selected Ion Source Electrode Potentials

(Measured with Respect to Filament)

Electrode	Potential in Volts
Filament	0.00
Filament Shield	-89.1
Electron Focus Slit	+15.7
Electron Accelerator Slit	+210.4
Ion Repeller	+99.5
Ion Accelerator	+67.0
Anode	+140.0
Rail I and II	+74.7

6.3.6 Discussion

It should be noted that the electron focus and filament shield potentials are a unique function of the filament position. The installation of a new filament normally requires a redetermination of the electron focus and filament shield voltages. These electrodes are adjusted to provide maximum electron current into the repeller-ion accelerator region as well as to allow proper operation of the emission regulator. If these two potentials are misadjusted, the emission regulator will not operate properly, and the filament will draw an excessive current and thus have a decreased life.

Shortly after installation of the present filament, an incident was observed where the electron distribution was changing although the electrode voltages were known to be constant. This phenomenon was attributed to a change in filament position. In future instruments, it would be desirable to use an improved filament mounting system.

One feature of the instrument which was considered undesirable was the regulation of total emission current rather than the more conventional regulation of anode current. Since the anode current is not necessarily the ionizing current; however, the question is raised as to how the ionizing current should be regulated.

Instability of the ion beam with time can be caused by an unstable source pressure or an unstable ionizing current. An unstable ionizing current can be due to changes in electron beam emission intensity or changes in position. The problem of Ion Source Stability is considered in more detail in the following section.

6.4 Source Stability and Sensitivity Evaluation

6.4.1 Objectives

The objectives of this section are to determine the causes of the source instability noted in Section 6.3 and to more conclusively determine the degree of instability. A by-product of these objectives is determination of the source pressure and sensitivity.

6.4.2 Conclusion

It was concluded that within the limits imposed by pump pressure changes, anode current changes and power supply changes, the ion source is stable. It was determined that the source sensitivity is approximately 1.90×10^{-8} amps per torr per microamp ionization current and that the source pressure is approximately 3.4×10^{-4} torr. It was calculated that the source to pump pressure ratio is only 11.4 with the existing pump and present analyzer outgassing.

6.4.3 Theory

It can be seen from Figure 33 that $Q_S = G_S (P_S - P_p)$, or rearranging terms, $P_S = Q_S/G_S + P_p$. Assuming that Q_S is a constant, the derivitive of source pressure with respect to pump pressure is 1, or a change in pump pressure causes an equal change in source pressure. With this information, the source output current can be corrected for changes in pump pressure in the following manner: The <u>increase</u> in pump pressure is multiplied by the sensitivity of the source at the given ionization current. The product is then <u>subtracted</u> from the higher output current to correct it back to the lower pump pressure. Of course, a drop in pump pressure can be similarly corrected by adding the product of the <u>decrease</u> in pump pressure times the source sensitivity to the lower output current.

6.4.4 Equipment

1 - Differential Volt Meter	John Fluke 803B	3439
1 - Power Supply	John Fluke 407	1161
1 - Power Supply	Hewlett-Packard 721A	304-14768

6.4.4 Equipment continued

1 - DC Micro Volt-Ammeter	Hewlett-Packard 425A	142-05861
1 - Pot Board	CSC	
3 - 0 - 50 Microamp Meters	Triplett	
2 - 0 - 100 Microamp Meters	Triplett	

6.4.5 Procedure

1. The electrode voltages called out in Table XXII were set up using the pot board and the regulated John Fluke supply.

2. The DC Micro Volt-Ammeter was connected between the high resistance positive sector pin and ground. The ion rails and negative sector electrodes were grounded. This connection provides a means of monitoring the ion current into the electric sector.

3. The mass spectrometer was placed in operation with the filament voltage adjusted to 105.5 volts above ground. Lens II was adjusted for maximum ion current. It was important to set the filament voltage using the scan supply before adjusting Lens II.

4. Ion current readings were periodically recorded for several hours. Pump pressure, pump speed, Throughput, I_{total}, I_{rep}, $I_{elec.\ acc.}$, and the John Fluke supply output voltage were simultaneously recorded.

5. The capillary line was leak checked, and the discovered leak was temporarily repaired using duct seal.

6. Step 4 was repeated.

7. From the data obtained in Step 6, calculations were made to determine the source sensitivity, source pressure and source pressure to pump pressure ratio.

6.4.6 Results

1. The results of the first ion stability measurement indicated that there were no correlations between fluctuations in ion current and any of the parameters simultaneously monitored. A plot of the ion current over a period of five hours is given in Table XXIII and Figure 34. During the five hour period over which it was monitored, the ion current was observed to vary plus or minus 11 percent from its mean value.

2. Upon leak checking the capillary line, it was found to have a leak. The leak was temporarily sealed with duct seal.

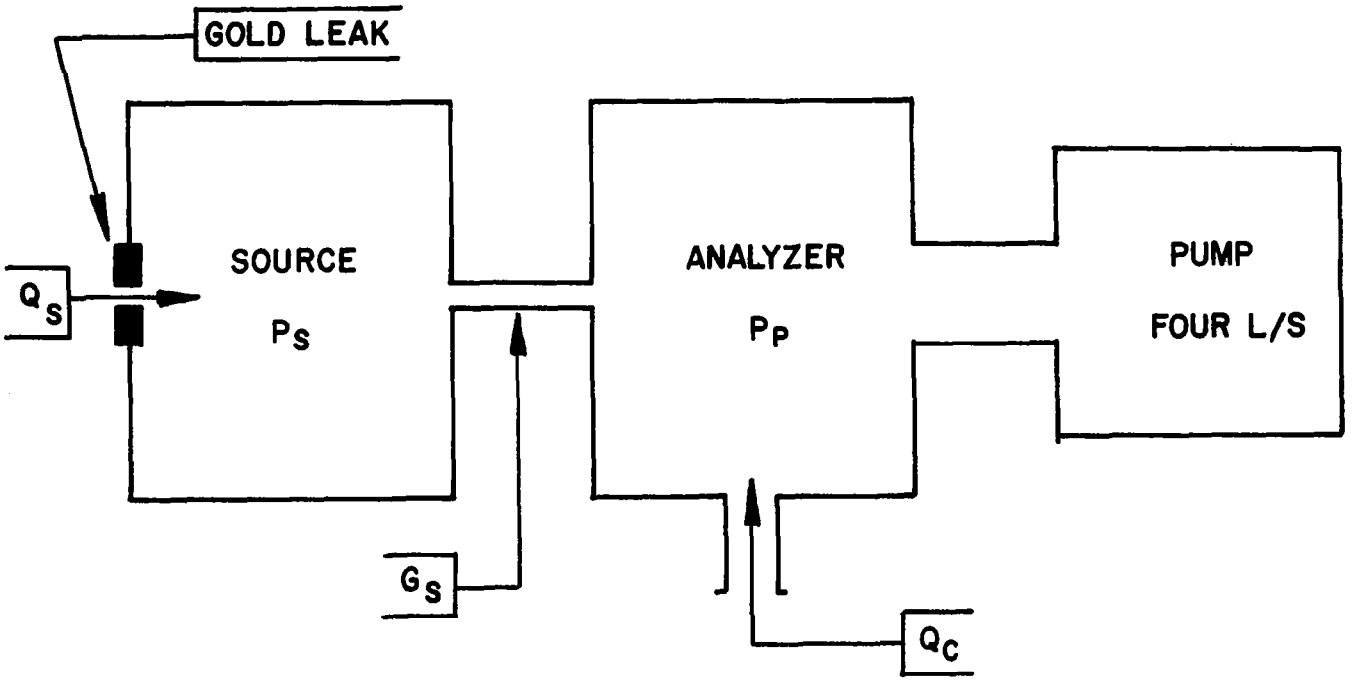

Q_S = GOLD LEAK THROUGHPUT - SAMPLE THROUGHPUT
Q_C = THROUGHPUT DUE TO OUTGASSING - CONTAMINATION THROUGHPUT
P_S = SOURCE PRESSURE
P_P = PUMP PRESSURE
G_S = SOURCE CONDUCTANCE

SIMPLIFIED VACUUM SYSTEM SCHEMATIC

FIG. THIRTY-THREE

3. When Step 4 of the Procedure was repeated, the ion current fluctuations correlated with changes in pump pressure and total emission current. The uncorrected ion current varied plus or minus 2.7 percent from its mean value over a period of four hours. This data is given in Table XXIV and Figure 35. The fluctuation in ion current corrected for changes in pump pressure and changes in total emission is plus or minus .6 percent from the mean value. This is approximately the experimental accuracy. The corrected data is shown in Table XXV and Figure 35.

4. In Step 7 of the Procedure, the source sensitivity and source pressure were calculated, and the ratio of source pressure to pump pressure was noted. The calculation is shown below. The calculation assumes a stable source throughput which is believed to be the case after repair of the capillary line.

$\Delta P_s = \Delta P_{pump} = 4.80 \times 10^{-5} - 3.0 \times 10^{-5} = 1.80 \times 10^{-5}$ torr.

$\Delta I_{out} = 22 \times 10^{-11} - 20.9 \times 10^{-11} = 1.1 \times 10^{-11}$ amps.

Source sensitivity $= \dfrac{1.1 \times 10^{-11}}{1.8 \times 10^{-5}} = .611 \times 10^{-6}$ amps/torr at 32.1 microamps emission.

Source sensitivity $= \dfrac{.611 \times 10^{-6}}{32.1} = 1.90 \times 10^{-8}$ $\dfrac{\text{amps}}{\text{torr-microamp.}}$

Source pressure $= \dfrac{20.9 \times 10^{-11}}{.611 \times 10^{-6}} = 3.42 \times 10^{-4}$ torr.

$\dfrac{\text{Source pressure}}{\text{Pump pressure}} = \dfrac{3.42 \times 10^{-4}}{3.00 \times 10^{-5}} = 11.4$

TABLE XXIII

Ion Beam Stability Data

(with capillary leak)

Time	Operation Time in Hours	Ion Current in Amps	Deviation From Mean in Percent
10:25	0.0	18.3×10^{-11}	-11.0
10:55	.5	21.9×10^{-11}	+ 6.57
11:25	1.0	22.5×10^{-11}	+ 9.50
11:55	1.5	22.6×10^{-11}	+ 9.98
12:25	2.0	22.8×10^{-11}	+11.0
12:55	2.5	22.1×10^{-11}	+ 7.55

TABLE XXIII continued

Time	Operation Time in Hours	Ion Current in Amps	Deviation From Mean in Percent
1:25	3.0	22.3×10^{-11}	+ 8.51
1:55	3.5	22.8×10^{-11}	+11.0
2:25	4.0	22.1×10^{-11}	+ 7.55
2:55	4.5	21.9×10^{-11}	+ 6.57
3:25	5.0	21.6×10^{-11}	+ 5.11
3:55	5.5	21.8×10^{-11}	+ 6.09

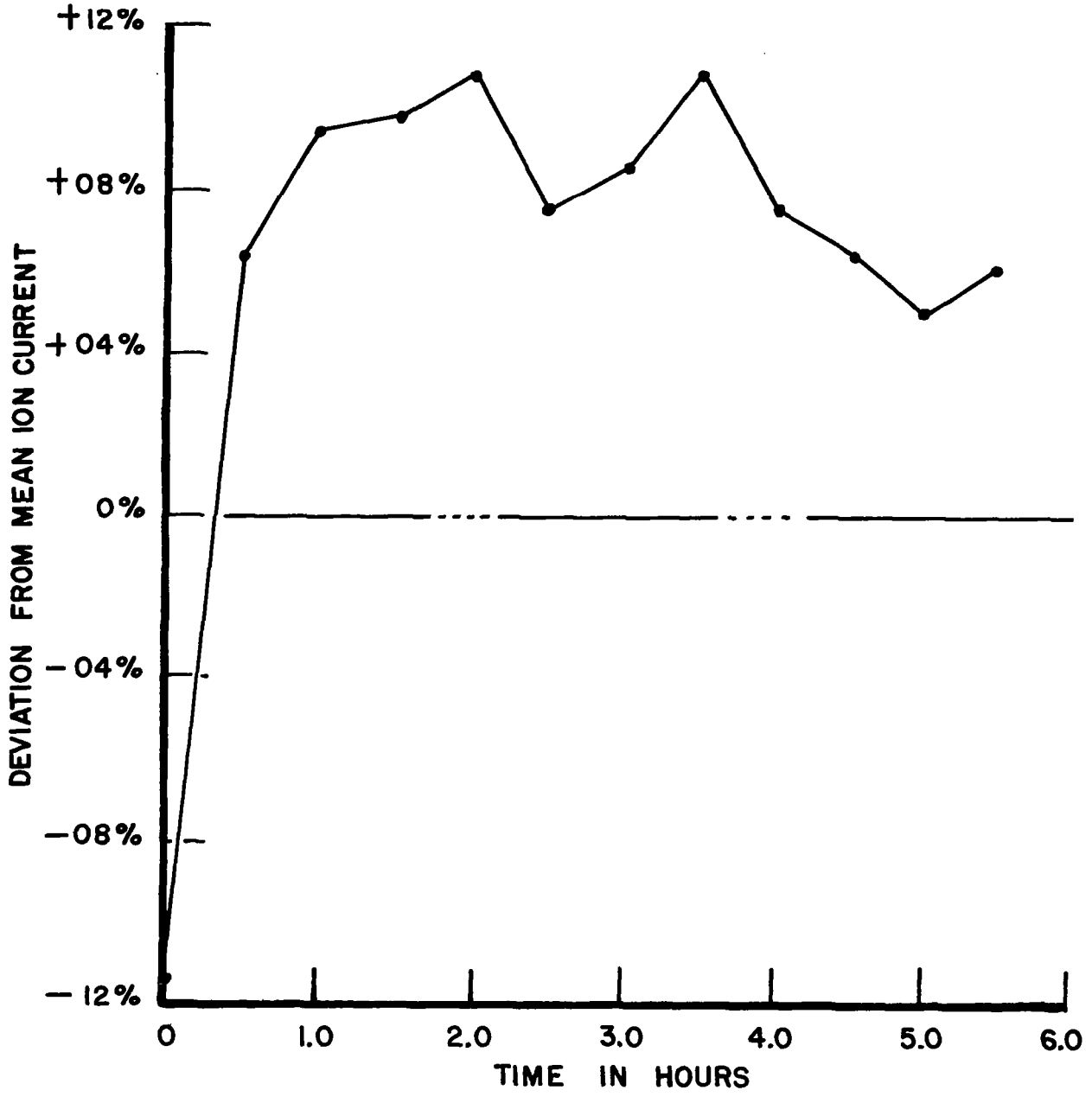

ION BEAM STABILITY
(with capillary leak)

FIG. THIRTY-FOUR

TABLE XXIV

Ion Beam Stability Data

(capillary repaired)

Time in Operation in Hours	I_2 in MA	I_1 in MA	Pump Speed in Liters/Sec.	Throughput in Torr-Liters/Sec.	Pressure in Torr	I_{Total} in Microamps	I_{anode} in Microamps	Source Power Supply Volts	Ion Current in Amps
0.0	1.00	.735	2.53	76.0×10^{-6}	3.00×10^{-5}	39.9	32.1	140.4	20.9×10^{-11}
.5	1.04	.76	2.46	76.8×10^{-6}	3.12×10^{-5}	39.9	32.2	140.4	21.0×10^{-11}
1.0	1.08	.80	2.60	84.1×10^{-6}	3.24×10^{-5}	39.9	32.1	140.4	21.0×10^{-11}
1.5	1.12	.84	2.74	92.0×10^{-6}	3.36×10^{-5}	39.9	32.0	140.5	21.1×10^{-11}
2.0	1.29	.98	2.87	115.0×10^{-6}	3.87×10^{-5}	39.9	32.0	140.5	21.2×10^{-11}
2.5	1.30	.98	2.78	108.2×10^{-6}	3.90×10^{-5}	39.9	32.1	140.5	21.3×10^{-11}
3.0	1.36	1.03	2.84	116.0×10^{-6}	4.08×10^{-5}	39.9	32.1	140.5	21.5×10^{-11}
3.5	1.40	1.06	2.84	119.0×10^{-6}	4.20×10^{-5}	39.7	31.8	140.5	21.4×10^{-11}
4.0	1.60	1.20	2.74	131.0×10^{-6}	4.80×10^{-5}	39.9	32.0	140.5	22.0×10^{-11}

TABLE XXV

Correction of Ion Beam Stability Data

Ion Current in Amps	Deviation From Mean in Percent	Ion Current Corrected for P_p in Amps	Ion Current Corrected for P_p & I_{anode} in Amps	Deviation From Mean of Corrected Ion Current in Percent
20.9×10^{-11}	-2.68	20.900×10^{-11}	20.90×10^{-11}	+.26
21.0×10^{-11}	-2.20	20.923×10^{-11}	20.86×10^{-11}	+.07
21.0×10^{-11}	-2.20	20.854×10^{-11}	20.85×10^{-11}	+.02
21.1×10^{-11}	-1.71	20.881×10^{-11}	20.95×10^{-11}	+.50
21.2×10^{-11}	-1.22	20.669×10^{-11}	20.73×10^{-11}	-.55
21.3×10^{-11}	- .73	20.750×10^{-11}	20.75×10^{-11}	-.45
21.5×10^{-11}	+ .24	20.840×10^{-11}	20.84×10^{-11}	+.02
21.4×10^{-11}	- .24	20.667×10^{-11}	20.86×10^{-11}	+.07
22.0×10^{-11}	+2.68	20.900×10^{-11}	20.96×10^{-11}	+.55

6.4.7 Discussion

The experiments described in this section indicate that the 4 Liter Ion Pump throughput increases by 72 percent (see Table XXIV) in a four hour period. If this 72 percent increase in total throughput had resulted from an increase in sample throughput, Q_s, a corresponding increase in output ion current would have occurred. Since the output current was observed to change only a fraction of this amount, it can be confidently assumed that the increase in pump throughput is not due to a change in Q_s but must be due to outgassing from the pump and walls of the vacuum system. This outgassing throughput is defined as the contamination throughput, Q_c.

When an inlet valve is opened and the sample throughput is first established, the power dissipation in the ion pump increases from less than one watt to over seven watts. The resulting rise in temperature, as would be expected, causes an increase in outgassing and consequently an increase in Q_c. This in turn causes a change in pump pressure, P_p, which, as pointed out in section 6.4.3 effects the source pressure and thus the output. It was indeed noted that the instrument was very unstable for the first 30 to 60 minutes after opening the inlet valve. In the experiments described above, data was not recorded for several minutes after

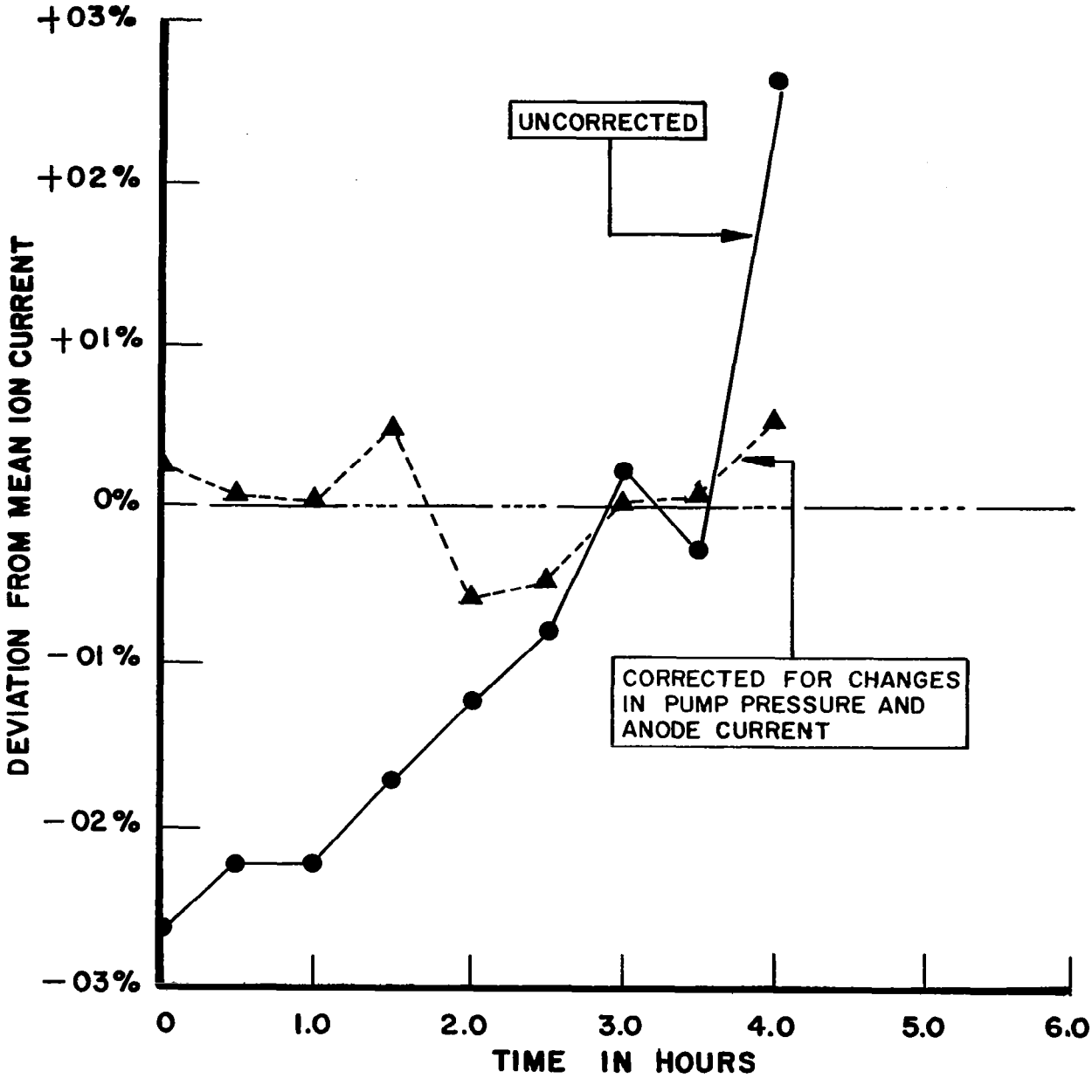

ION BEAM STABILITY
(with capillary repaired)

FIG. THIRTY--FIVE

opening the valve. The question is raised as to when adequate temperature stabilization (and thus stable outgassing) is reached. The results depicted in Figure 34 may be more indicative of an inadequate warm-up period than a leaking capillary.

In section 5.3.6, the effect of discrepancies from the design pump speed were discussed. This discussion assumed that the contamination throughput would be negligible. With the pump throughput limited to the sample throughput, the source to pump pressure ratio would be 34 based upon the source conductance computed by the manufacturer. The above experiments point out that a significant part of the pump throughput can be due to outgassing if the vacuum system is contaminated. The resulting throughput raises the pump pressure without a corresponding increase in source pressure. When this occurs, the more optimum source to pump pressure ratio of 34 decreases to a lesser, more undesirable value. The pressure ratio calculated in section 6.4.6 indicates that the pressure ratio is only 11.4 to 1. With this low pressure ratio, changes in pump pressure due to changes in outgassing rate or pump speed will have a much greater effect upon source pressure and thus the output.

7. ANALYZER EVALUATION

7.1 Description and Theory of Operation

The Analyzer can be divided into three parts: The Lens II region, the electric sector and the magnetic sector. The function and operation of the three areas are described below.

Lens II: The ribbon shaped ion beam emerging from the ion source tends to diverge due to the distortion of the electric field about the source exit slit. This is shown in Figure 36. The function of the Lens II electrode is to correct this divergence. Lens II is physically located six tenths of the distance between the ion source exit slit and the electric sector entrance slit measuring from the latter. The electric sector entrance slit is operated at ground potential. The ion source exit slit is maintained at the ion accelerator potential. If the potential of Lens II is maintained at 60 percent of the ion accelerator potential, the electric field in the region between the slits is not distorted by the Lens II electrode, and the divergent path of the ion beam is not influenced by the presence of Lens II. On the other hand, if Lens II is at a higher potential than 60 percent of the ion accelerator voltage, the field in the region between the slits is distorted in the manner shown in Figure 36. The distorted field causes the ion beam to be less diverging or converging depending upon the degree to which Lens II is raised above the 60 percent value of ion accelerator voltage. The beam intensity entering the electric sector is, therefore, improved by the focusing action of Lens II. Normally, the beam is not focused to a point at the entrance slit due to the resulting angular spread. The focusing is thus a compromise between the tolerable angular spread and a high beam intensity.

Electric Sector: The electric sector serves as an ion beam energy filter. The electric sector (See Figure 37) is bounded by four electrodes: a positive or outer sector, a negative or inner sector and a top and bottom rail. The positive and negative sectors are concentric and form a 60° arc. The ions travel in a circular path between the outer and inner electrodes due to the centripetal force, $F = eE$, [12] which results from the electric field in this region. The ions travel through the electric sector with a velocity v equal to $\sqrt{\frac{2eV}{m}}$ [13].

The radius of the ion path is given by the equation:

$$r = \frac{mv^2}{F} = \frac{mv^2}{eE} = \frac{m\,\frac{2eV}{m}}{eE} = \frac{2V}{E}$$

[12] F is the force in newtons, e is the change in coulombs of the particle and E is the electric field in volts/meter.

[13] v is the velocity in meters/sec., m is the mass in kilograms and V is the acceleration voltage - see Footnote 15.

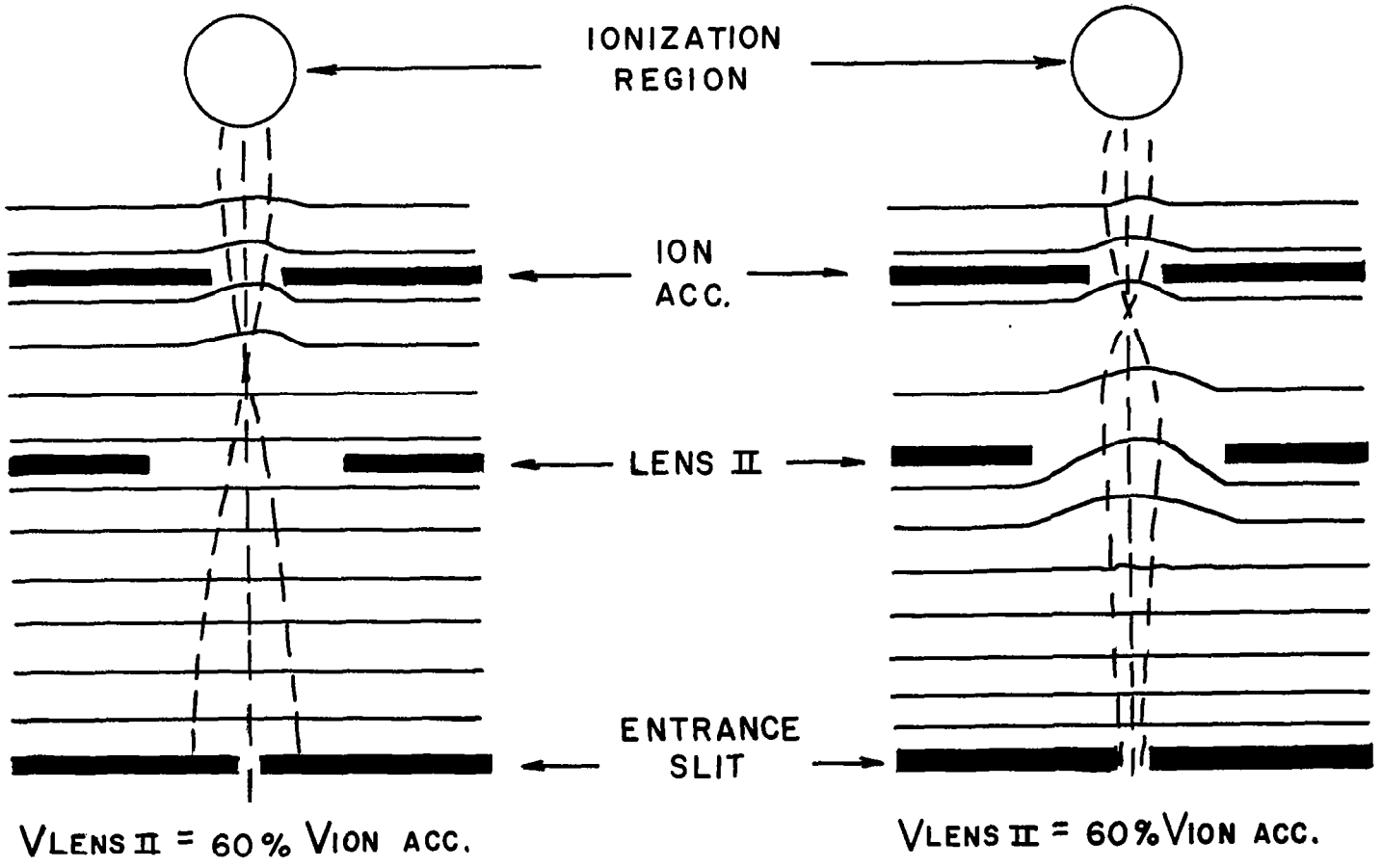

LENS II FOCUSING

FIG. THIRTY-SIX

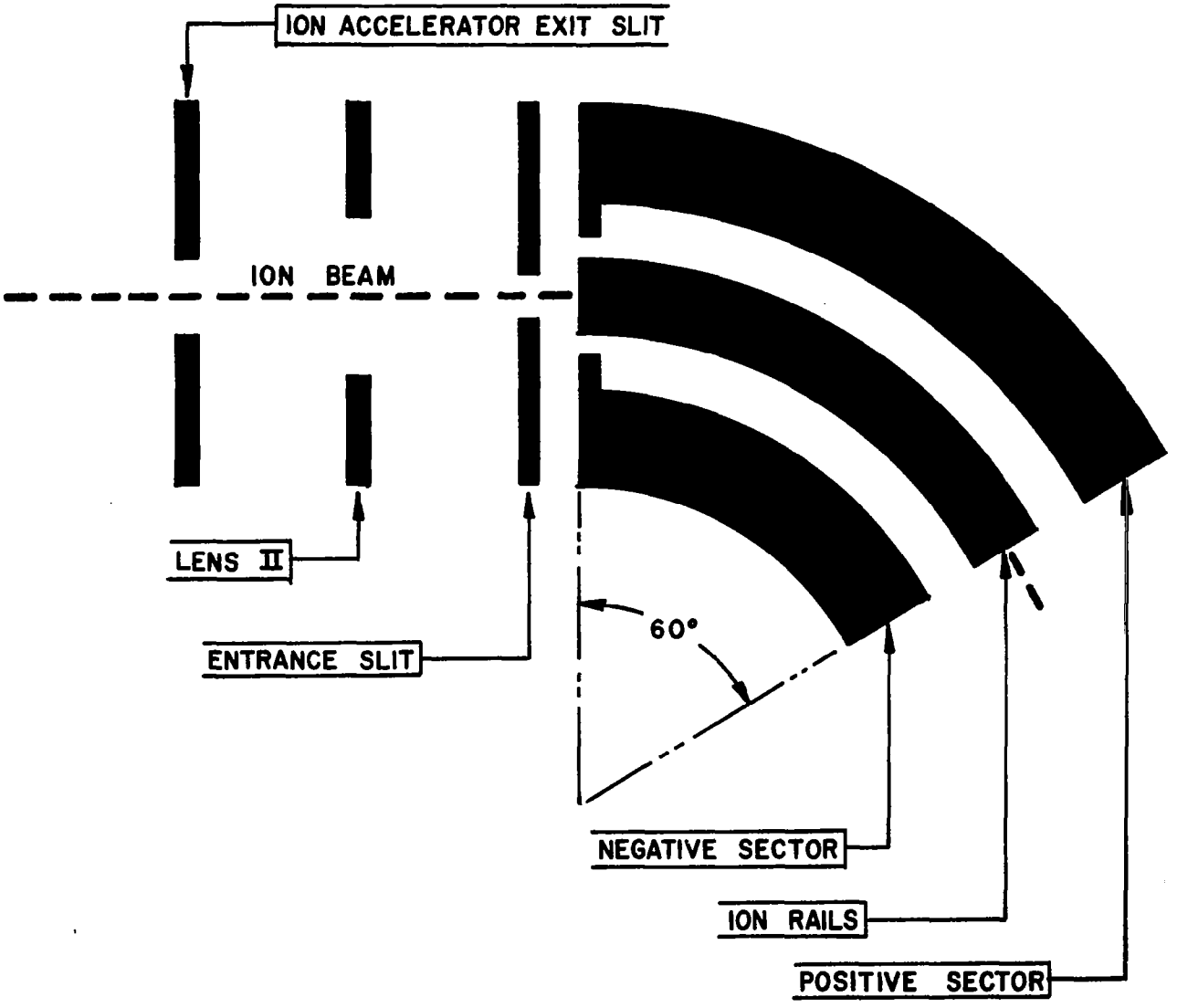

ELECTRIC SECTOR SCHEMATIC

FIG. THIRTY - SEVEN

It is seen from the preceding equation that all ions will simultaneously follow the same circular path regardless of mass.

The unique feature of the electric sector is that the electric field in this region can be changed from a spherical to a cylindrical to a toroidal configuration simply by changing the voltage on the rails. The top and bottom rails are at the same potential. If the rail voltage is at the center potential of the positive and negative sectors, the electric sector appears to the ion beam as a cylindrical condenser field. If the rail voltage is positive with respect to the center potential, the electric sector field approximates a spherical field. If the rail voltage is negative with respect to the center potential, the electric field approximates a toroidal field. This is shown in Figure 38.

Magnetic Sector: Upon emerging from the electric sector the ion beam enters the 90° magnetic sector. In this region, the monoenergetic beam is separated into beams of single m/e ratios. The ions of a given m/e ratio follow a path of radius r equal to $\frac{mv^2}{F_m} = \frac{mv^2}{evB} = \frac{1}{B}\sqrt{\frac{2mV}{e}}$ [14]

The different ion beams pass through their respective collector slits and are collected by the twelve collector buckets. Ions (or ion beams) which do not have one of the twelve m/e ratios necessary to enter one of the collector slits, strike the collector slit plate and are not measured by an electrometer. The ions strike the plane of the collector slits at an angle of 38°. The complete ion path is shown schematically in Figure 39. The ion deflections in the magnetic sector are shown in Figure 40. By construction of the square ABCD and the triangle ECD in Figure 40, it can be seen that the ion radius for any given collector bucket is $r = X\sin 38°$ where X is the distance of the collector bucket from the theoretical entrance point.

One of the most important measurements in evaluating the analyzer is a beam width measurement. The derivation of the equation used in this measurement is given below.

The slit distance X is equal to the radius divided by sin38°.

$$X = \frac{r}{\sin 38°} = \frac{1}{\sin 38°} \frac{1}{B}\sqrt{\frac{2mV_{acc}}{e}}$$

$$\frac{dX}{dV_{acc}} = \frac{1}{\sin 38°} \frac{1}{B}\sqrt{\frac{m}{2eV_{acc}}}$$

In measuring the beam width, the electrometer output is recorded on the y axis of an X-Y recorder while a voltage proportional to the acceleration voltage is recorded on the x axis. As the acceleration voltage is scanned, the beam moves across the slit drawing a trapezoidal (if the beam width is less than the slit width) shaped peak on the X-Y recorder. Although $\frac{dX}{dV_{acc}}$ is a function of V_{acc}, the change in V_{acc} required to sweep the beam across the slit is sufficiently small that

[14] F_m equals the magnetic force, B equals the magnetic field intensity in webers/meter

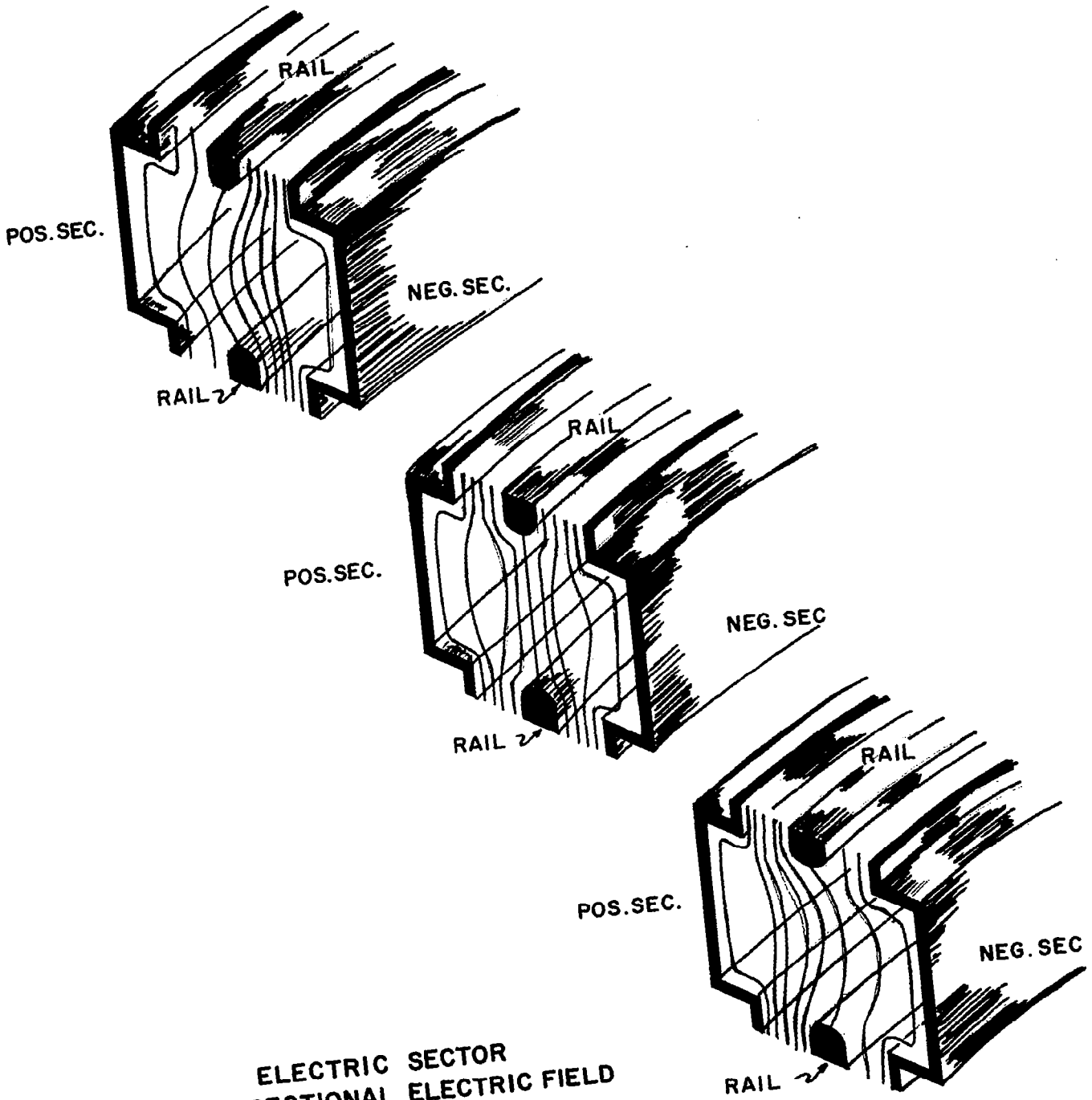

ELECTRIC SECTOR
CROSS SECTIONAL ELECTRIC FIELD

FIG. THIRTY-EIGHT

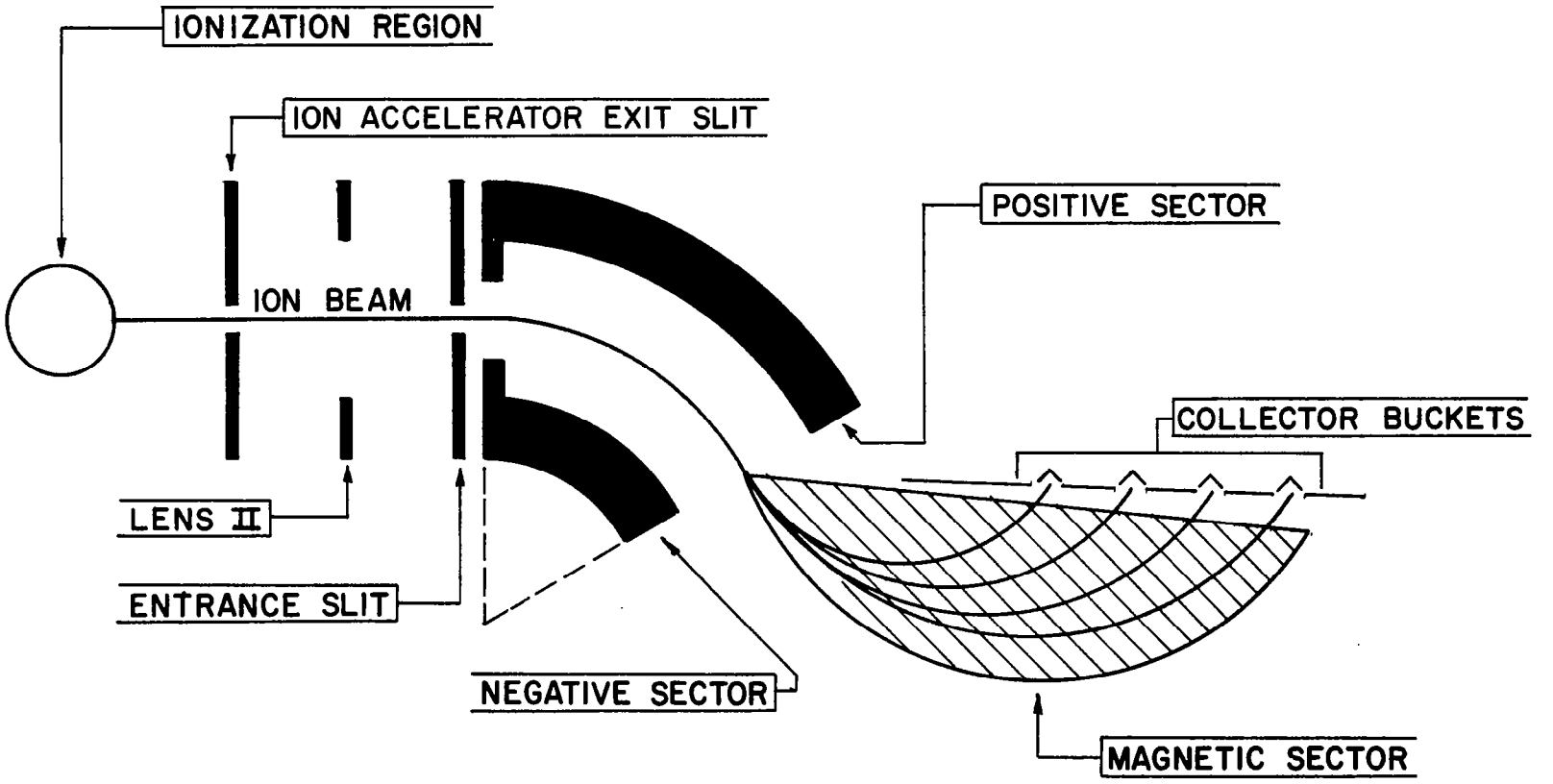

ION PATH SCHEMATIC

FIG. THIRTY - NINE

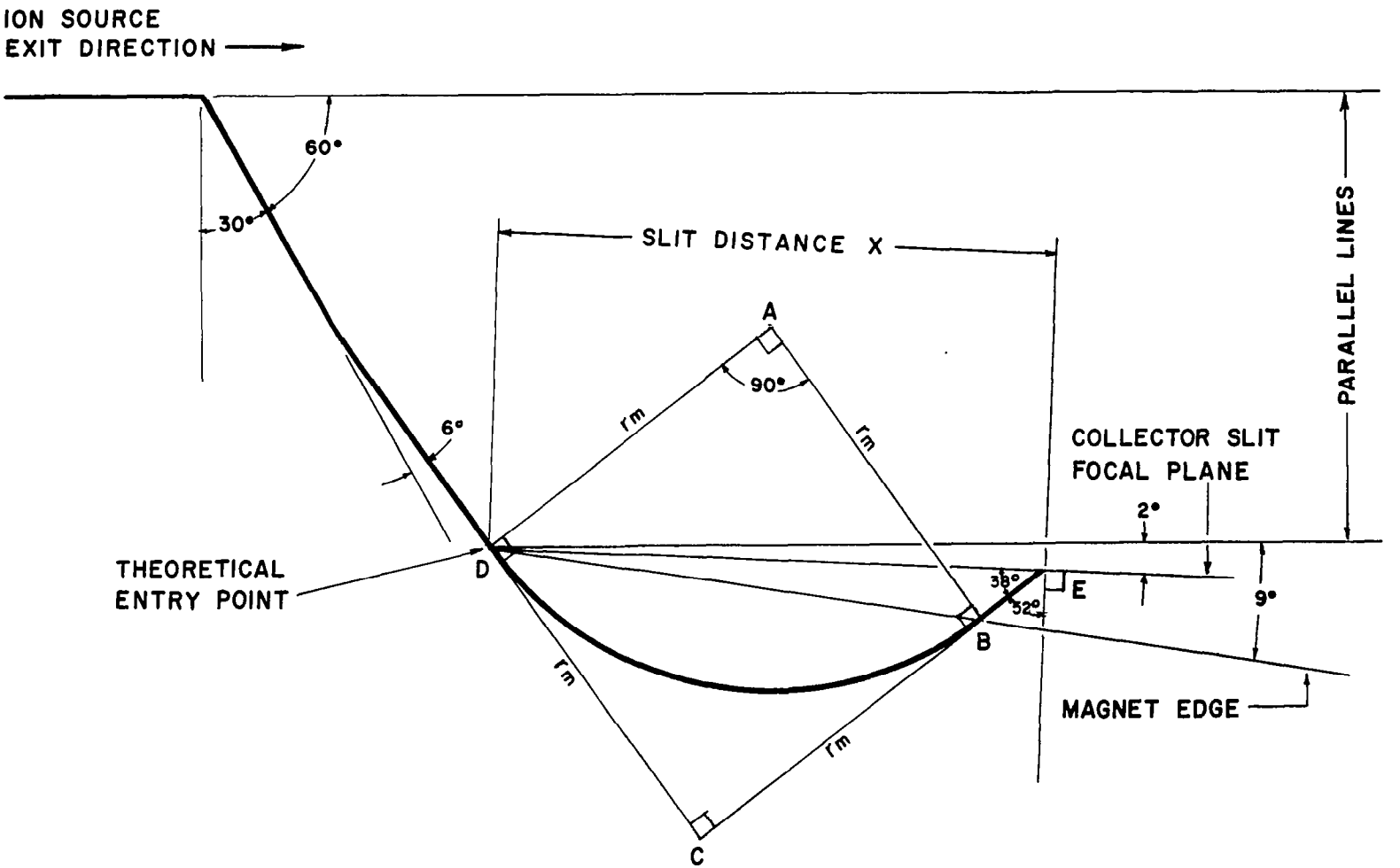

ION PATH ANGULAR DEFLECTIONS

FIG. FORTY

$\frac{dX}{dV_{acc}}$ can be considered a constant for the purpose of the measurement. The distance traveled by the beam is thus proportional to the change in acceleration voltage or to the change in acceleration voltage sample voltage recorded on the x axis.

$$\Delta X_{beam} = \frac{dX}{dV_{acc}} \cdot \Delta V_{acc} \simeq K\Delta_{acc} \propto \Delta V_{acc\ sample} \propto \Delta X_{recorder}.$$

If the slit width is known, it therefore becomes possible to determine the beam width by measuring the top and bottom of the recorded trapezoid with any arbitrary linear scale. The top, X_1, of the trapezoid is proportional to the slit width, S, minus the beam width, B, while the bottom X_2, of the trapezoid is proportional to the slit width plus the beam width. This is shown in Figure 41.

$$X_1 = K(S-B)$$

$$X_2 = K(S+B)$$

where K is the constant of proportionality.

$$(X_2 - X_1) = 2KB$$

$$B = \frac{(X_2 - X_1)}{2K}$$

$$(X_2 + X_1) = 2KS$$

$$K = \frac{(X_2 + X_1)}{2S}$$

Substituting for K

$$B = \frac{(X_2 - X_1)}{(X_2 + X_1)} = S\left(1 - \frac{2X_1}{X_2 + X_1}\right)$$

7.2 Selection of Analyzer Electrode Potentials

7.2.1 Objectives

The objectives of this section are to determine the optimum analyzer electrode potentials, to determine the advantages and disadvantages of a stronger analyzer magnet, to measure the analyzer ion efficiency and beam width and to draw conclusions as to the overall sensitivity and resolution to be expected from the mass spectrometer.

7.2.2 Conclusion

It was concluded that the best resolution would be obtained by adjusting the

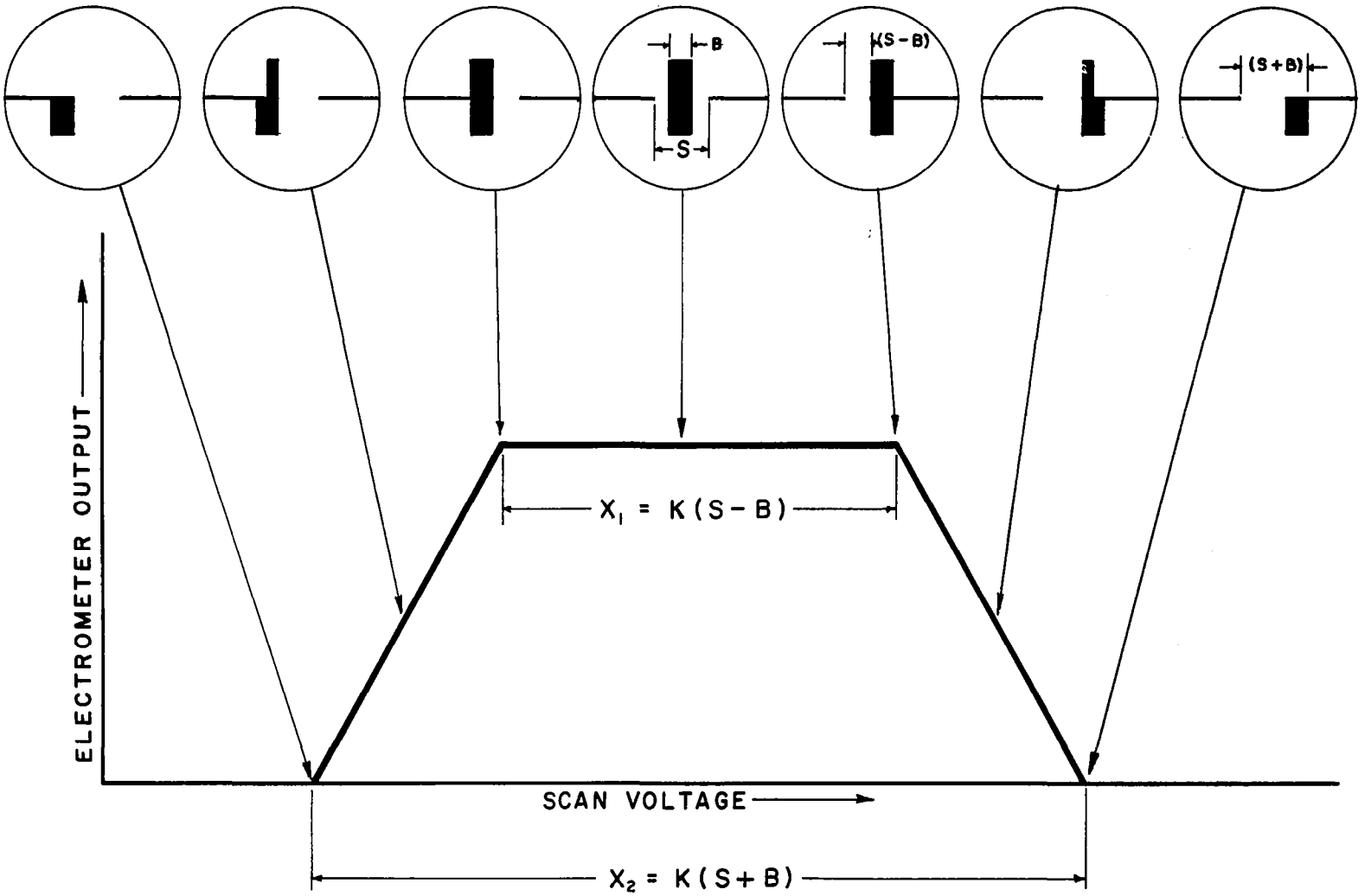

ION BEAM POSITION vs. ELECTROMETER OUTPUT

FIG. FORTY - ONE

delta sector voltage [16] to 80 to 85 percent of the acceleration voltage [15] and by adjusting the ion rail with respect to negative sector voltage to 42 to 47 percent of the delta sector voltage. It was determined that any increase in the Lens II potential above the 60 percent of ion accelerator voltage would depreciate the instrument resolution but increase the sensitivity. It was concluded that a Lens II voltage equal to approximately 80 percent of the ion accelerator voltage provides a reasonable compromise between instrument sensitivity and resolution. It was noted that the exit slit and entrance slit are not aligned.

Firm conclusions as to the proper operating potential of the Z-axis electrode are difficult to make due to the fact that this electrode at times behaves differently than at other times. This electrode has been normally adjusted to near ground potential; however, at times better resolution has been obtained by adjusting the Z-axis potential to approximately minus 30 volts with respect to ground.

The acceleration voltage necessary to focus the given beams in their proper slits was found to be 118 volts for the regular magnet and 230 volts for the spare magnet. It was concluded that better performance could be achieved by using the stronger magnet; although some modifications in the electronics and in the bucket positions would be necessary to do this.

Analyzer efficiencies in the neighborhood of 30 percent were obtained using the stronger magnet while an ion efficiency of 10 percent was the best obtainable with the weaker magnet. The stronger magnet also improves the overall instrument sensitivity by increasing the operating level of the ion accelerator voltage and thus improving the focusing action of the Lens II electrode.

Diagonal beam widths[17] of 7.5 mils for the 28 peak and 10.5 mils for the 44 peak were measured using the weaker magnet. The diagonal beam width with the instrument tuned for maximum sensitivity is estimated to be 50 mils using the weaker magnet. If the collector slit width would accommodate this beam width, it is estimated the instrument sensitivity could be increased by a factor of five over the high resolution mode of operation.

It was concluded that the filament position is a changing quantity which has a definite but yet unknown effect upon the operation of the analyzer.

---

[15] The acceleration voltage is defined as the total potential in volts through which the particle has been accelerated from the point of ionization to the potential at the center of the electric sector. Acceleration voltage is thus the algebraic sum of three potentials: the potential difference between the ionization region and the ion accelerator, the ion accelerator to entrance slit potential and the entrance slit to mean electric sector potential. When the acceleration voltage is discussed in conjunction with the magnet, the third potential is modified to be from the entrance slit to the mean magnetic sector potential (usually zero).

[16] The delta sector voltage is the voltage difference between the positive sector and negative sector electrodes.

[17] The term diagonal beam width is used as the beam does not enter the collector slit perpendicularly. The perpendicular beam width will equal the diagonal beam width times cos 52°.

It was concluded that without changing the magnet or performing the circuit and physical modifications implied by the change, the mass spectrometer would have a minimum detectable level of 800 ppm with a resolution of one part in forty-five and a usable mass range up to m/e equal 80.

7.2.3 Equipment

Differential Volt Meter	John Fluke 803B	3439
X-Y Recorder	Electronic Association 1120	118
DC Micro Volt-Ammeter	Hewlett-Packard 425A	142-05861
Potentiometer Board	CSC	

7.2.4 Procedure

1. The Micro-Ammeter was set up to measure the ion current into the electric sector. The meter was connected between the positive sector and ground. The negative sector and ion rails are grounded in making this setup.

2. The ion accelerator voltage was fixed at 100 volts.

3. The ion current into the electric sector was recorded as the Lens II potential was changed in increments of 10 percent of the ion accelerator potential.

4. Steps 2 and 3 were repeated at ion accelerator potentials of 150 and 200 volts.

5. The source potentials with respect to the filament were adjusted to the voltages recorded in Table XXII. Some modification of the filament shield potential and the electron focus potential were necessary due to a change in filament position.

6. An energy spread measurement was made using the procedure described in section 6.3. The potential of the ionization region with respect to the ion accelerator was determined by subtracting the ion accelerator voltage from the center ion potential.

7. The high voltage power supply was adjusted so that the 28 beam was centered in the center of the 28 collector slit. This is easily done by drawing a peak on the X-Y recorder using the scan switch and then setting the recorder pen to the center of the peak by adjusting the voltage manually.

8. ΔV_{sec} was measured and found to be approximately 100 volts. The ΔV_{sec} pot. was adjusted so this voltage was exactly 100 volts to simplify the calculations.

9. The positive and negative sector potentials were measured with respect to the entrance slit (ground), and the mean electric sector potential was calculated.

10. The potentials calculated in Steps 6 and 9 were algebraically subtracted. This difference voltage plus $V_{ion\ acc}$ comprise the acceleration voltage, V_{acc}.

11. A table was made up with the following column headings: $\frac{\Delta V_{sec}}{V_{acc}}$, V_{acc}, $V_{ion\ acc}$, Lens II. Values of V_{acc} were calculated for $\frac{\Delta V_{sec}}{V_{acc}}$ ratios from .80 to .95 assuming a value of 100 volts for ΔV_{sec}. $V_{ion\ acc}$ was calculated by subtracting the potential calculated in Step 10 from V_{acc}. Lens II was calculated by multiplying $V_{ion\ acc}$ by .6.

12. To set up a given $\frac{\Delta V_{sec}}{V_{acc}}$ ratio with constant $\frac{\text{Lens II}}{V_{ion\ acc}}$ and constant $\frac{V_{ion\ rail} - V_{neg.\ sec.}}{\Delta V_{sec}}$. The following procedure is used: Maintaining the ΔV_{sec} pot in one position, the ΔV_{sec} voltage is adjusted to 100 volts with the H. V. supply. While maintaining the ion accelerator pot in one position, the ion accelerator is adjusted to the value in the table using the injection pot.[18] The Lens II potential is then adjusted to the value listed in the table using the Lens II pot. The ion rail pot remains in one position. The z-axis electrode is adjusted to zero volts with the z-axis pot.

13. A peak was drawn with the instrument adjusted to each of the $\frac{\Delta V_{sec}}{V_{acc}}$ ratios listed in the table. It should be noted that the electrode voltage ratios are maintained to the first degree as the high voltage supply is scanned over a small range; although, it is necessary to make the setup at a high voltage setting which is approximately equal to the voltage present when the beam is in the slit. If the electrode voltages are not set up at approximately their operating potentials, the fixed potential between the ionization region and the ion accelerator will cause a change in the electrode voltage ratios as the high voltage is scanned.

14. The optimum $\frac{\Delta V_{sec}}{V_{acc}}$ ratio was selected from the results in step 13, and these conditions were again set up.

15. A table was made up of ion rail potentials for various $\frac{V_{ion\ rail} - V_{neg\ sec.}}{\Delta V_{sec}}$ ratios ranging from 20 to 70 percent. ΔV_{sec} was adjusted to be 100 volts. Increments of 2.5 percent were taken in the 50 percent region and larger increments in the less sensitive areas. A peak was drawn at each of the different rail settings.

16. The optimum $\frac{V_{ion\ rail} - V_{neg\ sec.}}{\Delta V_{sec}}$ was selected from the results in step

[18] The injection pot raises the potential of the source electrodes, ion acc., rep. etc., with respect to the analyzer electrodes ion rails, pos. sec. etc. while maintaining the potentials between the source electrodes constant.

15, and this condition was again set up.

17. The z-axis focus voltage was changed in increments of 10 volts both in a negative and positive direction, and a peak was drawn at each setting.

18. The optimum z-axis focus potential was selected from the results in step 17 and this z-axis potential was again set up.

19. Steps 12 through 18 were repeated.

20. The Lens II electrode was changed in increments of 5 percent of the ion accelerator voltage, and a peak was drawn at each setting.

21. The optimum Lens II potential was selected from the results in step 20, and this Lens II potential was again set up.

22. Steps 12 through 18 were again repeated.

23. The analyzer magnet was removed and replaced with the recently recharged spare magnet.

24. An investigation was made of the performance of the instrument with the stronger magnetic field.

25. The original magnet was re-installed.

26. The operation of the instrument was again evaluated to assure the change in performance noted in step 24 was due to the change in magnetic field.

27. The performance of the instrument with small changes in magnet position was noted. Changes in magnet position in three different axis were investigated.

28. The instrument was vented, and the filament position was purposely offset approximately 10 mills from its center position in a direction perpendicular to the slit and away from the center of the source.

29. After pump down, the operation of the instrument was noted and compared to the operation of the instrument with proper filament alignment.

30. The instrument was again vented. The filament was realigned, and the instrument pumped down.

31. Step 1 was repeated, and the total ion current into the electric sector was recorded.

32. The total ion current reaching the collector buckets was calculated by dividing the output voltage of each electrometer by its sensitivity and summing the results. The beams were scanned across their respective buckets to assure an accurate measurement.

33. The ion efficiency was calculated by dividing the results of Step 32 by the number of total ions recorded in Step 31.

34. Beam width measurements were made of the 28 and 44 beams. This was done using the procedure outlined in Section 7.1.

35. Using the selected electrode voltage ratios and the original magnet, the coincidence of the various beams focusing in their respective slits was studied.

36. The collector slits were adjusted according to the findings in Step 35.

37. An overall mass spectrometer minimum detectable signal was calculated. A 50 mv output on a 5 x 10^{12} ohm sensitivity amplifier was used as the criterion of a detectable signal.

7.2.5 Results

1. The results of Steps 1 through 4 of the Procedure are given in Tables XXVI through XXVIII and in Figure 42.

2. The results of Step 6 of the Procedure are given in Table XXIX and Figure 43. The potential of the ionization region with respect to the ion accelerator was found to be 117.3 - 105.7 = +11.6.

3. In Step 9 of the Procedure, the positive sector was found to be at a voltage of +48.4 and the negative sector at a voltage of -51.6. The mean was calculated to be -1.6 volts.

4. In Step 10, the voltage difference between V_{acc} and $V_{ion\ acc}$ was calculated to be 11.6 --1.6 = 13.2 volts.

5. In Step 11 of the Procedure, Table XXX was made up of the various electrode potentials for different $\frac{\Delta V_{sec}}{V_{acc}}$ ratios with constant $\frac{V_{Lens\ II}}{V_{ion\ acc}}$ and constant $\frac{V_{ion\ rail} - V_{neg\ sec}}{\Delta V_{sec}}$.

6. In Step 15, Table XXXI was made up to give the various Ion Rail voltages for different $\frac{V_{ion\ rail} - V_{neg\ sec}}{\Delta V_{sec}}$ ratios.

7. Steps 12 through 18 of the Procedure were repeated in Step 22. It is assumed that $\frac{\Delta V_{sec}}{V_{acc}}$, $\frac{V_{ion\ rail} - V_{neg\ sec}}{\Delta V_{sec}}$, $\frac{V_{Lens\ II}}{V_{ion\ acc}}$, and $V_{z\text{-}axis}$ were adjusted to their optimum values with this step. Best operation was experienced at the following ratios:

$$\frac{\Delta V_{sec}}{V_{acc}} = .825 \pm .025$$

$$\frac{V_{\text{ion rail}} - V_{\text{neg sec}}}{\Delta V_{\text{sec}}} = .450 \pm .025$$

$$\frac{V_{\text{Lens II}}}{V_{\text{ion acc}}} = .80 \pm .10$$

$$V_{\text{z-axis}} = -5v \pm 5v.$$

8. The result of replacing the original analyzer magnet with the recently recharged spare magnet was to improve the instrument sensitivity by a factor of four while simultaneously improving the instrument resolution. Since the field strength of the spare magnet was approximately 1.5 times the field strength of the original magnet and since the ratio of $\sqrt{V_{acc}}$ to B must be the same with each magnet due to the physical geometry, V_{acc} was approximately two and a quarter times greater with the stronger magnet. Since the largest part of V_{acc} is $V_{ion\ acc}$, $V_{ion\ acc}$ was approximately a factor of two larger with the stronger magnet. This would have improved the focusing properties of Lens II. In other words, the ion beam into the electric sector would have had greater intensity for the same angular spread. From Figure 42, it is noted that a factor of 1.5 of the improved sensitivity could be explained by an increase of ions into the electric sector due to better focusing in the Lens II region. It was concluded that the ion efficiency of the analyzer improved by a factor of approximately (4/1.5) = 2.6 with the stronger magnet.

9. When the original analyzer magnet was reinstalled, the instrument performance was as before the installation of the spare magnet. This provided confirmation that the noted improvement in instrument performance was due to the installation of the spare magnet.

10. In Step 27 of the Procedure, the performance of the instrument was evaluated at different magnet positions. The original magnet was used in this experiment. A factor of two improvement in instrument sensitivity was achieved by adjusting the magnet position. The final magnet position is shown in Figure 44.

11. Offsetting the filament in Step 28 of the Procedure did not notably effect instrument sensitivity or resolution. A change in the coincidence of the various mass beams in their respective slits did occur, however, with the change in filament position. It is believed that the filament moves with time and temperature. This is based upon the fact that the electron distribution changes during filament warm-up and from day to day.

12. In Step 31, the total ion current into the electric sector was found to be 125 picoamps.

13. The two most significant ion output currents with an air sample are the mass 28 and 32 collector currents. The 28 bucket current was found to be 2 volts/ 2×10^{11} ohms = 1×10^{-11} amps = 10 picoamps. The 32 bucket current was found to be 1.25 volts/5×10^{11} ohms = $.25 \times 10^{-11}$ amps = 2.5 picoamps. All other collector bucket currents were insignificant compared to the sum of these two, 12.5 picoamps.

14. In Step 33 of the Procedure, the analyzer efficiency was calculated by

dividing the results of Step 12 into the results of Step 13. Analyzer ion efficiency was calculated to be 12.5/125 = 10 percent. As was discussed in Step 8, the analyzer ion efficiency is much better than this with the stronger magnet; although, the measurement was not made directly.

15. In Step 34 of the Procedure, beam width measurements of the 28, and 44 mass beams were made at their respective buckets. The diagonal beam widths measured were 7.5 mils for the m/e 28 beam and 10.5 mils for the m/3 44 beam.

16. In Step 34 of the Procedure, it was noted that the 18, 28 and 32 beams were centered in their respective slits at a slightly lower high voltage setting than the 44 beam. The collector slits are fabricated in four assemblies: m/e 2; m/e 12, 15, 17 and 18; m/e 28, 29, 32 and 34; m/e 42, 44 and 45. Due to this construction, it is not possible to move the position of one collector slit without also moving the position of the other slits in that group. For example, it was noted that the m/e 28 and m/e 32 beams were not exactly coincident; although, the degree of mis-alignment was small enough to be tolerated. If this had not been the case, the 28, 29, 32 and 34 collector assembly would have had to been refabricated. It was determined that satisfactory coincidence could be achieved by moving the 28 bucket group 6.5 mils toward the 44 bucket and moving the 12 groups 5.0 mils in the same direction. The 42 group is the reference group, and it is not adjustable.

17. When the 12 and 28 collector slit assemblies were adjusted as indicated in Step 35 of the Procedure, the coincidence of the 18, 28, 29, 32 and 44 beams was observed and found to be satisfactory.

18. With an atmospheric sample, the total output ion current was found to be 12.5×10^{-12} amps. The minimum detectable output is considered to be 50 m.v. This is the peak to peak output noise of the 5×10^{12} ohm electrometers with a bandpass of 5 cps. The minimum detectable ion current is, thus, 50×10^{-3} volts/5×10^{12} ohms = 10×10^{-15} amps or 1×10^{-14} amps. The minimum detectable concentration is therefore $1 \times 10^{-14}/1.25 \times 10^{-11}$ equals $.8 \times 10^{-3}$ or 800 ppm. Minimum detectable levels of four times this value or 200 ppm were observed using the stronger analyzer magnet. There was no depreciation of the instrument resolution with the higher magnetic field. It is estimated that the sensitivity (and thus minimum detectable concentration) could be increased by a factor of five by tuning the instrument for maximum sensitivity. It is estimated that the resolution would be reduced to one part in eight under this condition.

19. The instrument resolution using the 44 collector was found to be one part in 45 for 2 percent crosstalk between adjacent peaks of the same height.

7.2.6 Discussion

The two most ambiguous parameters in the mass spectrometer are the filament position and the proper magnet position. The former is difficult to measure since filament position seems to change with time and with warm-up. A complete documented investigation of instrument performance with different magnet positions would be a prodigious task. This is due to the fact that the degradation in performance caused by a change in magnet position can often be compensated by a change in

electrode potentials. As the determination of the optimum electrode potentials for one magnet position is in itself a big job, it can be readily seen that a complete investigation of instrument performance with the magnet position varied vertically, horizontally and rotationally along two different axis with various combinations of movement would be an almost endless project. The problem is even further complicated by variations in magnet strength and charging patterns. Sufficient evaluation of magnet position and strength has been made to definitely say that these parameters are critical to proper operation.

TABLE XXVI

Total Ion Current vs. Lens II Voltage

($V_{ion\ acc}$ = 100 volts)

Lens II Voltage in Volts	Lens II Voltage in Percent of $V_{ion\ acc}$	Total Ion Current in Amps
10	10	7.2×10^{-11}
20	20	8.0×10^{-11}
30	30	9.0×10^{-11}
40	40	10.2×10^{-11}
50	50	11.5×10^{-11}
60	60	12.5×10^{-11}
70	70	13.2×10^{-11}
80	80	14.0×10^{-11}
90	90	14.9×10^{-11}
100	100	2.8×10^{-11}

TABLE XXVII

Total Ion Current vs. Lens II Voltage

($V_{ion\ acc}$ = 150 volts)

Lens II Voltage in Volts	Lens II Voltage in Percent of $V_{ion\ acc}$	Total Ion Current in Amps
15	10	6.7×10^{-11}
30	20	7.4×10^{-11}
45	30	8.3×10^{-11}
60	40	9.7×10^{-11}
75	50	11.8×10^{-11}
90	60	14.5×10^{-11}
105	70	17.2×10^{-11}
120	80	19.2×10^{-11}
135	90	16.8×10^{-11}
150	100	4.0×10^{-11}

TABLE XXVIII

Total Ion Current vs. Lens II Voltage

($V_{ion\ acc}$ = 200 volts)

Lens II Voltage in Volts	Lens II Voltage in Percent of $V_{ion\ acc}$	Total Ion Current in Amps
20	10	6.3×10^{-11}
40	20	6.9×10^{-11}
60	30	7.7×10^{-11}
80	40	8.9×10^{-11}
100	50	10.8×10^{-11}
120	60	14.1×10^{-11}

TABLE XXVIII continued

Lens II Voltage in Volts	Lens II Voltage in Percent of $V_{ion\ acc}$	Total Ion Current in Amps
140	70	19.0×10^{-11}
160	80	23.0×10^{-11}
180	90	14.5×10^{-11}
200	100	1.8×10^{-11}

TABLE XXIX

Determination of Injection Voltage

Electrometer Repelling Voltage in Volts	Ion Current in Amps
105	50.5×10^{-12}
110	50.5×10^{-12}
114	48.0×10^{-12}
115	44.0×10^{-12}
116	38.0×10^{-12}
118	20.0×10^{-12}
120	4.0×10^{-12}

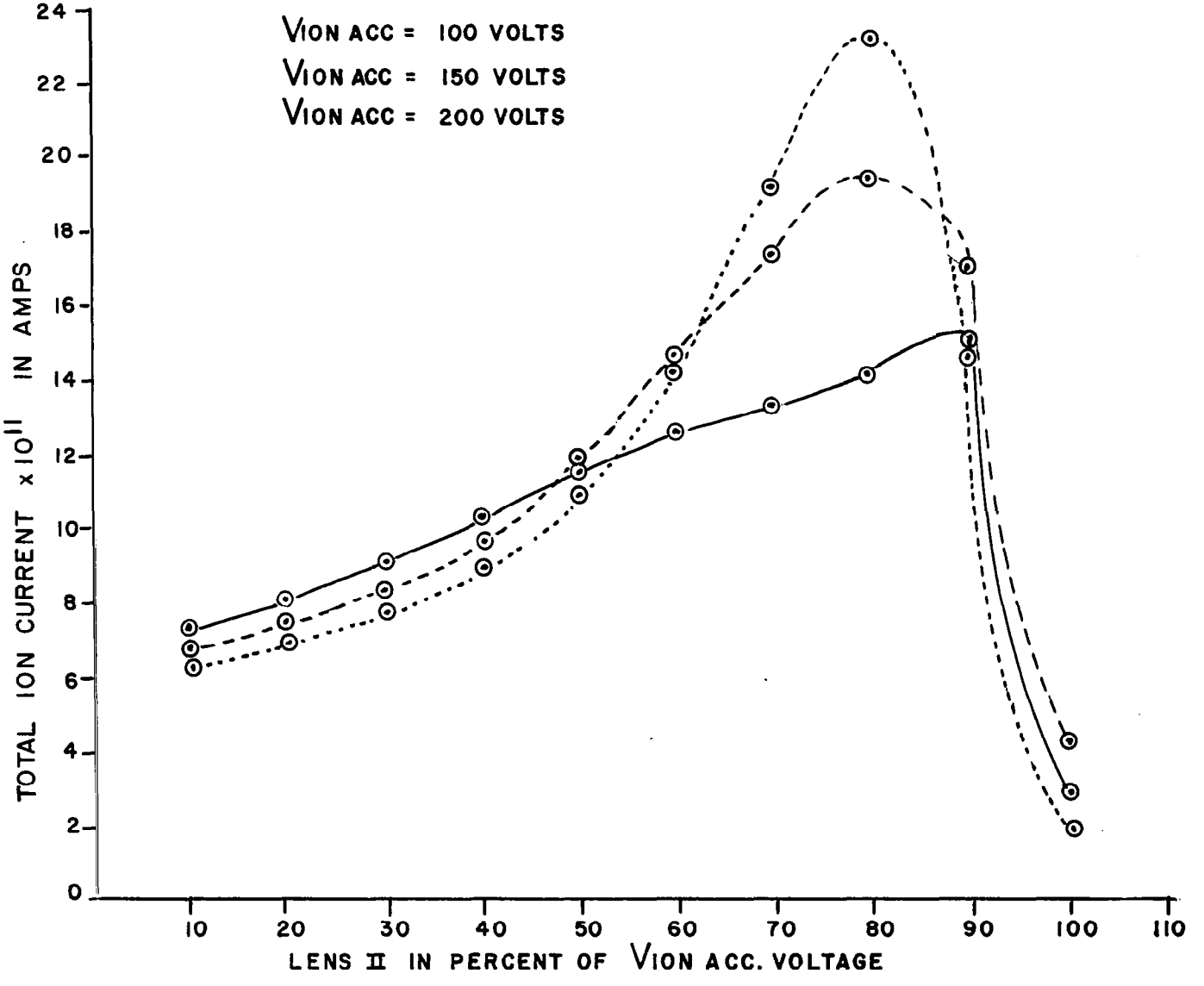

TOTAL ION CURRENT VS LENS II VOLTAGE

FIG. FOURTY-TWO

DETERMINATION OF IONIZATION POTENTIAL WITH RESPECT TO ION ACCELERATOR

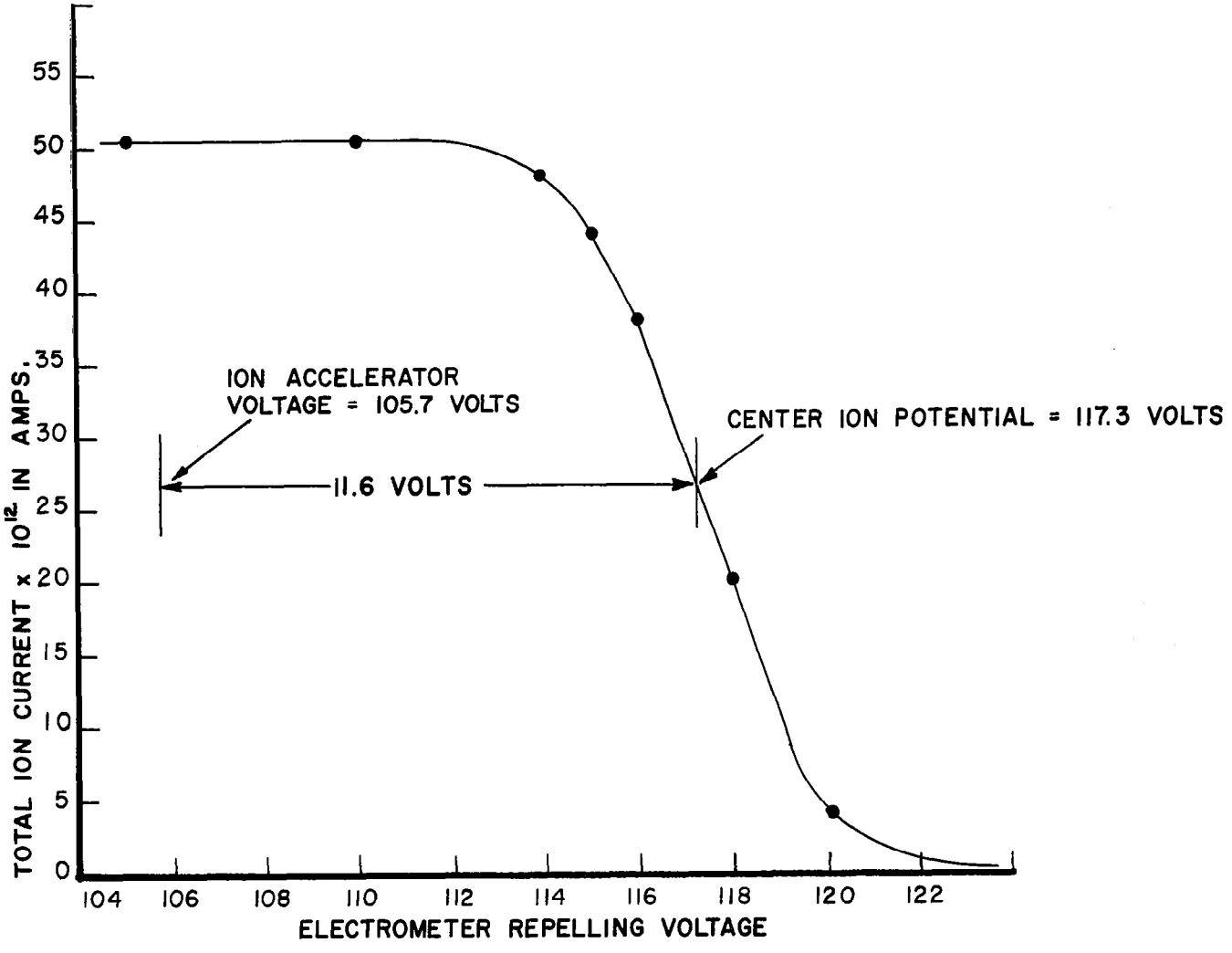

FIG. FORTY-THREE

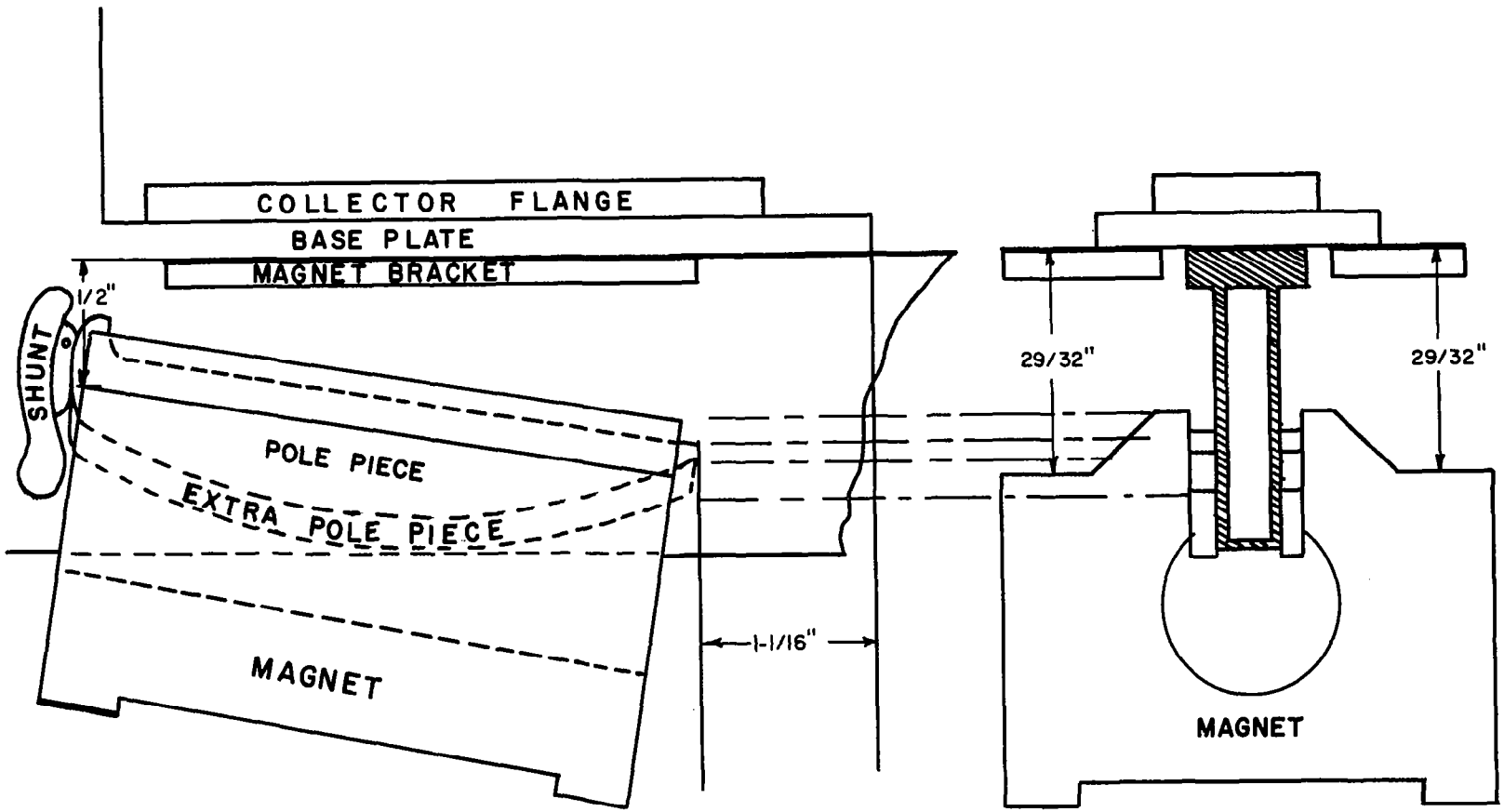

MAGNET POSITION

FIG. FOURTY-FOUR

TABLE XXX

Table for Setting Up $\frac{\Delta V_{sec}}{V_{acc}}$ Ratios

ΔV_{sec} = 100 volts, $\frac{V_{ion\ rail} - V_{neg\ sec}}{\Delta V_{sec}}$ = .45, $V_{z\text{-}axis}$ = 0

$\frac{\Delta V_{sec}}{V_{acc}}$	V_{acc} in Volts	$V_{ion\ acc}$ in Volts	$V_{Lens\ II}$ in Volts
.800	125.0	111.8	67.0
.825	121.1	107.9	64.6
.850	117.9	104.7	62.6
.875	114.2	101.0	60.5
.900	111.0	97.8	58.6
.925	108.1	94.9	56.9
.950	105.2	92.0	55.2

TABLE XXXI

Table for Setting Up $\frac{V_{ion\ rail} - V_{neg\ sec.}}{\Delta V_{sec}}$ Ratios

ΔV_{sec} = 100 Neg Sec. = -51.6 Pos Sec = +48.4

$\frac{V_{ion\ rail} - V_{neg\ sec}}{\Delta V_{sec}}$	$V_{ion\ rail}$ in Volts
.20	-31.6
.30	-21.6
.40	-11.6
.425	- 9.1
.450	- 6.6
.475	- 4.1

TABLE XXXI continued

$\frac{V_{ion\ rail} - V_{neg\ sec}}{\Delta V_{sec}}$	$V_{ion\ rail}$ in Volts
.500	- 1.6
.550	+ 3.4
.600	+ 8.4
.700	+18.4

7.3 Analyzer Magnet Evaluation

7.3.1 Objectives

The objectives of this report are to determine if there is a depreciation of the analyzer magnet's field strength with time, to determine the temperature coefficient of the analyzer magnet, to predict the effect of a given temperature change upon the ion beam position and to determine the maximum magnetic field intensity in the area about the analyzer magnet.

7.3.2 Conclusions

It was concluded that the analyzer magnet field strength depreciates significantly (11 percent) in the first three months after recharging. It was noted that the analyzer magnet must remain within a narrow temperature range for the mass spectrometer to operate properly. It was concluded that the magnetic field intensity is less than 5 gauss at a distance of 9 inches from the magnet in any direction

7.3.3 Equipment

Spare Analyzer Magnet	CSC C320717-A	7
Gaussmeter	Radio Frequency Labs 525	161
Standard Magnet	Radio Frequency Labs HB16660	----
Temperature Chamber	Statham TC-4	2045

7.3.4 Procedure

1. The magnet was returned to CSC for recharging per their specification C320717-A.

2. Upon return of the magnet, a measurement was made of the maximum field strength obtainable with the probe centered between the magnet pole pieces. This number was recorded in a log.

3. Step 2 of the Procedure was repeated periodically over a period of three months during which time the magnet was isolated from shunting ferromagnetic materials and AC fields. The magnet shunt was removed during this period to simulate the conditions in the mass spectrometer.

4. A wooden jig was fabricated to position the gaussmeter probe between the magnet pole pieces. The jig was placed in position and not repositioned for the duration of the temperature testing.

5. The 0 to 5 kilogauss scale of the gaussmeter was calibrated using the two kilogauss standard magnet.

6. A reading of the magnetic field was taken at room temperature.

7. The analyzer magnet was placed in the temperature chamber, and the ambient temperature was lowered to -40°C.

8. After the chamber had been at temperature for a period of one hour, the magnet was removed and the field quickly measured. This procedure permitted the gaussmeter probe to remain at room temperature. The mass of the magnet is such that its temperature did not appreciably change in the 15 second period required to make the reading. The gaussmeter was recalibrated seconds before removal of the magnet from the chamber.

9. After a period of 16 hours during which the magnet remained at room temperature, the field was again measured. As before, the gaussmeter was calibrated just prior to making the measurement.

10. The analyzer magnet was again placed in the temperature chamber and the ambient temperature was raised to +65°C.

11. Step 8 of the Procedure was repeated.

12. A cutout was formed in the center of a plywood sheet which permitted the magnet to be positioned in either of two directions with the plywood cutting the center line of the magnet. See Figure 45.

13. The cutout sheet was elevated above the table top with props. The analyzer magnet, also resting on props, was positioned in the center of the plywood and a good distance from any magnetic material.

14. The plywood sheet was covered with vellum paper. One corner of the magnet was selected as the origin. See Figure 46.

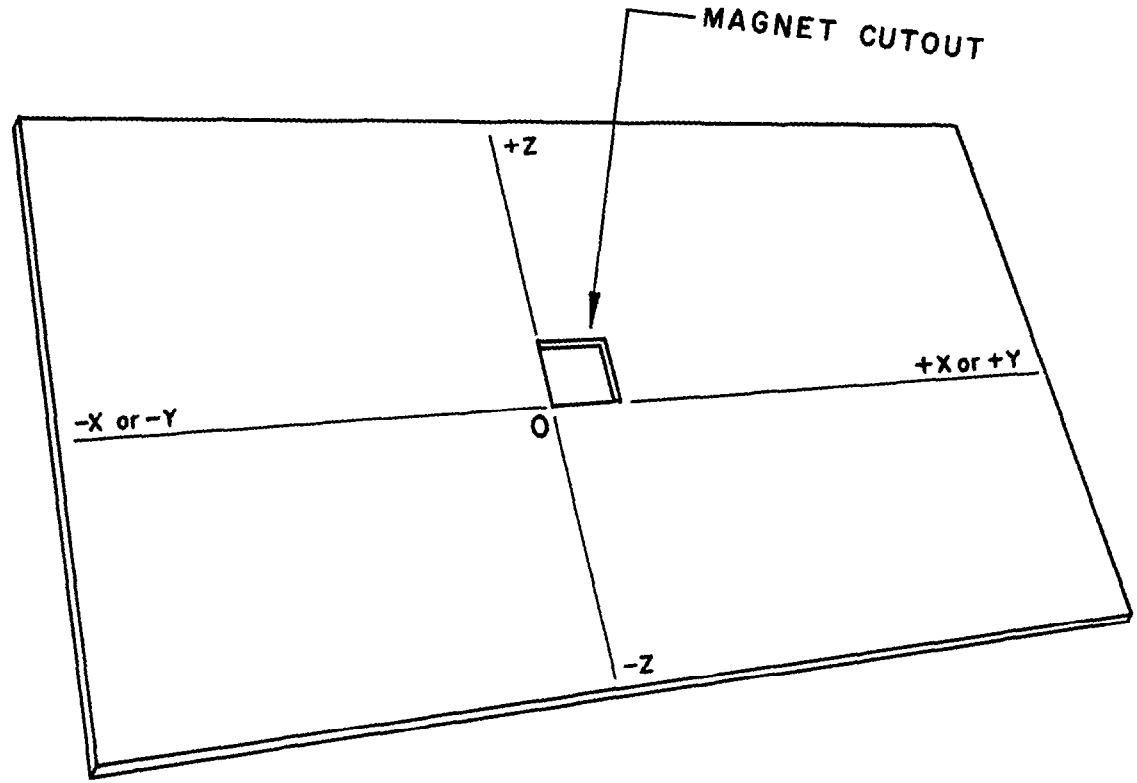

PLYWOOD SHEET FOR PLOTTING STRAY FIELD

FIG. FORTY-FIVE

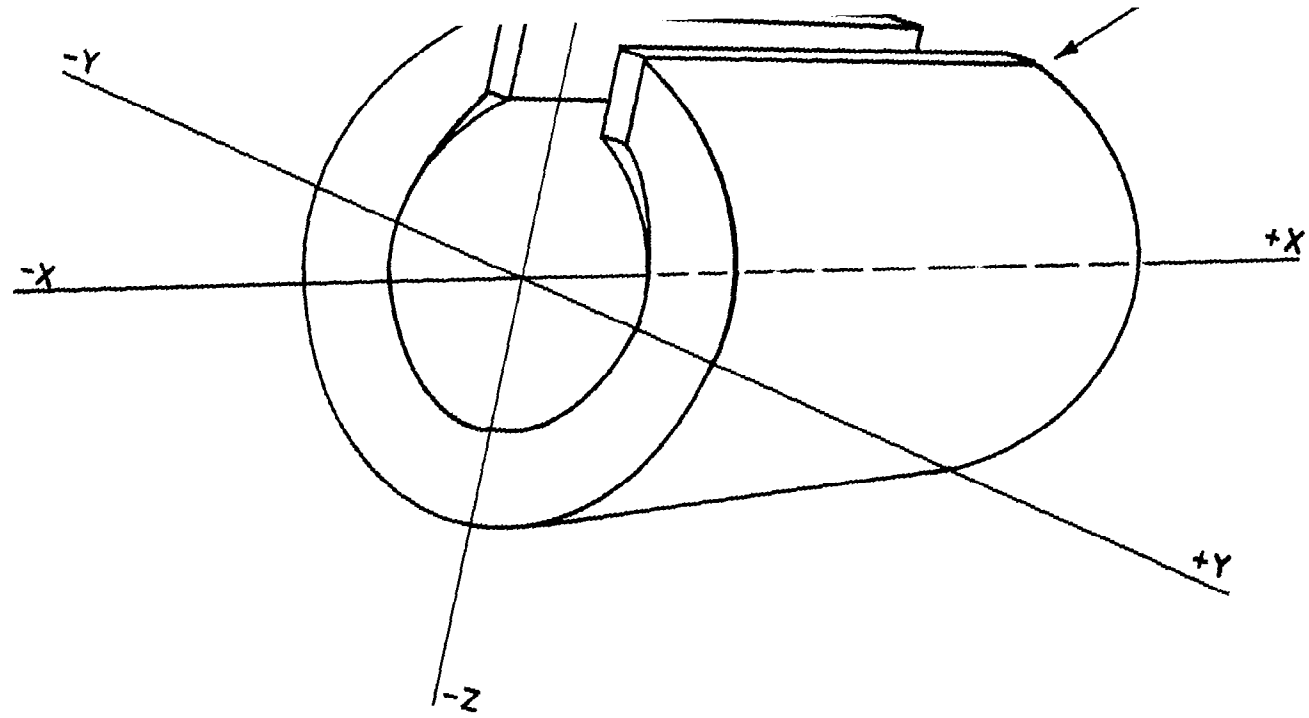

ANALYZER MAGNET

FIG. FORTY-SIX

15. The gaussmeter was calibrated using the standard magnet.

16. Working in the XZ plane, points on the 5, 10, 20, 50 and 100 gauss maximum field intensity loci were marked on the vellum paper approximately every 30° around the magnet. Each reading was made by turning the gaussmeter probe in every direction and taking the largest reading obtainable at that point. The gaussmeter was frequently recalibrated in the process of making the readings.

17. The magnet was repositioned and Step 16 was repeated in the YZ plane.

7.3.4 Results

1. The results of Steps 2 and 3 of the Procedure are recorded in Table XXXII and in Figure 47.

2. The results of Steps 4 through 11 are given in Table XXXIII and Figure 48. The average temperature coefficient was found to be $\frac{3.30 - 3.19}{105} = .001047$ kgauss/°C = $\frac{.001047}{3.25} = .0322$ percent/°C.

3. The results of Steps 12 through 17 are given in Tables XXXIV and XXXV and in Figures 49 and 50.

TABLE XXXII

Magnetic Field vs. Elapsed Time

Date	Time From Initial Reading in Days	Field Strength in Gauss	Change from Initial Reading in Percent
7/7/65	0	3600	00.0
7/14/65	7	3500	- 2.8
7/16/65	Temperature Evaluation	3410	- 5.3
8/2/65	19	3380	- 6.1
8/9/65	26	3380	- 6.1
8/27/65	44	3380	- 6.1
9/27/65	75	3200	-11.1
10/8/65	88	3200	-11.1

MAXIMUM ANALYZER MAGNET FIELD STRENGTH MEASURED
IN CENTER OF POLE PIECES vs TIME ELAPSED SINCE RECHARGING

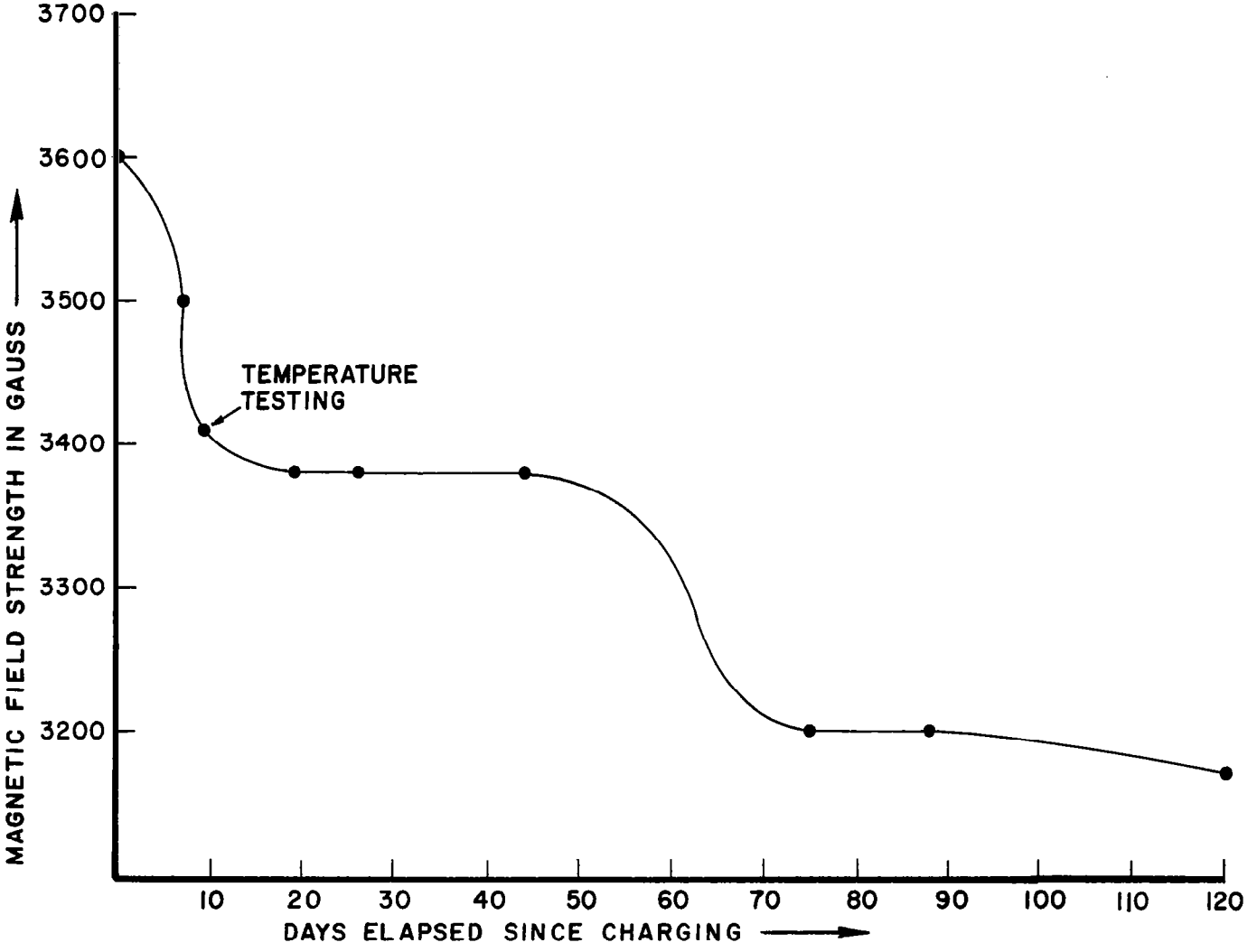

MAGNETIC FIELD vs. ELAPSED TIME

FIG. FORTY-SEVEN

TABLE XXXIII

Magnet Field vs. Temperature

Temperature °C	Magnet Field in Gauss
+22.5	3220
-40.0	3300
+22.5	3220
+65.0	3190

7.3.5 Discussions

The question of magnetic field stability with time was first raised when it was noted that the maximum magnetic field of the regular analyzer magnet had apparently dropped from a value of 3200 gauss to a value of 2200 gauss in one year. As far as is known, the magnet was neither exposed to a strong AC field nor had its temperature raised to near the Curie point during this time, nor had the magnet experienced an unusual mechanical shock. As the noted change in magnetic field strength was only an informal observation and as the magnetic field strength is critical to proper operation of the instrument, the decision was made to more formally investigate the magnet stability with both time and temperature.

The distance[19] (measured along the focal plane) at which the ion beam intersects the focal plane is proportional to 1/B.[20] It can be seen that a small percentage change in B will cause an almost direct percentage change in this distance. The beam width of the 44 ion beam is 10.5 mils. Assuming this beam is centered in the 23 mil slit, the distance of the edge of the beam to the edge of the slit is 23 - 10.5 ÷ 2 or 6.2 mils. The slit is 3.2 inches from the theoretical entry point. Thus a change in magnetic field of .0062/3.2 or approximately .2 percent will move the beam to the edge of its slit causing the m/e 44 output to decrease and become unstable. With a temperature coefficient of .0322 percent/°C, the tolerable temperature variation is .2/.0322 or 6.2 degrees centigrade. This result assumes that the high voltage supply changes do not compensate for the changes in magnetic field. The lower masses are less susceptable to changes in magnetic field, and stable operation can be maintained over a wider temperature range.

[19] Measured from the theoretical entry point.

[20] B is the magnetic field strength.

The gaussmeter used in the stray field experiment was purchased for measuring the analyzer magnet field strength in the center of the gap. This particular gaussmeter is less than ideal for measuring magnetic fields in the 5 to 50 gauss range. For this reason, it is entirely possible that the 5 gauss measurements are only accurate to plus or minus 20 or 30 percent. The higher field strength measurements would be more accurate.

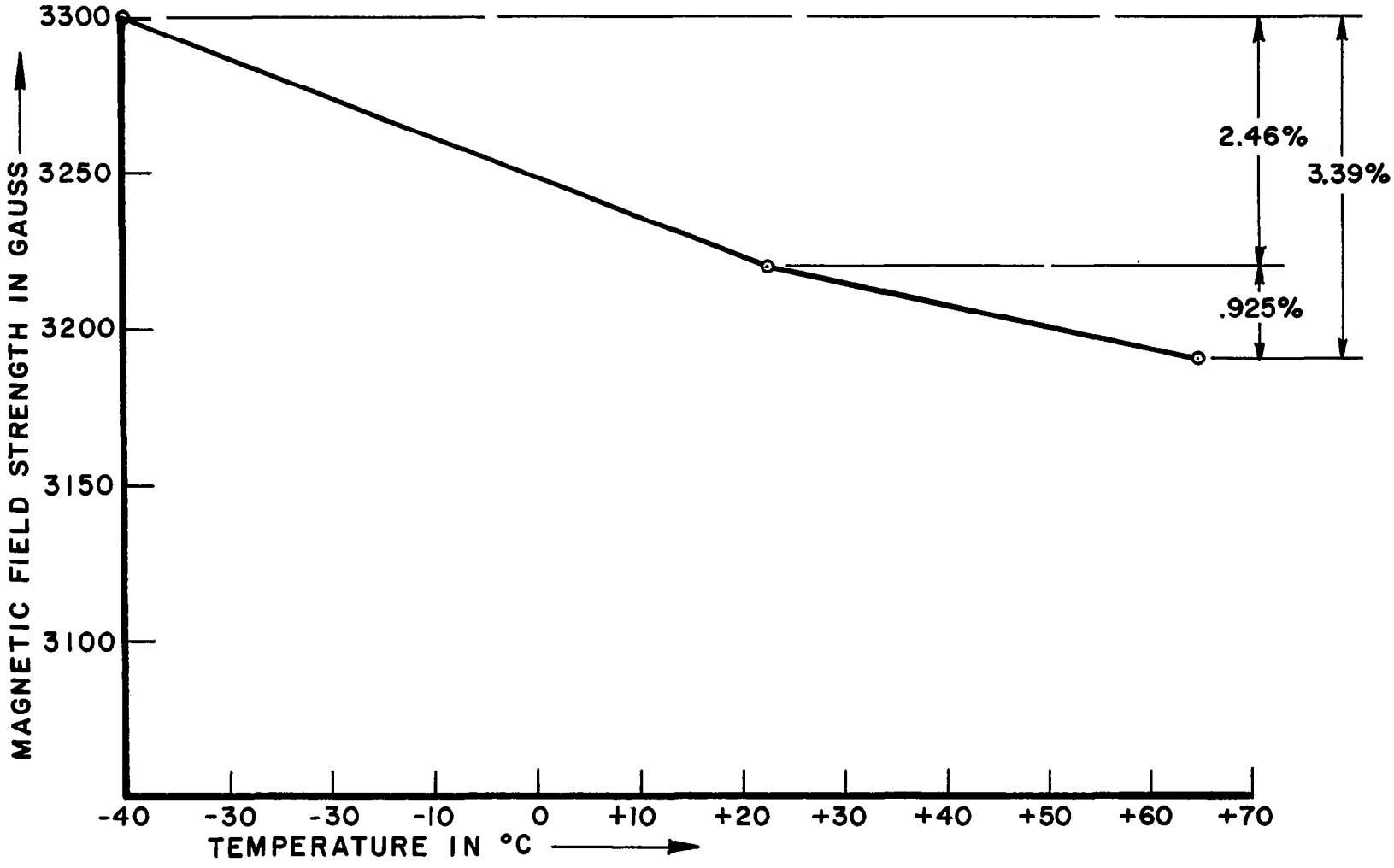

MAGNETIC FIELD vs. TEMPERATURE

FIG. FORTY-EIGHT

TABLE XXXIV

Stray Field Intensity in the XZ Plant

Pt. No.	Magnetic Field Intensity in Gauss	X Coordinate in Inches	Z Coordinate in Inches
1	5	+8.7	- .1
2	5	+8.9	+4.6
3	5	+6.2	+9.0
4	5	+1.9	+10.2
5	5	-2.2	+9.5
6	5	-4.7	+6.7
7	5	-6.2	+2.0
8	5	-5.7	-1.9
9	5	-3.2	-4.5
10	5	+1.2	-5.6
11	5	+6.0	-4.3
12	10	+7.7	+ .3
13	10	+7.7	+4.4
14	10	+5.1	+7.8
15	10	+1.8	+8.9
16	10	-1.3	+8.4
17	10	-4.1	+5.8
18	10	-5.1	+2.0
19	10	-4.3	-1.1
20	10	-2.1	-3.2
21	10	+1.5	-4.3
22	10	+5.4	-3.1
23	20	+6.2	+ .5

TABLE XXXIV continued

Pt. No.	Magnetic Field Intensity in Gauss	X Coordinate in Inches	Z Coordinate in Inches
24	20	+6.4	+3.9
25	20	+4.2	+6.8
26	20	+1.7	+7.3
27	20	- .7	+6.9
28	20	-3.1	+5.0
29	20	-3.9	+2.1
30	20	-3.0	- .2
31	20	-1.2	-2.0
32	20	+1.5	-2.6
33	20	+4.4	-1.9
34	50	+5.1	+ .9
35	50	+5.2	+3.3
36	50	+3.6	+5.5
37	50	+1.7	+6.1
38	50	- .1	+5.9
39	50	-2.2	+4.2
40	50	-2.7	+2.0
41	50	-2.1	+ .2
42	50	- .6	-1.2
43	50	+1.3	-1.6
44	50	+3.8	- .9
45	100	+4.3	+1.1
46	100	+4.6	+2.8
47	100	+3.7	+4.5

TABLE XXXIV continued

Pt. No.	Magnetic Field Intensity in Gauss	X Coordinate in Inches	Z Coordinate in Inches
48	100	+1.9	+5.4
49	100	+ .3	+5.3
50	100	-1.7	+3.9
51	100	-1.9	+1.9
52	100	-1.5	+ .7
53	100	- .2	- .6
54	100	+1.4	- .7
55	100	+3.3	- .3

TABLE XXXV

Stray Field Intensity in the YZ Plane

Pt. No.	Magnetic Field Intensity in Gauss	Y Coordinate in Inches	Z Coordinate in Inches
1	5	+12.2	+ 2.0
2	5	+10.8	+ 6.3
3	5	+ 7.1	+ 9.8
4	5	+ 1.8	+10.8
5	5	- 2.4	+10.1
6	5	- 5.1	+ 9.2
7	5	- 7.2	+ 5.8
8	5	- 8.2	+ 1.9
9	5	- 7.2	- 2.6
10	5	- 3.7	- 4.8
11	5	+ 1.2	- 5.7

TABLE XXXV continued

Pt. No.	Magnetic Field Intensity in Gauss	Y Coordinate in Inches	Z Coordinate in Inches
12	5	+ 5.7	- 5.1
13	5	+ 9.3	- 4.5
14	5	+11.3	- 1.2
15	10	+ 9.6	+ 1.7
16	10	+ 9.2	+ 5.4
17	10	+ 6.1	+ 8.0
18	10	+ 1.6	+ 8.9
19	10	- 1.6	+ 8.4
20	10	- 5.7	+ 5.8
21	10	- 6.5	+ 2.0
22	10	- 5.1	- 1.3
23	10	- 2.3	- 3.6
24	10	+ 1.5	- 4.2
25	10	+ 4.9	- 3.9
26	10	+ 8.2	- 1.5
27	20	+ 8.2	+ 2.0
28	20	+ 7.9	+ 4.8
29	20	+ 5.7	+ 6.9
30	20	+ 1.9	+ 7.7
31	20	- 1.1	+ 7.6
32	20	- 4.0	+ 5.7
33	20	- 4.9	+ 2.1
34	20	- 4.1	- .4
35	20	- 2.1	- 2.5

TABLE XXXV continued

Pt. No.	Magnetic Field Intensity in Gauss	Y Coordinate in Inches	Z Coordinate in Inches
36	20	+1.6	-3.1
37	20	+4.1	-2.9
38	20	+7.0	- .9
39	50	+6.4	+2.2
40	50	+5.2	+5.1
41	50	+1.8	+6.4
42	50	- .5	+6.1
43	50	-2.5	+4.4
44	50	-3.1	+2.5
45	50	-2.6	+ .4
46	50	- .9	-1.2
47	50	+1.3	-1.6
48	50	+3.4	-1.5
49	50	+5.6	- .2
50	100	+4.3	+ .1
51	100	+5.4	+3.5
52	100	+3.5	+5.2
53	100	+1.5	+5.4
54	100	-1.1	+4.6
55	100	-2.2	+2.2
56	100	- .8	+ .1
57	100	+1.9	- .9

ANALYZER MAGNET STRAY FIELD INTENSITY IN THE XZ PLANE

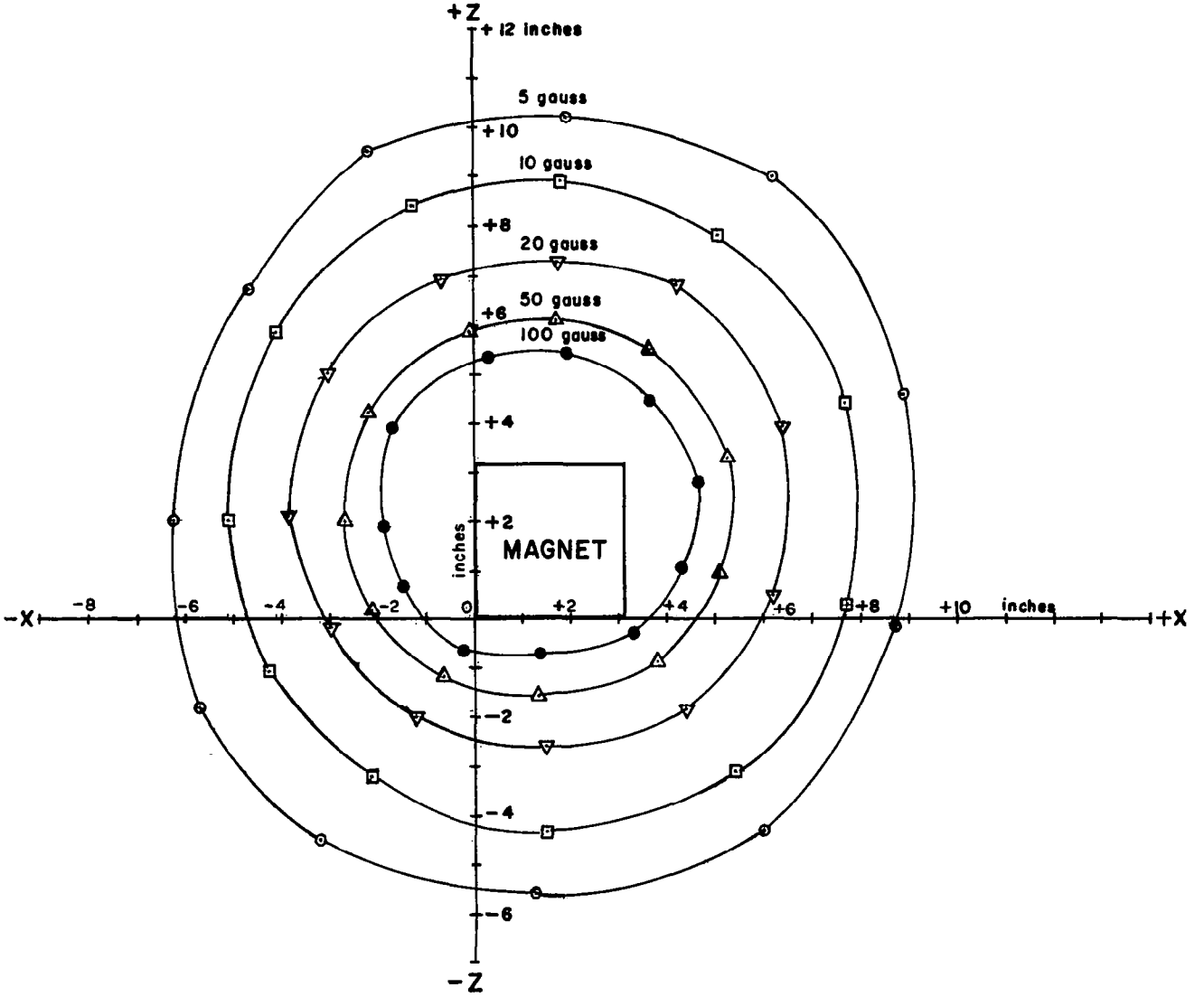

FIG. FORTY-NINE

ANALYZER MAGNET STRAY FIELD INTENSITY IN THE YZ PLANE

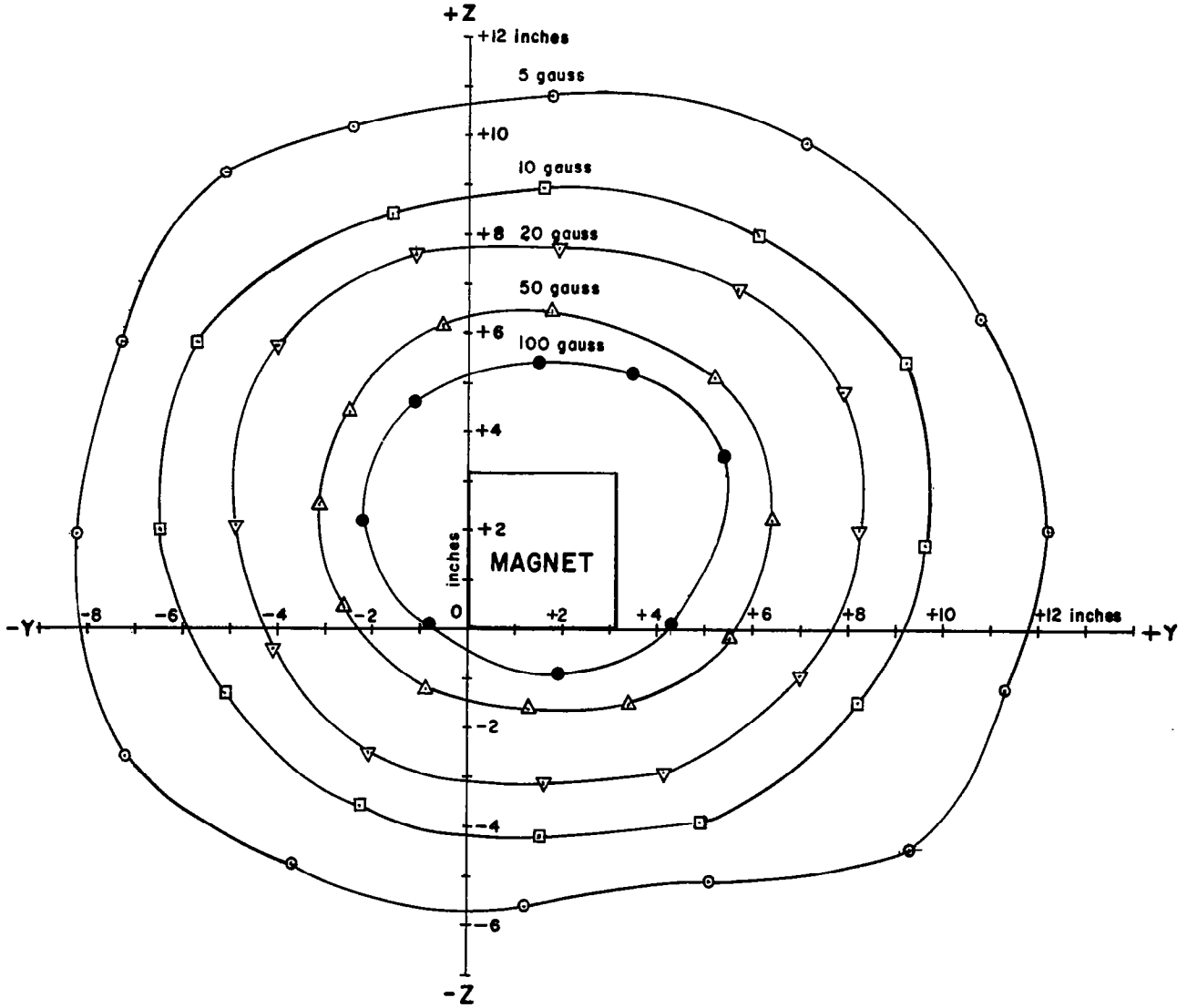

FIG. FIFTY

8. EVALUATION OF ELECTRONICS

8.1 Functions of the Electronic Circuits

Electronic circuits perform nine basic functions in the mass spectrometer. Electronic circuits do the following: one, power the filament; two, control electron emission from the filament; three, provide controlled analyzer electrode voltages; four, provide regulated ion source electrode potentials[21]; five, detect and measure the output ion currents; six, supply high voltage power to operate the ion pump; seven, provide a means of monitoring the pump pressure; eight, provide protection from filament burn-out due to vacuum loss; and nine, select the source of sample gas.

The mass spectrometer electronics is comprised of the following circuits: Master Oscillator, Emission Regulator and Filament Supply, Fixed High Voltage Supply, Scan High Voltage Supply, Potentiometer Board, Shield Supply, Anode Supply, Electrometers, Electrometer Power Supply, Ion Pump Power Supply and Ground Support Remote Control Box. The function of each of these circuits is given below.

Master Oscillator: The Master Oscillator converts the DC input power into a square wave voltage source which is used to drive several different power supply transformers. With this converter technique, all of the various supplies have the same ripple frequency. This eliminates the possibility of different frequency ripple frequencies beating together and generating undesirable modulated ripple voltages

Emission Regulator and Filament Supply: The function of the Filament Supply is to provide power for heating the filament. The power to the filament is controlled by the Emission Regulator in such a manner that constant emission current is maintained.

Fixed High Voltage Supply: The function of the Fixed High Voltage Supply is to provide a regulated fixed voltage to the potentiometer board divider string which supplies the analyzer electrode potentials.

Scan High Voltage Supply: The function of the Scan High Voltage Supply is to provide a regulated scan voltage to the potentiometer board divider string which supplies the analyzer electrode potentials. When the mass spectrometer is switched to the scan mode, two relay contacts switch the divider string from the Fixed High Voltage Supply to the Scan High Voltage Supply.

Potentiometer Board: Three voltage divider circuits are mounted on the Potentiometer Board. One divider circuit is connected across the shield supply. One divider string is connected across the anode supply, and the third divider string is across either the fixed high voltage supply or the scan high voltage supply. The

[21]The supply of ion source electrode potentials is differentiated from the supply of analyzer electrode potentials as the source potentials are fixed while the analyzer potentials are scanned when the instrument is used in the scan mode.

relay which selects the power source for the third string is also mounted on the Potentiometer Board. The divider string which is across the shield supply provides electrode potentials for the electron gun electrodes: filament shield, filament, electron focus and electron accelerator. The divider string which is across the anode supply furnishes electrode potentials to the remaining ion source electrodes. The third divider string supplies electrode potentials to the analyzer and provides the ground reference point for all the electrode potentials. The shield, anode and selected high voltage supply are referenced to one another in the Potentiometer Board circuitry.

Shield Supply: The Shield Supply furnishes the regulated voltage across the divider string supplying electrode potentials to the electron gun section of the ion source.

Anode Supply: The Anode Supply furnishes the regulated voltage across the divider string supplying the ion source electrode potentials not supplied by the shield supply string.

Electrometers: The function of the Electrometers is to transform the small ion currents striking the collector buckets into low impedance voltage signals which can be easily measured and recorded.

Electrometer Power Supply: The Electrometer Power Supply furnishes four regulated voltages (+35, +10, +2.6 and -20) to the twelve electrometers.

Ion Pump Power Supply: The Ion Pump Power Supply performs three functions. Primarily, the Ion Pump Power Supply provides a high voltage power source for the four liter ion pump. A second function of the supply is to furnish a logarithmic pump pressure signal to the ground support control box. The third function of the Ion Pump Power Supply is to provide a filament protection interlock which shuts off the filament when the ion pump pressure reaches a preset level.

Ground Support Remote Control Box: The function of the Ground Support Remote Control Box is to monitor the operation of the mass spectrometer upon installation in the airplane. Connection between the Remote Control Box and the mass spectrometer is made through one large connector and cable which is easily removed just prior to flight. The Remote Control Box has provisions for opening any one of the five inlet valves as well as monitoring the emission current, high voltage or any one of the twelve electrometer outputs. A momentary depress switch is located in the Remote Control Box for switching from the fixed high voltage supply to the scan high voltage supply.

8.2 Evaluation of the Master Oscillator, Filament Supply and Emission Regulator

The Master Oscillator, Filament Supply and Emission Regulator are constructed on one printed circuit board. During the testing period no particular difficulty was experienced with either the Master Oscillator or Filament Supply. The regulation of the total emission current by the Emission Regulator is not as good as

might be expected. Changes in total emission current of 2.5 percent have been observed in an eight hour period with the unit maintained at room temperature. The temperature regulation of the Emission Regulator was not investigated.

8.3 Evaluation of Fixed High Voltage Supply

8.3.1 Objective

The objective of this section is to determine the voltage variation of the Fixed High Voltage Supply.

8.3.2 Conclusion

It was concluded that the Fixed High Voltage Power Supply varies ± .146 percent from its mean over the temperature range, that it varies ± .019 percent from its mean over the input voltage range and that it varies ± .146 percent randomly.

8.3.3 Equipment

Power Supply Kepco	CK36-1.5	H-40117
Differential Volt Meter	John Fluke 803B	3439

8.3.4 Procedure

1. Power was supplied to the emission regulator circuit which in turn provided power to the Fixed High Voltage Supply.

2. Both the emission regulator and the Fixed High Voltage Supply were placed in a temperature chamber.

3. The filament load was simulated to duplicate operation conditions.

4. The Fixed High Voltage output was monitored and recorded as the temperature was varied from -45° to +65°C.

5. The Fixed High Voltage output was monitored and recorded as the input voltage to the emission regulator was varied from 24 to 32 volts. This was done at room temperature.

6. The Fixed High Voltage output was measured and recorded at random intervals over a period of 24 hours. The supply was turned on and off several times during this period.

8.3.5 Results

The results are recorded in Tables XXXVI, XXXVII and XXXVIII and Figures 51, 52 and 53.

TABLE XXXVI

Variation of Fixed High Voltage Supply With Temperature

Temperature in °C	Output Voltage in Volts	Deviation From Mean Voltage in Volts	Deviation From Mean in Percent
+23.0	346.595	+.137	+.040
-45.0	346.965	+.507	+.146
-20.0	346.826	+.368	+.106
0.0	346.608	+.150	+.043
+22.0	346.373	-.085	-.025
+40.0	346.244	-.214	-.062
+65.0	345.951	-.507	-.146

TABLE XXXVII

Variation of Fixed High Voltage Supply with Input Voltage

Input Voltage in Volts	Output Voltage in Volts	Deviation From Mean Voltage in Volts	Deviation From Mean Voltage in Percent
32	346.98	+.065	+.019
28	346.95	+.035	+.010
24	346.85	-.065	-.019

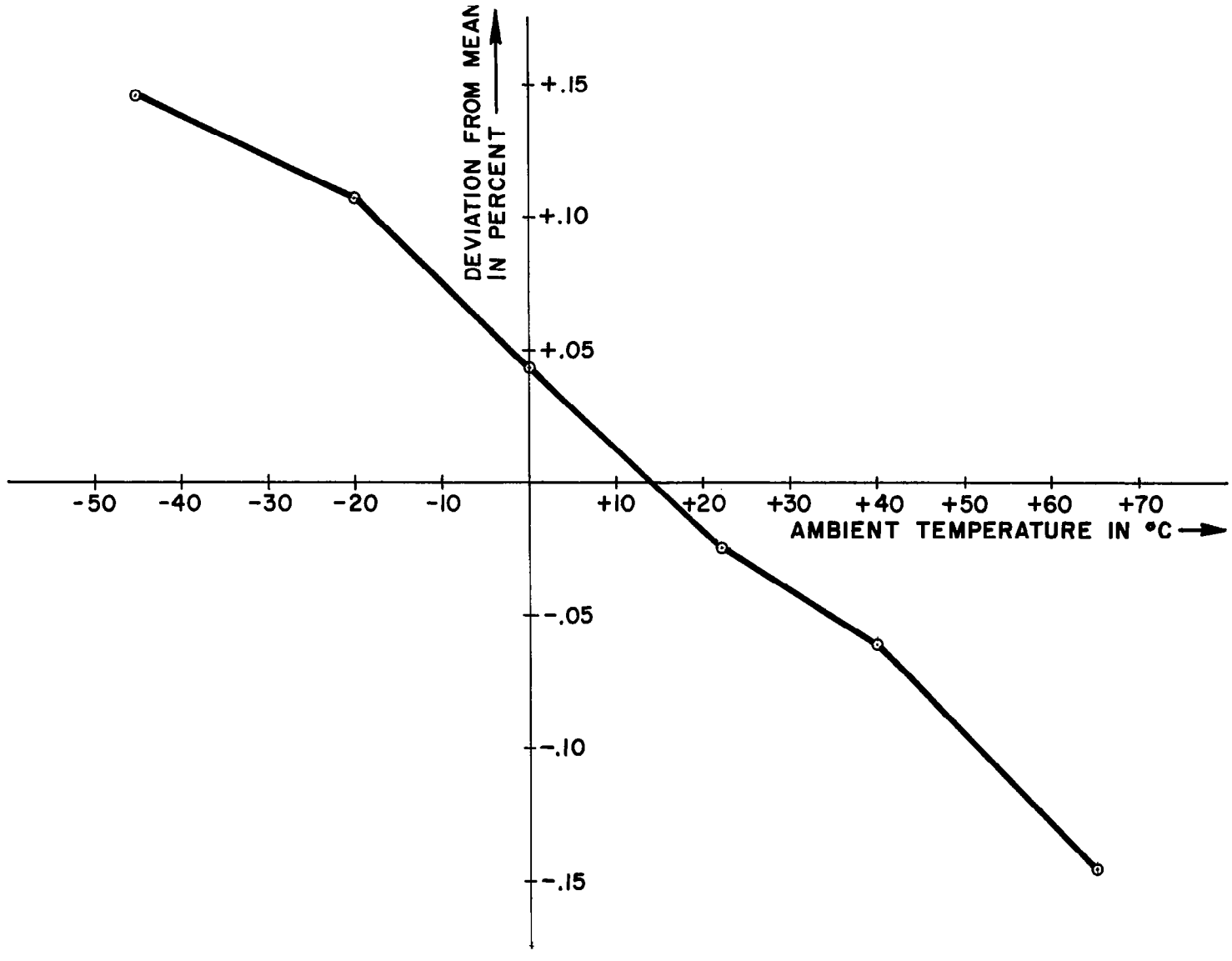

VOLTAGE VARIATION WITH TEMPERATURE OF FIXED HIGH VOLTAGE SUPPLY

FIG. FIFTY-ONE

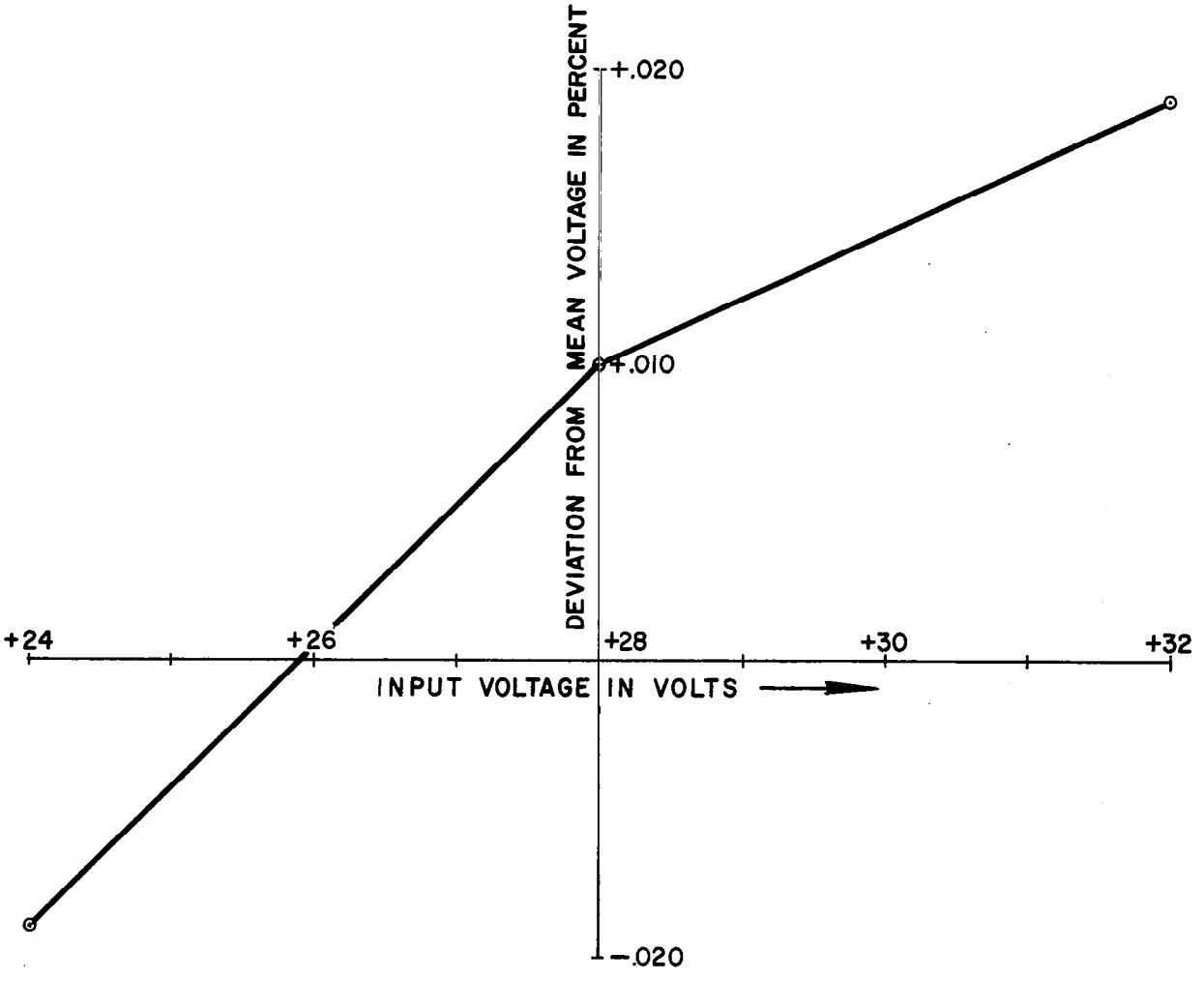

VOLTAGE VARIATION WITH INPUT VOLTAGE OF FIXED HIGH VOLTAGE SUPPLY

FIG. FIFTY-TWO

TABLE XXXVIII

Variation of Fixed High Voltage Supply

Observed Randomly Over 24 Hours Period

Output Voltage in Volts	Deviation From Mean Voltage in Volts	Deviation From Mean Voltage in Percent
346.95	-.135	-.039
347.20	+.115	-.033
347.57	+.485	+.140
347.40	+.315	+.091
347.00	-.085	-.024
347.20	+.115	+.033
346.86	-.225	-.065
346.60	-.485	-.140

8.4 Evaluation of Scan High Voltage Supply

8.4.1 Objective

The objective of this section is to determine the voltage variation of the Scan High Voltage Supply.

8.4.2 Conclusion

It was concluded that the Scan High Voltage Supply output voltage varies ± .558 percent over the temperature range, ± .003 percent over the input voltage range and ± .229 percent randomly.

8.4.3 Equipment

Power Supply	Kepco CK36-1.5	H-40117

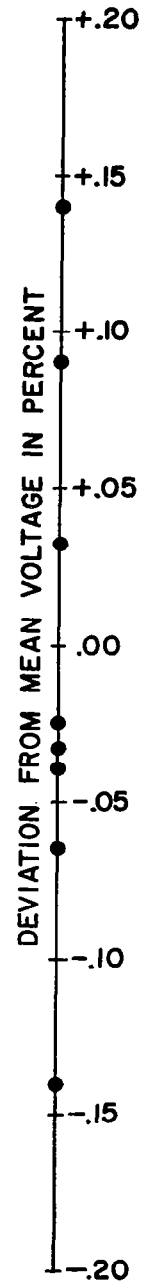

VARIATION OF FIXED HIGH VOLTAGE SUPPLY
OBSERVED AT RANDOM OVER 24 HOUR PERIOD

FIG. FIFTY-THREE

8.4.3 Equipment

Power Supply	Kepco CK36-1.5	H-40108
Differential Volt Meter	John Fluke 803B	3439

8.4.4 Procedure

1. The 1N945B reference diode was removed from the circuit, and a laboratory power supply was substituted for the reference voltage. The lab. supply provided a means of adjusting the supply output to a voltage similar to the Fixed High Voltage Supply output.

2. Power was supplied to the emission regulator circuit which in turn furnishes power to the Scan High Voltage Supply.

3. Both the emission regulator and the Scan High Voltage Supply were placed in a temperature chamber.

4. The Scan High Voltage Supply output was monitored and recorded as the ambient temperature was varied from -43° to +65°C.

5. The Scan High Voltage Supply output was monitored and recorded as the input voltage to the emission regulator was varied from 24 to 32 volts. This was done at room temperature.

6. The Scan High Voltage Supply output was measured and recorded at random intervals. During the monitoring period, the supply was turned on and off several times. Readings were corrected for changes in the reference voltage.

8.4.5 Results

The results are recorded in Tables XXXIX, XL and XLI and Figures 54 and 55.

TABLE XXXIX

Variation of Scan High Voltage Supply With Temperature

Temperature in °C	Output Voltage in Volts	Deviation From Mean Voltage in Volts	Deviation From Mean Voltage in Percent
-43	349.54	+1.945	+.561
-20	348.84	+1.245	+.359

TABLE XXXIX continued

Temperature in °C	Output Voltage in Volts	Deviation From Mean Voltage in Volts	Deviation From Mean Voltage in Percent
0	348.06	+ .465	+.134
+21	347.30	- .295	-.085
+45	346.37	-1.225	-.354
+65	345.65	-1.945	-.561

TABLE XL

Variation of Scan High Voltage Supply With Input Voltage

Input Voltage in Volts	Output Voltage in Volts	Deviation From Mean Voltage in Volts	Deviation From Mean Voltage in Percent
24	347.976	-.005	-.001
28	347.980	-.001	-.000
32	347.986	+.005	+.001

TABLE XLI

Variation of Scan High Voltage Supply Observed Randomly

Over a 24 Hours Period

Output Voltage in Volts	Deviation From Mean Voltage in Volts	Deviation From Mean Voltage in Percent
347.300	+.795	+.229
345.710	-.795	-.229
346.448	-.057	-.016
346.080	-.425	-.122
346.379	-.126	-.036

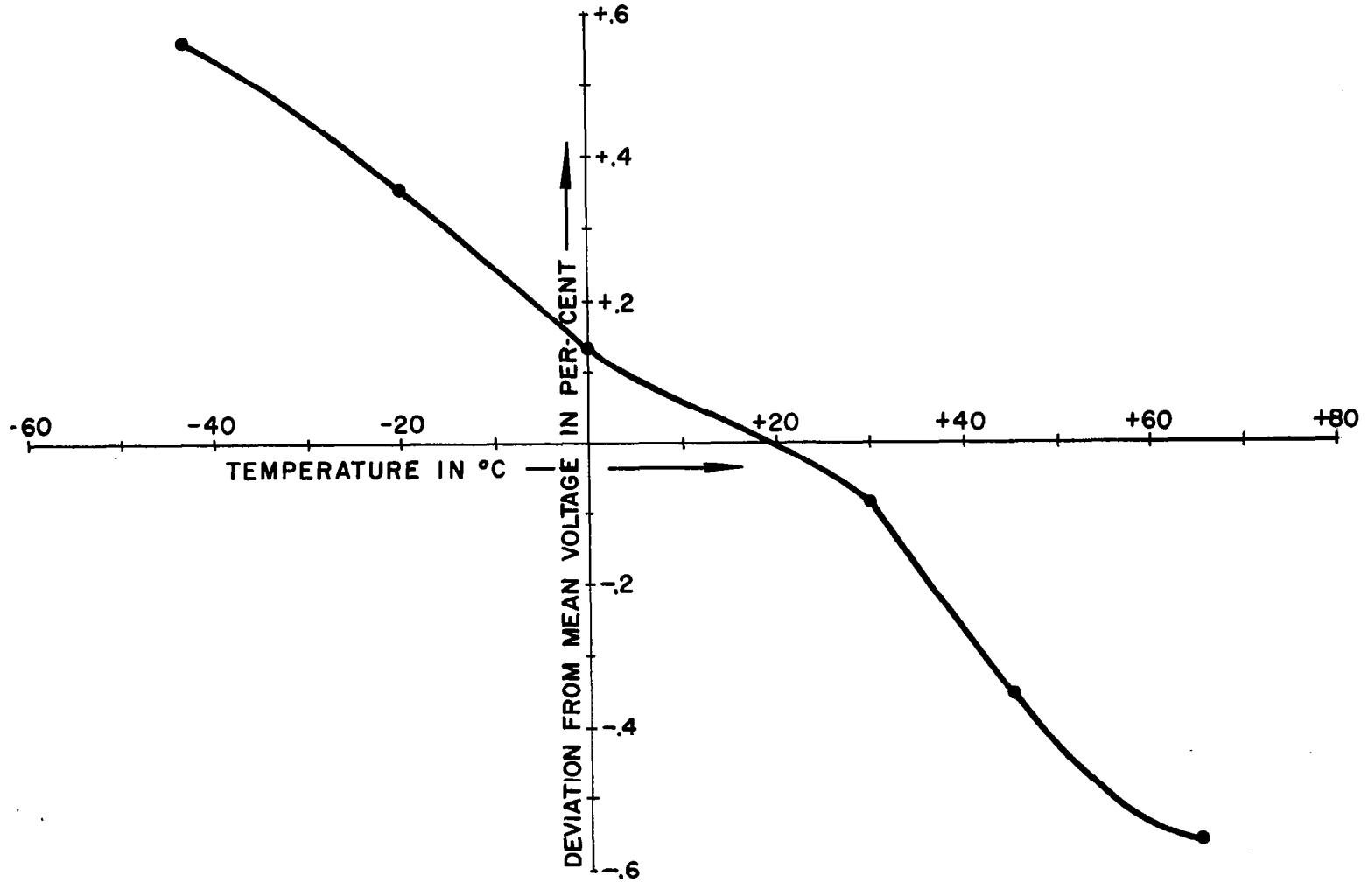

VOLTAGE VARIATION WITH TEMPERATURE OF SCAN HIGH VOLTAGE SUPPLY

FIG. FIFTY-FOUR

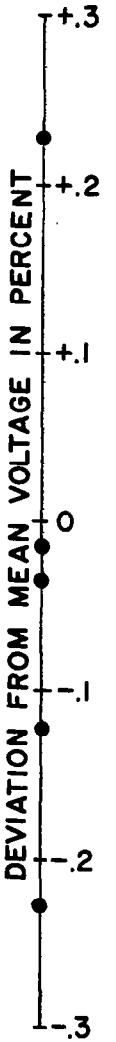

VARIATIONS OF SCAN HIGH VOLTAGE SUPPLY
OBSERVED AT RANDOM OVER 24 HOUR PERIOD

FIG. FIFTY-FIVE

8.5 Scan High Voltage Supply Ripple Analysis[22]

8.5.1 Objectives

The objectives of the following experiments were to determine the causes of unusually high AC ripple observed on the Scan High Voltage Supply, to eliminate the causes of unusual ripple and establish a normal ripple level which would not depreciate the shape of a scanned peak.

8.5.2 Conclusion

It was concluded that there were three causes of the unusually high ripple level observed on the supply. The cause of random supply fluctuations was a shorting rectifier. One cause of the high sinusoidal ripple was oscillations in the circuit. A second cause of the excessive ripple was the absence of several components in the supply filtering circuit.

8.5.3 Equipment

Power Supply	Kepco CK36-1.5	H-40117
Differential Volt Meter	John Fluke 803B	3439
Oscilloscope	Tektronix 545B	367

8.5.4 Procedure

1. The supply was connected across its standard load.

2. The Fluke meter was connected across the supply and monitored. A number of abrupt fluctuations in voltage were observed. At this time, a small steady arcing was seen in the center of one of the high voltage rectifiers. As the rectifiers were not a flight qualified type, they were replaced by Unitrode type 653-2.

3. The Fluke meter was removed from across the supply and connected between the positive side of the supply and ground. This step eliminated from the circuit the ripple which had been imposed from the ungrounded negative side of the meter.

---

[22]During the period the Scan High Voltage Supply was being evaluated for DC voltage variations, the ripple on the supply was not observed. Later, it was noted that a high level of ripple was present on this supply. At that time, the following analysis and correction procedure were carried out.

4. With the ripple reduced by the previous step, it was observed that a high frequency oscillation existed in the circuit. The capacitor which shunts the feedback resistor of the circuit's operational amplifier was missing. As this capacitor is required to avoid oscillations, an appropriate capacitor was selected and added to the circuit.

5. The ripple was again measured and found to still be above the levels experienced on the breadboard circuit. It was noted that one filtering capacitor had been omitted from the circuit. This was added.

6. The ripple was again measured. The ripple was observed as the circuit was scanned to assure that the circuit did not break into oscillations at any voltage level.

7. The ripple was observed as the temperature was raised to 65°C.

8.5.5 Results

The result of the above procedures was to reduce the ripple from a 20 volt peak to peak value to a 40 millivolt peak to peak value. It was observed that the ripple increased to 200 millivolts when the temperature was raised to 65°C.

8.5.6 Discussion

Upon correction of the ripple problem, it would have been desirable to re-evaluate the DC voltage fluctuations. It is assumed that a significant decrease in the random voltage variations would have been experienced upon elimination of the ripple. At the time, it was not deemed worthwhile to re-examine the DC voltage variations for the decisions had been made to continue using the Fixed High Voltage Supply for the continuous mode of operation. At the beginning of the evaluation, the idea had been entertained of eliminating the fixed high voltage supply and using the scan high voltage supply for both the continuous and scan modes of operation.

8.6 Evaluation of the Potentiometer Board

The Potentiometer Board circuitry was found to be satisfactory with the exception of a noisy potentiometer and shorted resistor which were replaced. Upon conclusion of the ion source and analyzer evaluations, the pot. board divider strings were modified; so the various electrode potentials could be adjusted to the values selected in the evaluations.

8.7 Evaluation of the Shield Voltage Supply

8.7.1 Objective

The objective of this section is to determine the voltage variation of the Shield Voltage Supply.

8.7.2 Conclusion

It was concluded that the Shield Voltage Supply varies ± 3.90 percent from its mean value over the temperature range, that it varies ± .09 percent from its mean value over the input voltage range, that it varies ± .46 percent randomly.

8.7.3 Equipment

Power Supply	Kepco CK36-1.5	H40117
Differential Volt Meter	John Fluke 803B	3439
Temperature Chamber	Statham TC-4	2045

8.7.4 Procedure

1. Power was supplied to the emission regulator circuit which in turn applied power to the Shield Voltage Supply.

2. The high voltage box was inserted into the test chamber. The emission regulator was connected to the high voltage box. The Shield Supply is located in the high voltage box.

3. The Shield Voltage Supply was monitored and recorded as the temperature was varied from -40° to +65°C.

4. The Shield Voltage Supply output was monitored and recorded as the input voltage to the emission regulator was varied from 24 to 32 volts. This was done at room temperature.

5. The Shield Voltage Supply output was measured and recorded at random intervals over a period of 24 hours. The supply was turned on and off several times during this period.

8.7.5 Results

See Tables XLII, XLIII and XLIV and Figures 56, 57 and 58.

8.7.6 Discussion

It was noted that it required 15 to 20 minutes for the Shield Voltage Supply to stabilize after turn on.

TABLE XLII

Variation of Shield Supply With Temperature

Temperature in °C	Time at Temperature in Minutes	Output Voltage in Volts	Deviation From Mean Voltage in Volts	Deviation From Mean Voltage in Percent
19	20	323.96	+ 4.36	+1.37
-40	20	307.15	-12.45	-3.90
-20	18	312.99	- 6.61	-2.06
0	22	317.83	- 1.77	-0.55
40	25	326.74	+ 7.14	+2.24
65	20	332.05	+12.45	+3.90

TABLE XLIII

Variation of Shield Supply With Input Voltage

Input Voltage in Volts	Output Voltage in Volts	Deviation From Mean Voltage in Volts	Deviation From Mean Voltage in Percent
32	323.13	+0.22	+0.068
30	323.19	+0.28	+0.086
28	322.86	-0.05	-0.016
26	322.73	-0.18	-0.056
24	322.63	-0.28	-0.086

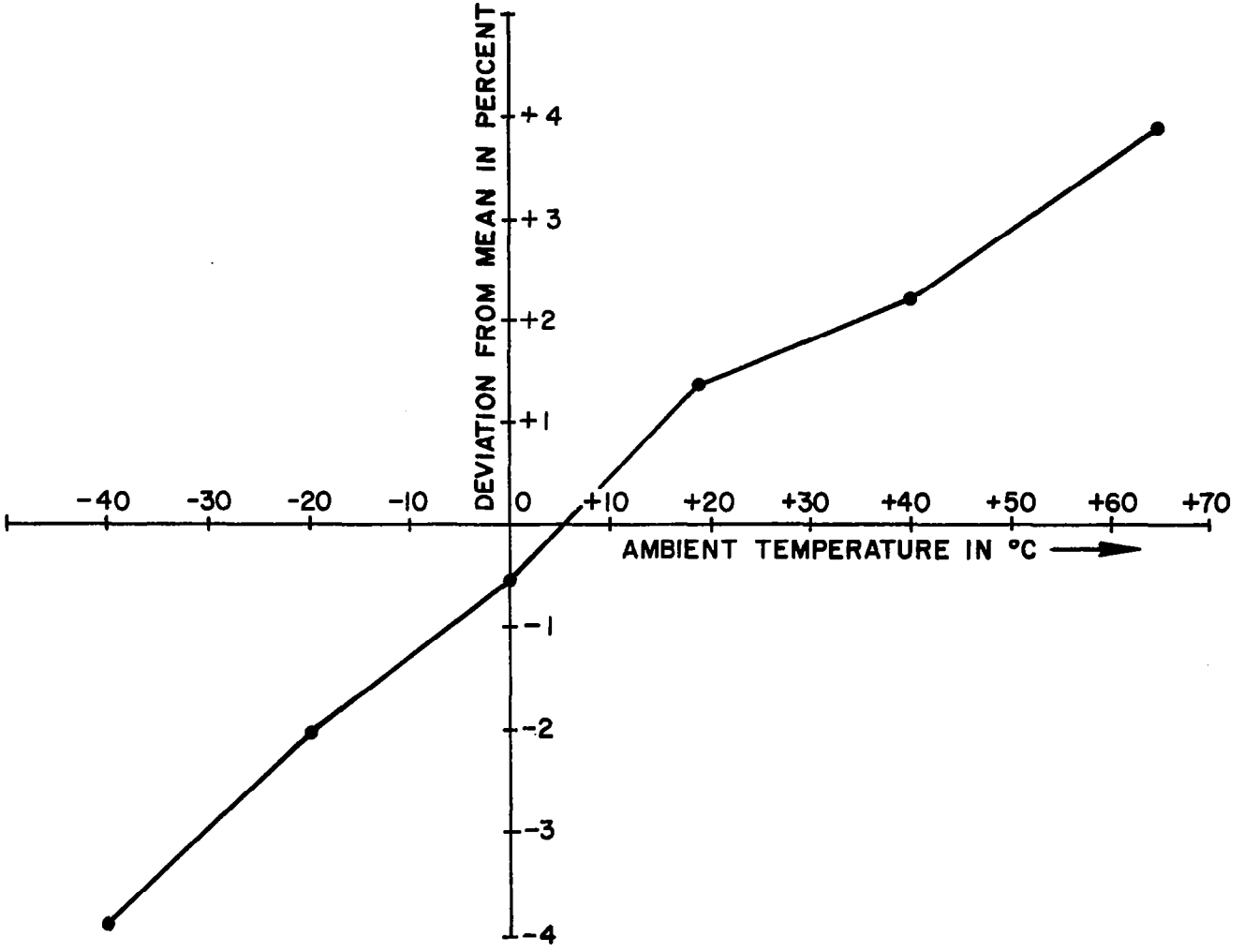

VOLTAGE VARIATION OF SHIELD SUPPLY WITH TEMPERATURE

FIG. FIFTY-SIX

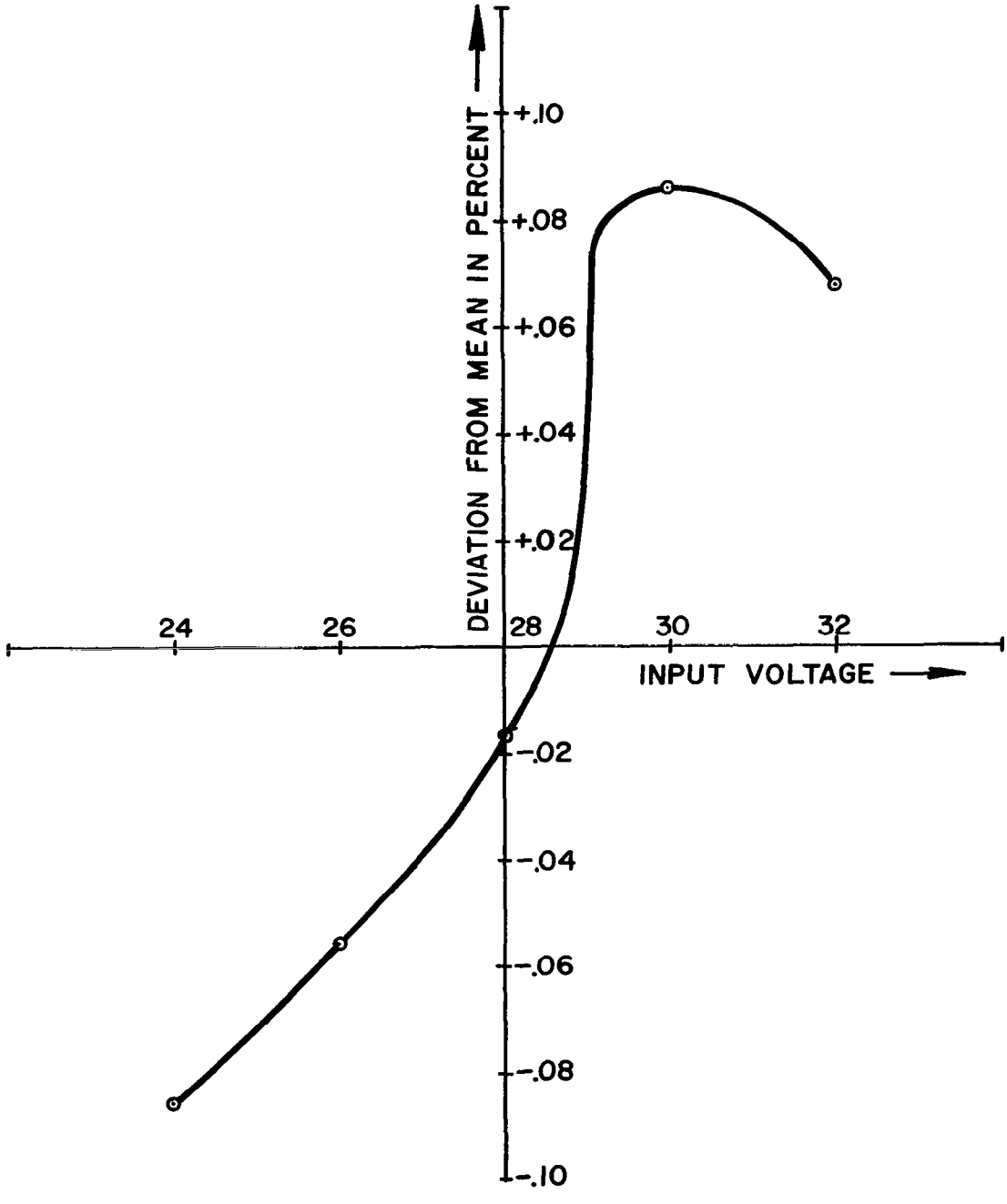

VOLTAGE VARIATION OF SHIELD SUPPLY WITH INPUT VOLTAGE

FIG. FIFTY-SEVEN

TABLE XLIV

Variation of Shield Supply Randomly Observed

Over a 24 Hour Period

Output Voltage in Volts	Deviation From Mean Voltage in Volts	Deviation From Mean Voltage in Percent
323.70	-0.48	+0.148
325.57	+1.39	+0.429
322.86	-1.32	-0.408
322.69	-1.49	-0.460
325.67	+1.49	+0.460
325.59	+1.41	+0.435
325.54	+1.36	+0.420

8.8 Evaluation of the Anode Voltage Supply

8.8.1 Objective

The objective of this section is to determine the voltage variation of the Anode Voltage Supply.

8.8.2 Conclusion

It was concluded that the Anode Voltage Supply output varies ± 3.68 percent from its mean value over the temperature range, that it varies ± .109 percent from its mean value over the input voltage range and that it varies ± .396 percent randomly.

8.8.3 Equipment

Power Supply	Kepco CK36-1.5	H-40117

VARIATION OF SHIELD SUPPLY VOLTAGE
OBSERVED AT RANDOM OVER 24 HOUR PERIOD

FIG. FIFTY-EIGHT

8.8.3 Equipment continued

Differential Volt Meter	John Fluke 803B	3439
Temperature Chamber	Statham TC-4	2045

8.8.4 Procedure

1. Power was supplied to the emission regulator circuit which in turn applied power to the Anode Voltage Supply.

2. The high voltage box was inserted into the test chamber, and the emission regulator was connected to the high voltage box. The Anode Supply is located in the high voltage box.

3. The Anode Voltage Supply output was monitored and recorded as the temperature was varied from -40° to +65°C.

4. The Anode Voltage Supply output was monitored and recorded as the input voltage to the emission regulator was varied from 24 to 32 volts. This was done at room temperature.

5. The Anode Voltage Supply output was measured and recorded at random intervals for a period of 24 hours. The supply was turned on and off several times during this period.

8.8.5 Results

The results are given in Tables XLV, XLVI and XLVII and Figures 59, 60 and 61.

TABLE XLV

Variation of Anode Supply With Temperature

Temperature in °C	Output Voltage in Volts	Deviation From Mean Voltage in Volts	Deviation From Mean Voltage in Percent
+19	156.35	+1.14	+0.73
-40	149.46	-5.75	-3.68
-20	151.57	-3.64	-2.33
0	153.61	-1.60	-1.02
+40	158.30	+3.09	+1.98
+65	160.96	+5.75	+3.68

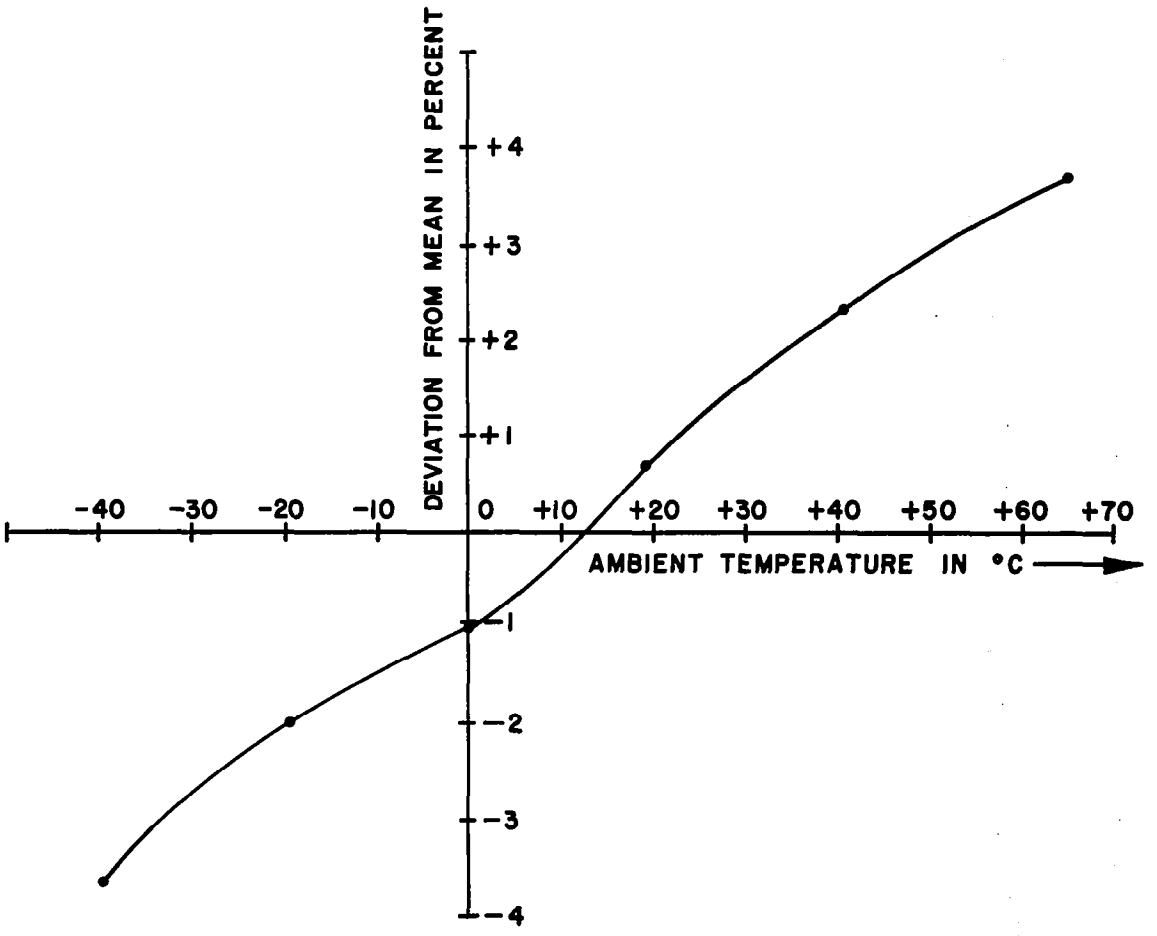

VARIATION OF ANODE SUPPLY WITH TEMPERATURE

FIG. FIFTY-NINE

TABLE XLVI

Variation of Anode Supply With Input Voltage

Input Voltage in Volts	Output Voltage in Volts	Deviation From Mean Voltage in Volts	Deviation From Mean Voltage in Percent
32	156.35	+0.16	-.102
30	156.31	+0.13	+.083
28	156.31	+0.13	+.083
26	156.04	-0.14	+.089
24	156.02	-0.17	+.109

TABLE XLVII

Variation of Anode Supply Randomly

Observed Over a 24 Period

Output Voltage in Volts	Deviation From Mean Voltage in Volts	Deviation From Mean Voltage in Percent
156.65	+0.02	+.013
157.15	+0.52	+.333
156.02	-0.61	-.391
156.29	-0.34	-.218
157.25	+0.62	+.396
157.21	+0.58	+.371
157.18	+0.55	+.352

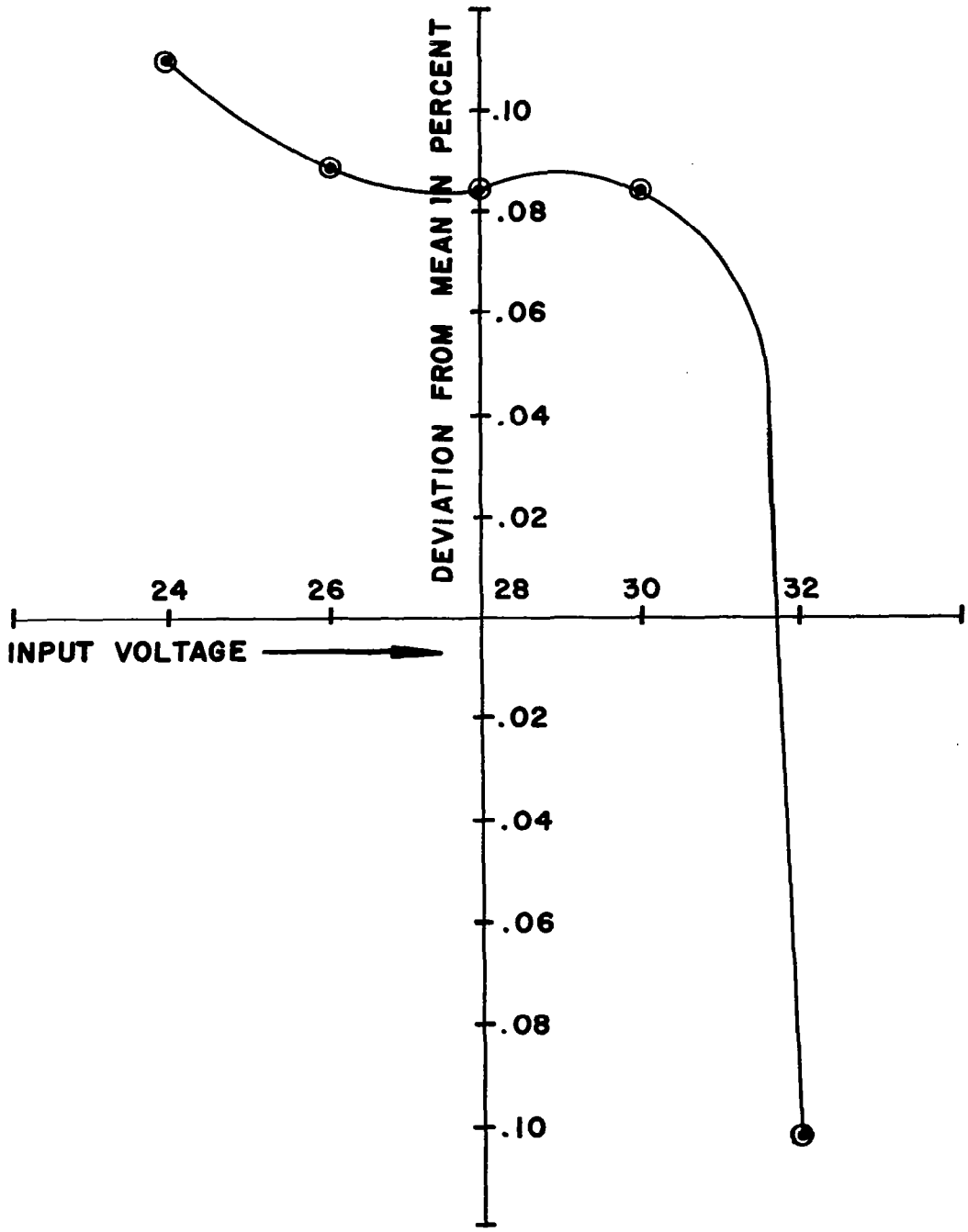

VARIATION OF ANODE SUPPLY WITH INPUT VOLTAGE

FIG. SIXTY

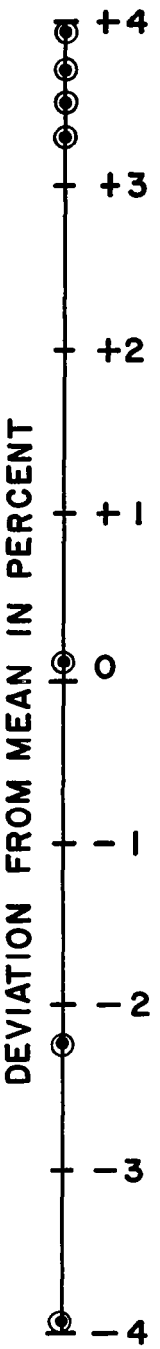

VARIATION OF ANODE SUPPLY RANDOMLY OBSERVED OVER A 24 HOUR PERIOD

FIG. SIXTY-ONE

8.9 Evaluation of the Electrometer Amplifiers

There are twelve electrometer amplifiers. Nine of the electrometers have a sensitivity of 5×10^{12} ohms; two have a sensitivity of 5×10^{11} ohms; and one electrometer has a sensitivity of 2×10^{11} ohms. The minimum detectable current on the 5×10^{12} ohm amplifiers is 1×10^{-14} amperes. This minimum detectable level assumes a 50 m.v. peak to peak noise level which is typical of the amplifiers properly adjusted for a zero to five cps bandwidth. The feedback components were not properly selected in most of the electrometers, and therefore, the peak to peak output noise levels ranged from 50 to 200 m.v.

The electrometer output is from zero to minus five volts DC. The amplifiers are capable of driving a 10 kohm load. The dynamic output impedance of the electrometers is less than one ohm. A check on the output zero six months after adjustment showed all the outputs to be within plus or minus 50 m.v. of zero. During this six month period, the amplifiers were switched on and off many times; however, it has been the practice to leave the electrometers on as much as possible.

The twelve electrometer amplifiers and the electrometer power supply are mounted together in a package which in turn is mounted to the mass spectrometer. It was noted that the mounting of the electrometer package to the instrument proper is not sufficiently rigid.

8.10 Evaluation of Electrometer Amplifier Power Supply

8.10.1 Objective

The objective of this section is to determine the voltage variation of the four supplies which comprise the Electrometer Amplifier Power Supply.

8.10.2 Conclusion

Maximum variations of the four supplies observed over the temperature range, over the voltage range and at random are tabulated in Table XLVIII.

TABLE XLVIII

Summary of Electrometer Power Supply Performance

Summary	Variation Over Temperature Range in Percent	Variation Over Input Voltage in Percent	Variations Observed Over 48 Hour Period in Percent
+35	±.12	±.028	±.06
-20	±.35	±.04	±.06
+10	±.07	±.03	±.04
+ 2.6	+.16	+.19	±.06

8.10.3 Equipment

Power Supply	Kepco CK36-15	H 40117
Differential Volt Meter	John Fluke 803B	3439
Temperature Chamber	Statham TC	2045

8.10.4 Procedure

1. Power was applied to the Electrometer Power Supply.

2. The Electrometer Amplifier Power Supply was placed in the temperature chamber and connected to its normal load of electrometers.

3. The Electrometer Power Supply outputs were monitored and recorded as the temperature was varied from -45° to +65°C.

4. The Electrometer Power Supply outputs were monitored and recorded as the input voltage was varied from 24 to 32 volts. This was done at room temperature.

5. The Electrometer Amplifier Power Supply outputs were measured and recorded over a period of 48 hours at random intervals.

8.10.5 Results

The results are given in Tables IL through LX and Figures 62 through 73.

TABLE IL

Variation of -20 Volt Supply With Temperature

Temperature in °C	Output Voltage in Volts	Deviation From Mean Voltage in Volts	Deviation From Mean Voltage in Percent
+21	19.993	+0.009	+ .045
-45	20.053	+0.69	+0.346
-20	20.044	+0.060	+0.302
0	20.013	+0.029	+0.146
+20	19.979	-0.005	+0.025
+40	19.945	-0.039	-0.196
+65	19.914	-0.070	- .352

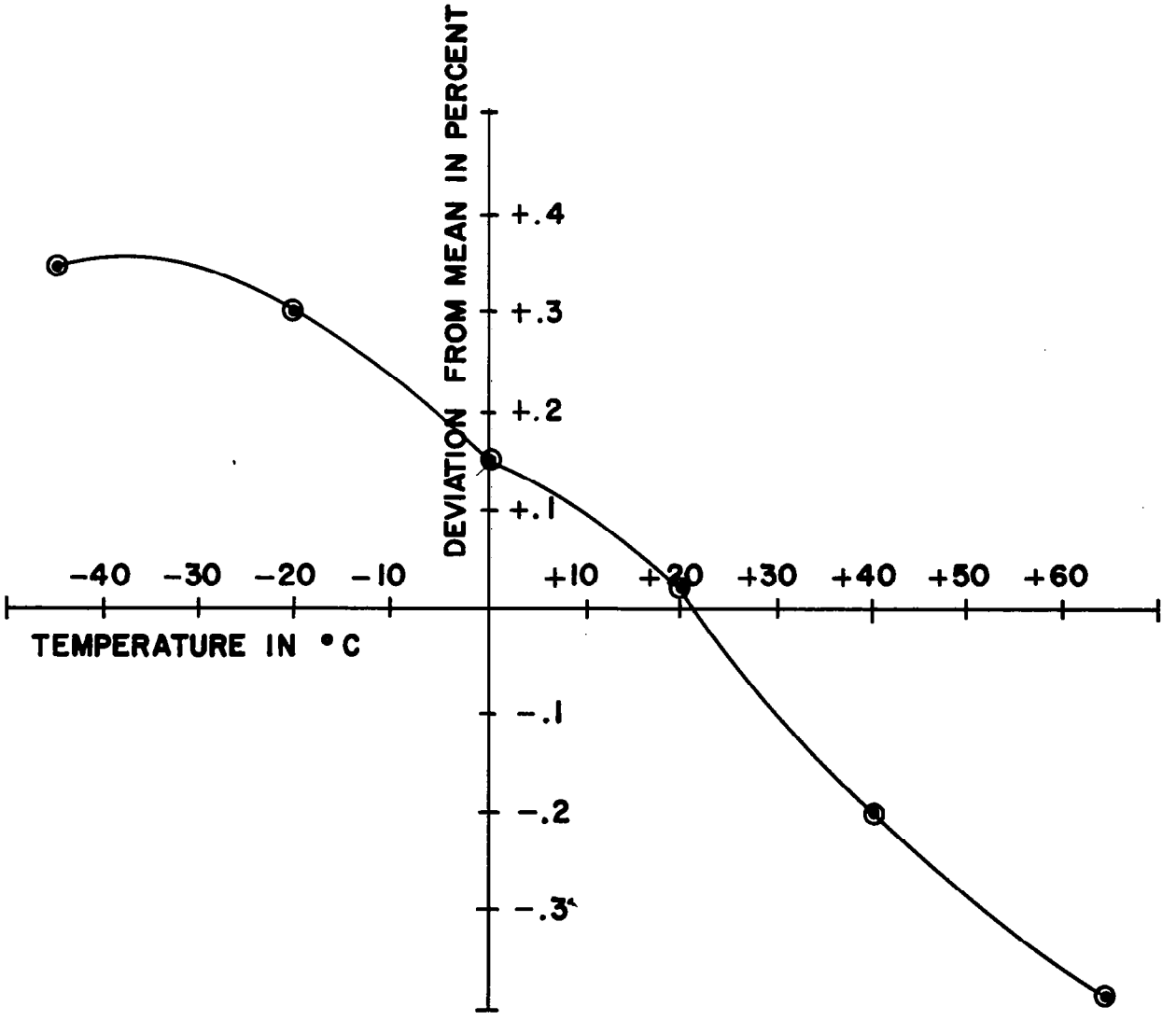

VARIATION OF -20 VOLT SUPPLY WITH TEMPERATURE

FIG. SIXTY-TWO

TABLE L

Variation of -20 Volt Supply With Input Voltage

Input Voltage in Volts	Output Voltage in Volts	Deviation From Mean Voltage in Volts	Deviation From Mean Voltage in Percent
32	19.978	+.008	+.040
28	19.977	+.007	+.035
24	19.963	-.007	-.035

TABLE LI

Variation of -20 Volt Supply Randomly Observed Over a 48 Hour Period

Output Voltage in Volts	Deviation From Mean Voltage in Volts	Deviation From Mean Voltage in Percent
19.993	+0.012	+0.06
19.969	-0.012	-0.06
19.993	+0.012	+0.06
19.977	-0.004	-0.02

TABLE LII

Variation of +35 Volt Supply With Temperature

Temperature in °C	Output Voltage in Volts	Deviation From Mean Voltage in Volts	Deviation From Mean Voltage in Percent
-45	34.949	+.036	+.103
-20	34.954	+.041	+.117
0	34.929	+.016	+.046
+20	34.911	-.002	+.006

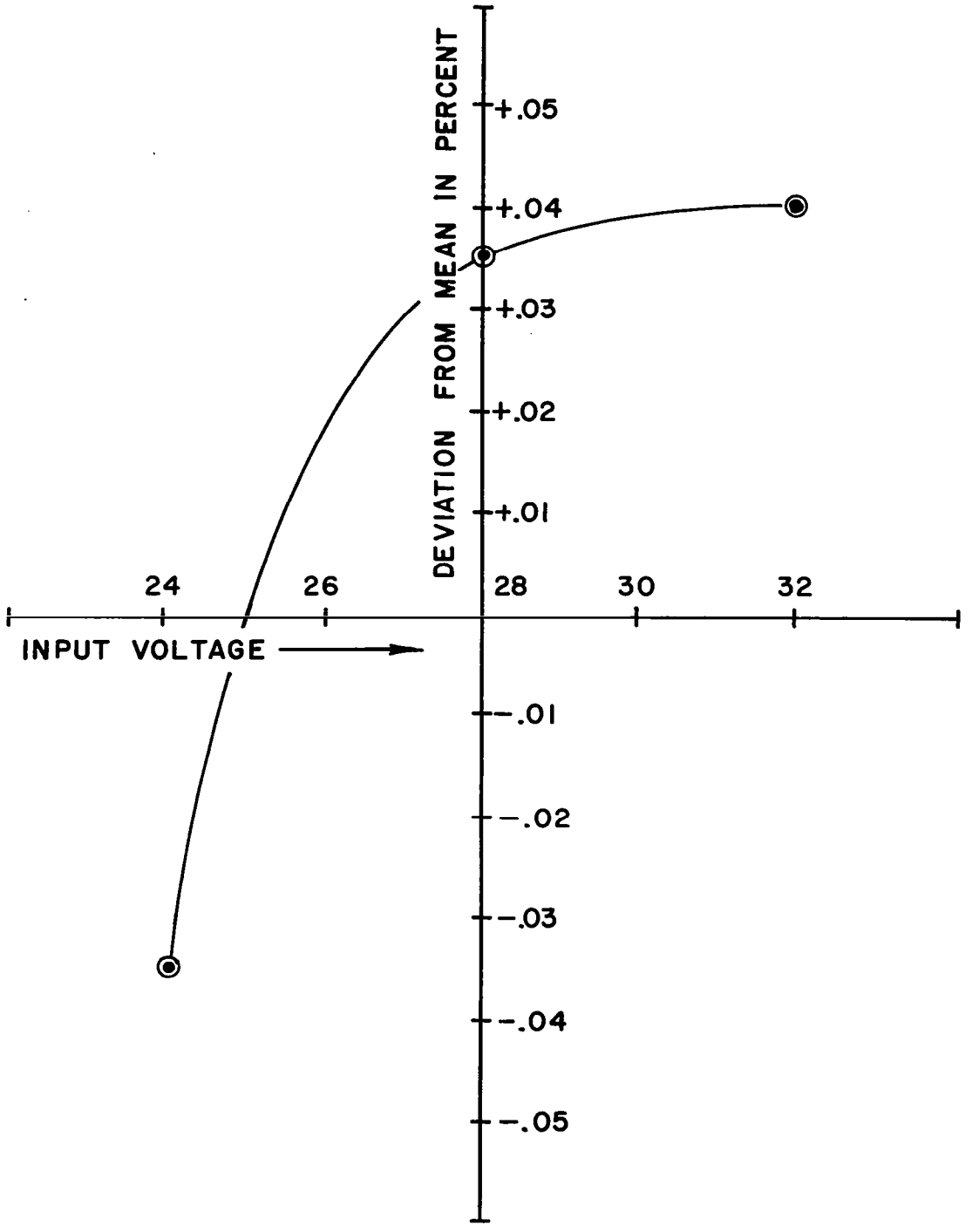

VARIATION OF -20 VOLT SUPPLY WITH INPUT VOLTAGE

FIG. SIXTY-THREE

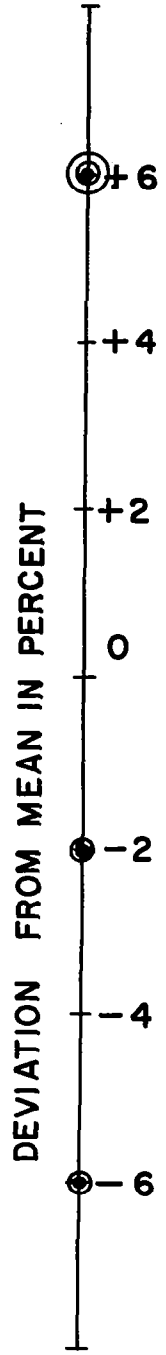

VARIATION OF -20 VOLT SUPPLY RANDOMLY OBSERVED OVER A 24 HOUR PERIOD

FIG. SIXTY-FOUR

TABLE LII cont.

Variation of +35 Volt Supply With Temperature

Temperature in °C	Output Voltage in Volts	Deviation From Mean Voltage in Volts	Deviation From Mean Voltage in Percent
+40	34.890	-.023	-.066
+65	34.872	-.041	-.117

TABLE LIII

Variation of +35 Volt Supply With Input Voltage

Input Voltage in Volts	Output Voltage in Volts	Deviation From Mean Voltage in Volts	Deviation From Mean Voltage in Percent
32	34.934	+0.010	+0.028
28	34.930	+0.006	+0.017
26	34.914	-0.010	-0.028

TABLE LIV

Variation of +35 Volt Supply Randomly Observed

Over a 48 Hour Period

Output Voltage in Volts	Deviation From Mean Voltage in Volts	Deviation From Mean Voltage in Percent
34.952	+0.021	+0.060
34.911	-0.020	-0.057
34.945	+0.014	+0.040
34.930	-0.001	-0.003

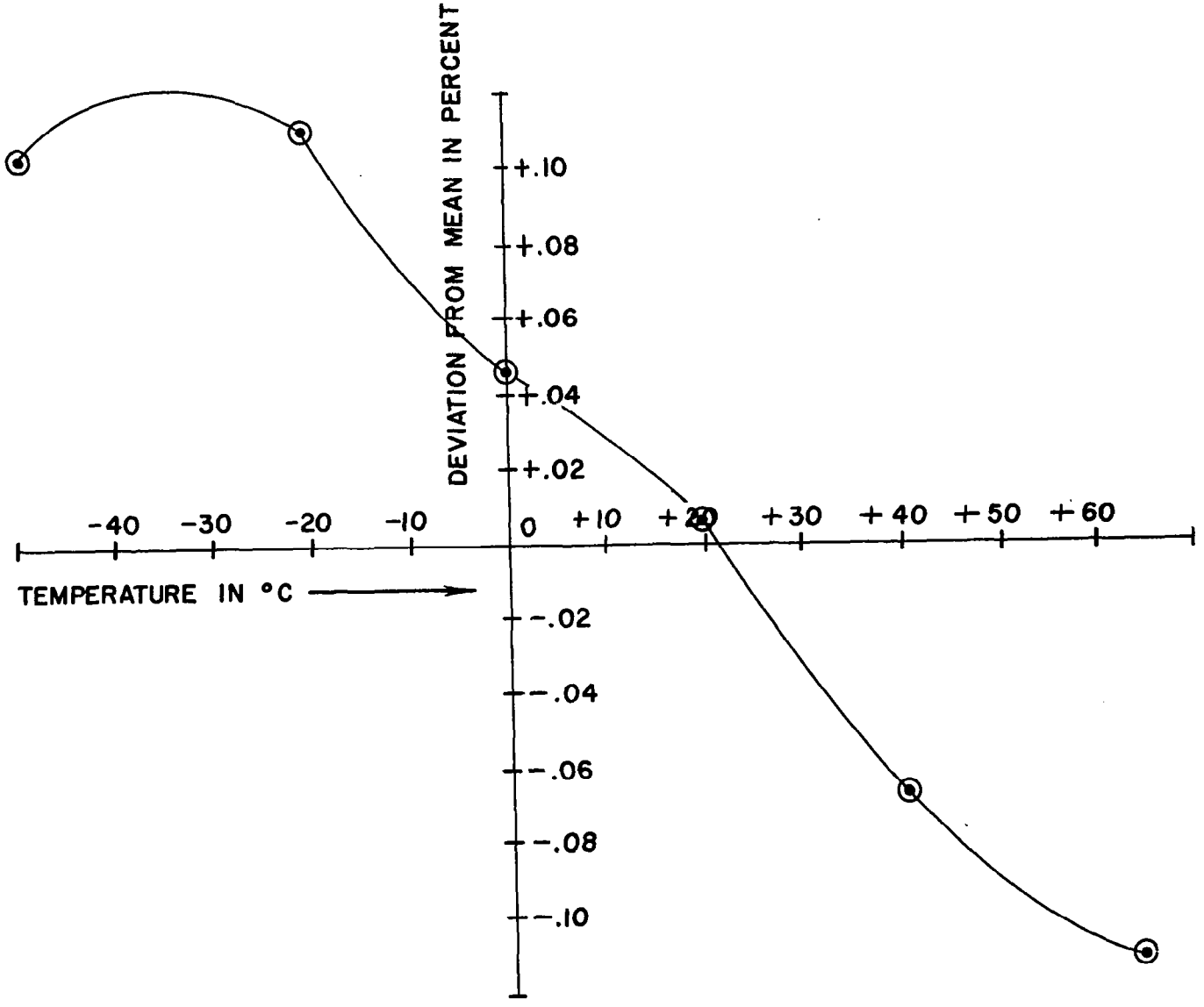

VARIATION OF +35 VOLT SUPPLY WITH TEMPERATURE

FIG. SIXTY-FIVE

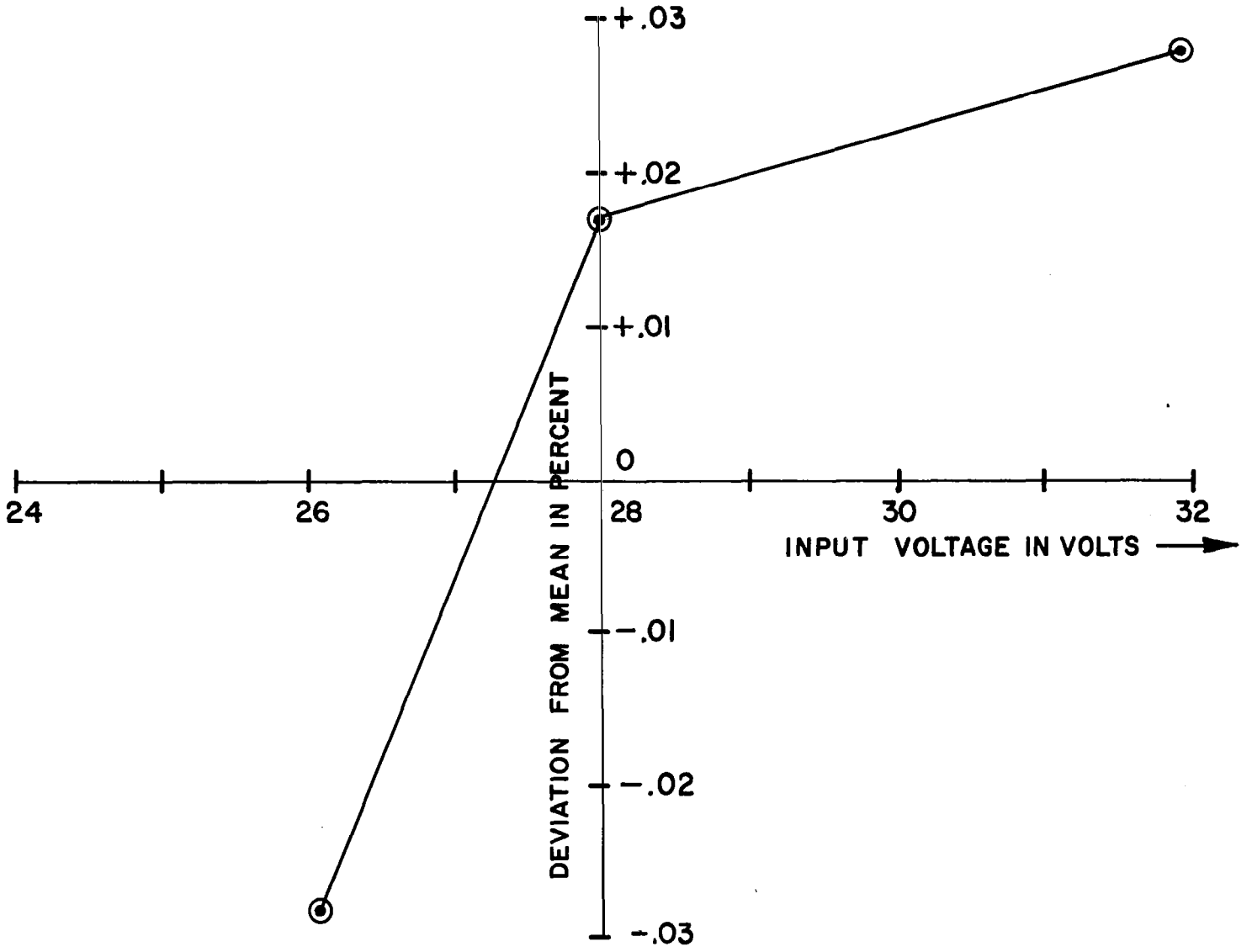

VARIATION OF +35 VOLT SUPPLY WITH INPUT VOLTAGE

FIG. SIXTY-SIX

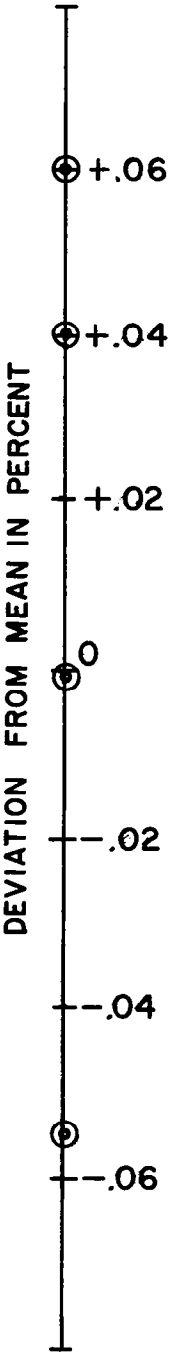

VARIATION OF +35 VOLT SUPPLY RANDOMLY OBSERVED OVER A 24 HOUR PERIOD

FIG. SIXTY-SEVEN

TABLE LV

Variation of +10 Volt Supply With Temperature

Temperature in °C	Output Voltage in Volts	Deviation From Mean Voltage in Volts	Deviation From Mean Voltage in Percent
+21	9.984	+0.003	.03
-45	9.980	-0.001	.01
-20	9.988	+0.007	.07
0	9.987	+0.006	.06
+20	9.984	+0.003	.03
+40	9.976	-0.005	.05
+65	9.974	-0.007	.07

TABLE LVI

Variation of +10 Volt Supply With Input Voltage

Input Voltage in °C	Output Voltage in Volts	Deviation From Mean Voltage in Volts	Deviation From Mean Voltage in Percent
32	9.983	+0.003	.03
28	9.983	+0.003	.03
24	9.978	-0.002	.02

TABLE LVII

Variation of +10 Volt Supply Randomly Observed

Over a 48 Hour Period

Output Voltage in Volts	Deviation From Mean Voltage in Volts	Deviation From Mean Voltage in Percent
9.988	+.004	.04
9.981	-0.003	.03

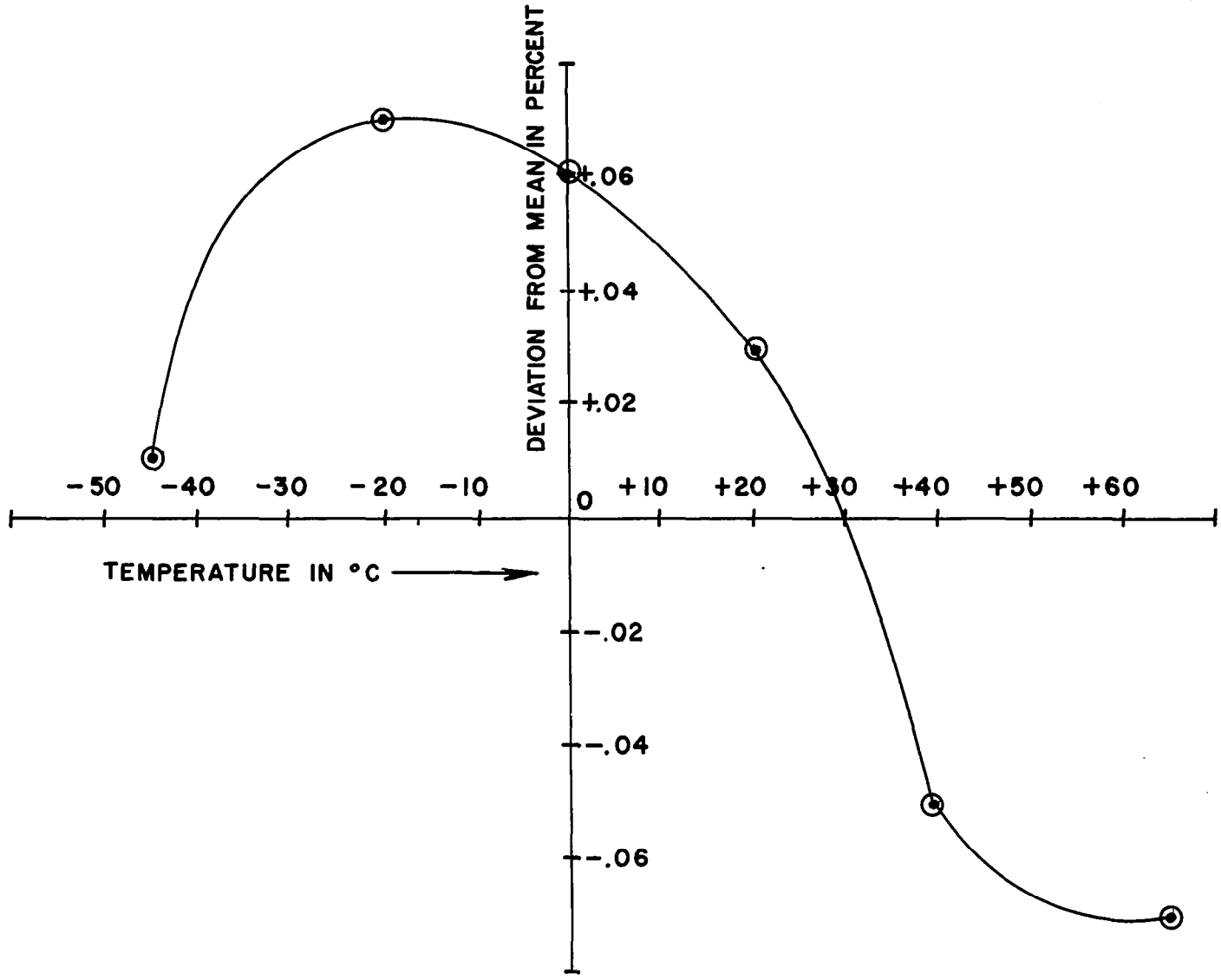

VARIATION OF +10 VOLT SUPPLY WITH TEMPERATURE

FIG. SIXTY-EIGHT

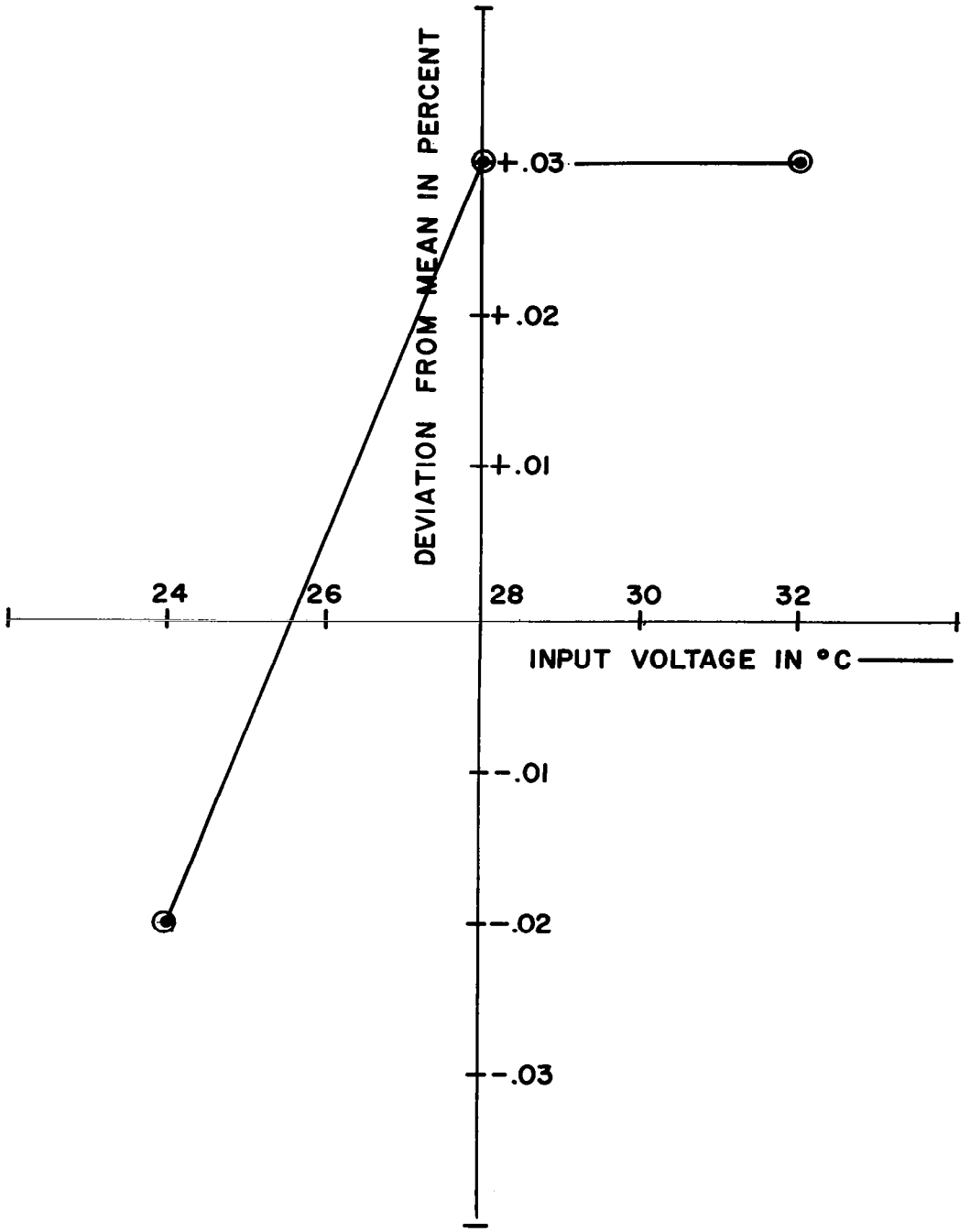

VARIATION OF + 10 VOLT SUPPLY WITH INPUT VOLTAGE

FIG. SIXTY-NINE

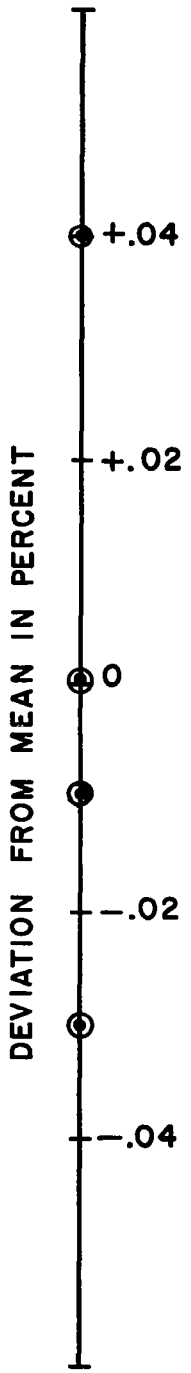

VARIATION OF +10 VOLT SUPPLY RANDOMLY OBSERVED OVER A 24 HOUR PERIOD

FIG. SEVENTY

TABLE LVII continued

Output Voltage in Volts	Deviation From Mean Voltage in Volts	Deviation From Mean Voltage in Percent
9.984	-0.000	0.00
9.983	-0.001	.01

TABLE LVIII

Variation of +2.6 Volt Supply With Temperature

Temperature in °C	Output Voltage in Volts	Deviation From Mean Voltage in Volts	Deviation From Mean Voltage in Percent
+21	2.594	+.003	+ .116
-45	2.592	+.001	+0.039
-20	2.595	+.004	+0.155
0	2.593	+.002	+0.078
+20	2.592	+.001	+0.039
+40	2.589	-.002	-0.077
+65	2.588	-.003	-0.116

TABLE LIX

Variation of +2.6 Volt Supply With Input Voltage

Input Voltage in Volts	Output Voltage in Volts	Deviation From Mean Voltage in Volts	Deviation From Mean Voltage in Percent
32	2.597	+ .005	+0.192
28	2.592	0.000	0.000
24	2.587	-.005	-0.192

TABLE LX

Variation of +2.6 Volt Supply Randomly Observed Over a 48 Hour Period

Output Voltage in Volts	Deviation From Mean Voltage in Volts	Deviation From Mean Voltage in Percent
2.595	+.0015	+.058
2.592	-.0015	-.058

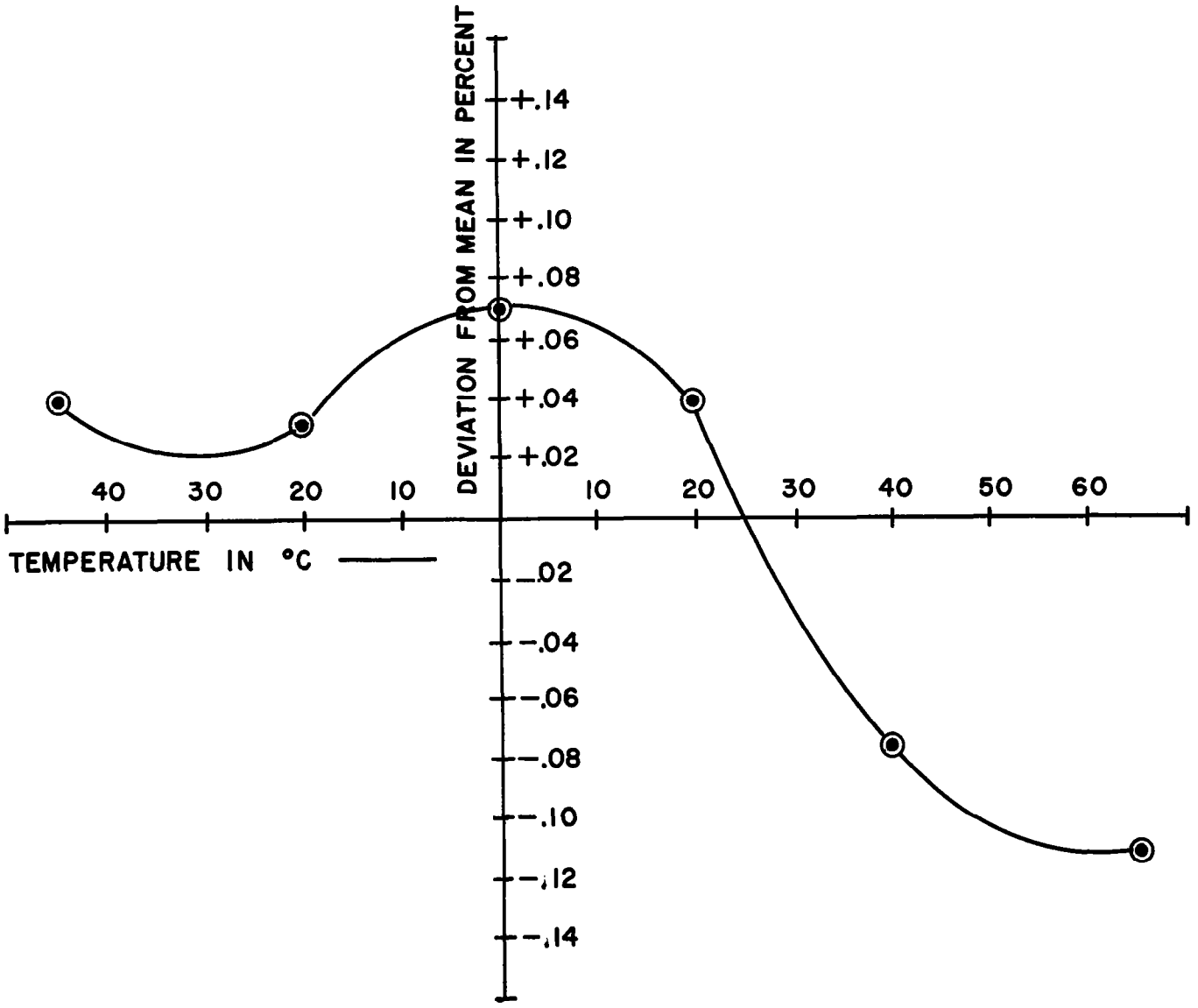

VARIATION OF +2.6 VOLT SUPPLY WITH TEMPERATURE

FIG. SEVENTY- ONE

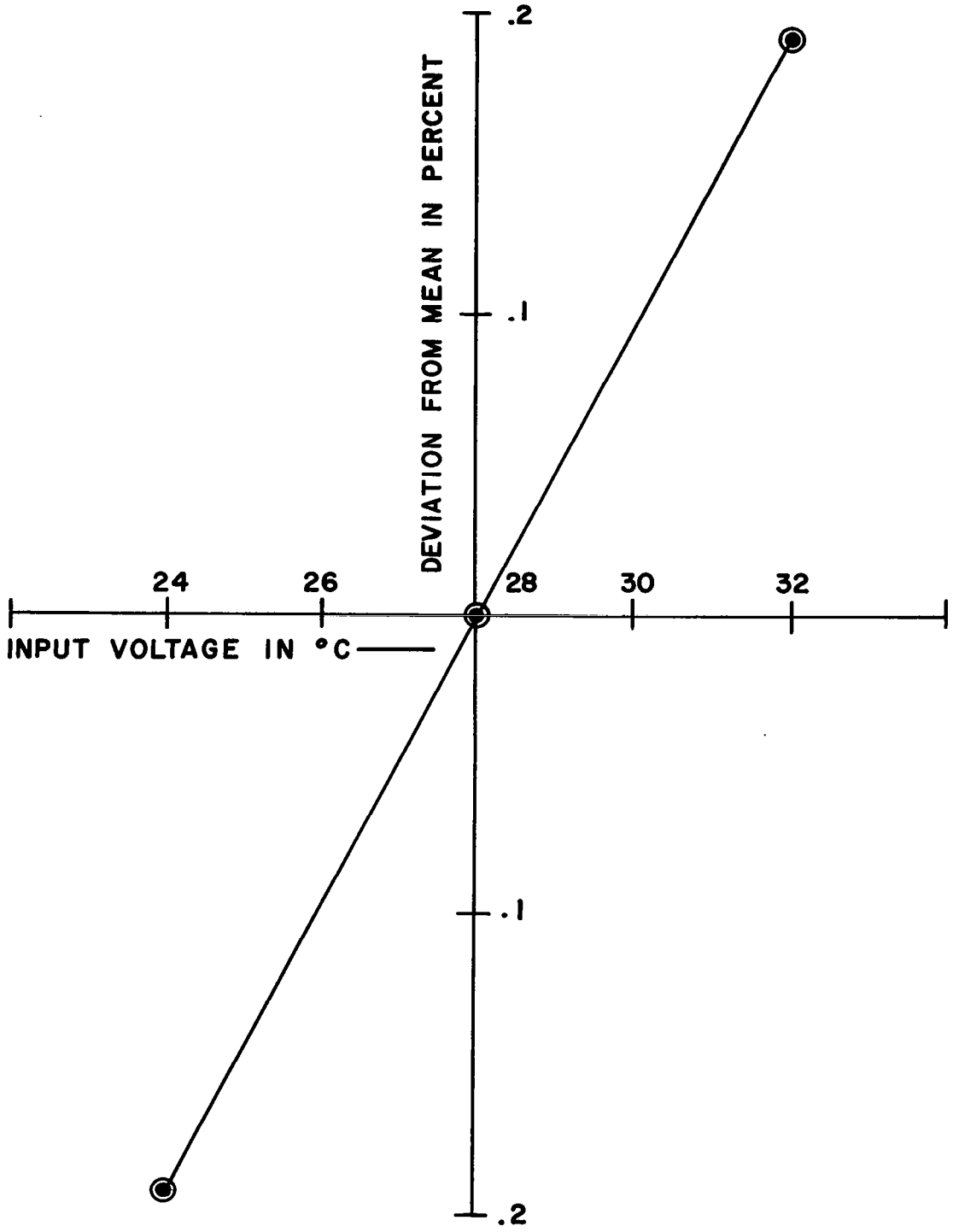

VARIATION OF +2.6 VOLT SUPPLY WITH INPUT VOLTAGE

FIG. SEVENTY-TWO

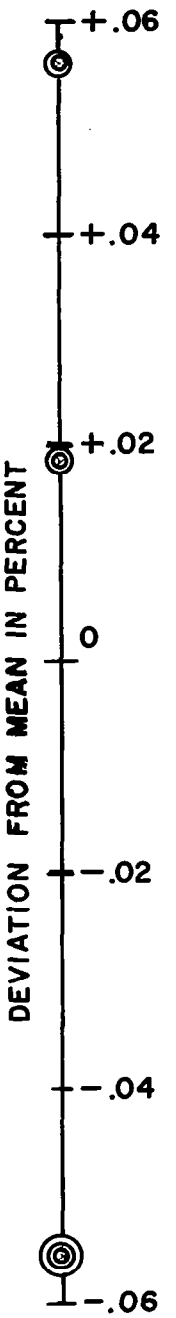

VARIATION OF +2.6 VOLT SUPPLY RANDOMLY OBSERVED OVER A 24 HOUR PERIOD

FIG. SEVENTY-THREE

TABLE LX continued

Output Voltage in Volts	Deviation From Mean Voltage in Volts	Deviation From Mean Voltage in Percent
2.594	+.0005	+.019
2.592	-.0015	-.058

8.11 Evaluation of the Ion Pump Power Supply

It is difficult to separate the performance of the Ion Pump Power Supply from the operation of the pump itself. The combination of pump and power supply functioned in a marginal manner for three months after delivery of the instrument. At that time, the performance of the pump-supply combination had depreciated to the point that the instrument was completely unusable. Whether the change in performance was due to a change in the pump or a change in the supply is unknown. Neither unit had been evaluated at that time. The pump was returned to Varian Associates for refurbishing. Upon the return of the pump, the performance of the pump-supply combination was again examined and found to be still unusable. For the remainder of the testing period the ion pump was operated from a larger supply which is part of the ground support equipment. This combination yielded a performance approximately equal to the performance of the instrument upon delivery. The larger supply had the properties of both higher voltage output and higher power output.

Shortly after delivery of the instrument and during one of the initial evaluation flights it was noted that arcing occured in the original supply over 27,000 feet. A closer investigation of the problem showed that the packaging in this module was particularly dense. The dual problem of high altitude arcing and insufficient output was solved with the purchase of a new flight power supply. The new supply had an output voltage of 7000 volts and was capable of delivering 4 m.a. current at this voltage.[23] The volt-ampere characteristics of the original supply were recorded and are shown in Figure 74. The interlock and metering circuits which are physically located in the Ion Pump Power Supply module were found to operate satisfactorily.

8.12 Evaluation of the Remote Control Box

No difficulties were experienced in operation of the Remote Control Box.

[23]With the use of a regulated supply, it is essential that a fair vacuum be established in the instrument before the ion pump is turned on.

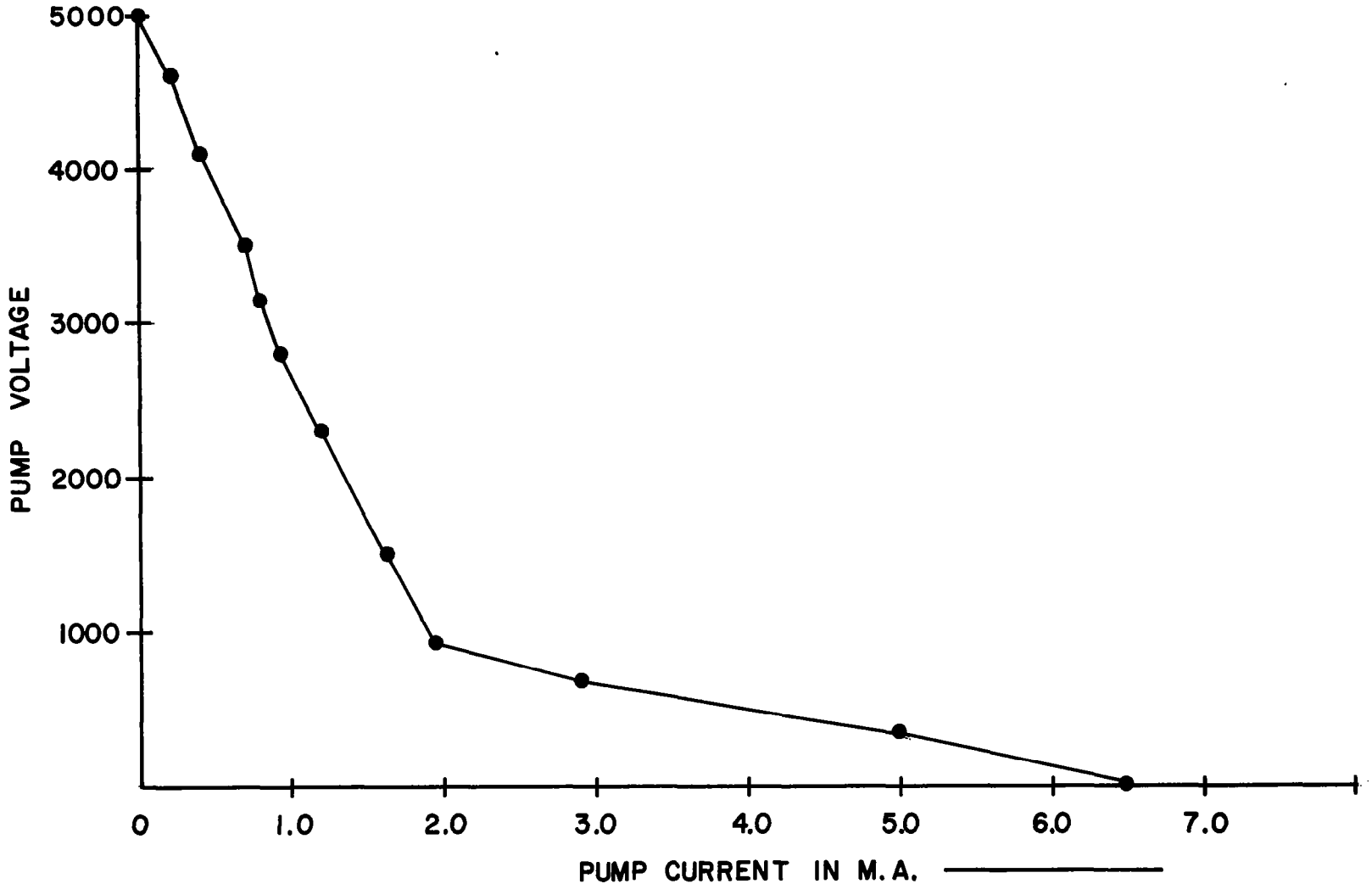

VOLT-AMPERE CHARACTERISTICS OF THE ORIGINAL
ION PUMP POWER SUPPLY
FIG. SEVENTY—FOUR

9. CONCLUSIONS AND RECOMMENDATIONS

The general conclusion which was drawn from the investigation is that the double-focusing mass spectrometer shows considerable promise as a practical means of measuring gas concentrations in a flight environment. It is recommended that simplicity, reliability, small size and lower cost be the design goals of any future development effort. Several specific recommendations are discussed below.

The mass spectrometer evaluated in this report was equipped with a vacuum system for operation in the earth's atmosphere. In an instrument designed for operation in outer space, the vacuum system could be excluded. This would eliminate the vacuum problems discussed in the report as well as reduce the size of the instrument by a factor of two. In any future application where space pumping is not available, it is imperative that a more effective ion pump be used. The vacuum pump capacity not only limits the stability of the instrument as is explained in the section on the vacuum system but also limits the size of the gold leak used. With a higher pumping capability, a larger and more reliable gold leak could be utilized in conjunction with a larger source conductance to produce the same source pressure.

In any future design of the electron source, it would be desirable to either reduce the filament movement or to redesign the electron-gun in such a manner that filament movement would have a less pronounced effect upon electron distribution. It is believed that this would increase the stability of the instrument both as to output and resolution.

It would be desirable to improve several different features of the analyzer magnet. The analyzer evaluation indicated that better resolution could be obtained with the instrument by using a stronger magnetic field. Due to the relatively small pole area compared to the wide gap, the magnetic field was extremely non-uniform. It is assumed that better focusing could be achieved with a magnetic field which began and ended more abruptly and which was more uniform in the center. A third desirable improvement in the magnet design would be better stability with time. A fourth, and probably the most important improvement to be desired in the magnet design would be better temperature stability. As the temperature coefficient of the present magnet approaches practical limits, special techniques to attain better temperature stability should be investigated.

It is recommended that in future designs an electrode current which is directly related to ionization current be regulated rather than regulating the total filament emission. Doing this should make the mass spectrometer more stable and less sensitive to changes in filament position.

LIST OF SPECIAL SYMBOLS

B	Magnetic field intensity of the analyzer magnet. Also Ion Beam width.
ΔV_{sec}	Delta electric sector voltage. The voltage between the positive sector electrode and the negative sector electrode.
e	Electric charge.
E	Electric field intensity.
F	Force.
F_m	Force resulting from magnetic field.
G_A	Conductance of pinch-off tube aperature.
$G_{G.L.}$	Conductance of gold leak.
G_P	Conductance of pinch-off tube.
G_v	Conductance of valve between pinch-off tube and 15 liter pump.
G_s	Source conductance.
G_1	Pumping speed of 4 liter pump and pinch-off tube line combination.
G_2	Pumping speed of 4 liter pump.
G_{15}	Pumping speed of pinch-off tube line to 15 liter pump.
I_{anode}	Electron current to anode electrode.
$I_{elec.\ acc.}$	Electron current to the electron accelerator electrode.
$I_{ion\ acc.}$	Electron current to the ion accelerator electrode.
I_{rep}	Electron current to ion repeller electrode.
I_{total}	Total filament emission current.
I_1	Pump current of 4 liter pump with both 4 liter and 15 liter pump pumping on system.
I_2	Pump current of 4 liter pump with only 4 liter pump pumping on system.

P_p	Pump pressure of 4 liter pump.
P_{p1}	Pump pressure of 4 liter pump with inlet valve closed.
P_{p2}	Pump pressure of 4 liter pump with inlet valve open.
P_s	Ion Source Pressure.
P_1	Pressure on high side of gold leak in gold leak test system.
P_2	Pressure on low side of gold leak in gold leak test system.
P_3	Fifteen liter pump pressure.
Q	Throughput.
Q_s	Sample throughput.
Q_c	Contamination throughput.
r	Radius.
S	Slit width. Also Pump Speed.
S_4	Speed of four liter pump.
S_{15}	Speed of fifteen liter pump.
v	Velocity.
V_{acc}	Acceleration voltage.
V_{anode}	Anode voltage.
$V_{elec.\ acc.}$	Electron accelerator voltage.
$V_{elec.\ focus}$	Electron focus voltage.
$V_{elec.\ rails}$	Electron rail voltage.
$V_{fil.}$	Voltage of filament with respect to ground.
$V_{fil.\ shield}$	Filament shield voltage.
$V_{Lens\ II}$	Lens II voltage.
V_{ion}	Ionization voltage.
$V_{ion\ acc.}$	Ion accelerator voltage.

$V_{ion\ rails}$	Ion rail voltage.
$V_{inj.}$	Injection voltage.
$V_{neg.\ sec.}$	Negative sector voltage.
$V_{pos.\ sec.}$	Positive sector voltage.
$V_{rep.}$	Repeller voltage.
$V_{z\text{-axis focus}}$	Z-axis focus voltage.
X	The distance of a collector bucket from the theoretical entrance point, the slit distance.
X_1	Top dimension of scanned peak as measured on recorder scale.
X_2	Bottom dimension of scanned peak as measured on recorder scale.

NASA-Langley, 1966 CR-605